NASA TECHNICAL REPORT

NASA TR R-302

NASA TR R-302

USE OF SUPERPOSITION IN DIGITAL COMPUTERS TO OBTAIN WIND-TUNNEL INTERFERENCE FACTORS FOR ARBITRARY CONFIGURATIONS, WITH PARTICULAR REFERENCE TO V/STOL MODELS

by Harry H. Heyson

Langley Research Center
Langley Station, Hampton, Va.

NATIONAL AERONAUTICS AND SPACE ADMINISTRATION • WASHINGTON, D. C. • FEBRUARY 1969

NASA TR R-302

USE OF SUPERPOSITION IN DIGITAL COMPUTERS TO OBTAIN WIND-TUNNEL INTERFERENCE FACTORS FOR ARBITRARY CONFIGURATIONS, WITH PARTICULAR REFERENCE TO V/STOL MODELS

By Harry H. Heyson

Langley Research Center
Langley Station, Hampton, Va.

NATIONAL AERONAUTICS AND SPACE ADMINISTRATION

For sale by the Clearinghouse for Federal Scientific and Technical Information
Springfield, Virginia 22151 – CFSTI price $3.00

CONTENTS

USE OF SUPERPOSITION IN DIGITAL COMPUTERS TO OBTAIN WIND-TUNNEL INTERFERENCE FACTORS FOR ARBITRARY CONFIGURATIONS, WITH PARTICULAR REFERENCE TO V/STOL MODELS

By Harry H. Heyson
Langley Research Center

SUMMARY

A superposition method utilizing a digital computer is developed to obtain wall interference for arbitrary configurations. A variety of specific configurations are treated. Sample numerical results indicate that a large number of variables, such as wind-tunnel configuration, model configuration, wake deflection, model location, span of wing and tail, load distribution, sweep, angle of attack, pivot location, tail length, and tail height, may individually or collectively produce substantial effects on wall interference. Interference is particularly severe at the rear rotor of tandem systems; the maximum size of such systems for reasonable wall effects is discussed.

INTRODUCTION

The interference flow at a model engendered by the presence of the wind-tunnel boundaries has been recognized and studied for over 50 years. (A recent summary is presented in ref. 1.) This interference has been found to depend upon a great many configuration variables such as span and sweep. In many cases, interference values have been calculated for systematic variations of the pertinent parameters, and these values may be found in many papers. In other cases, superposition schemes, often using supplementary charts and tables, have been set up for general types of wings.

Actual wind-tunnel practice is not always optimum with regard to obtaining the correct wall interference factors for a given test. Unless the proper factors are readily available, without supplementary calculations, there is a tendency to use an available "small model" factor rather than the appropriate finite-span factor; for instance, wing sweep may be ignored, particularly since the average wind-tunnel test engineer does not have an inclination toward manual superposition calculations. These trends are particularly common in the testing of V/STOL models, where the configurations range over such a wide variety of types that the required factors are seldom available. Indeed, the

practice in V/STOL tests, other than those intended specifically to study wall effects, is to ignore wall interference, largely because of the inconvenience of obtaining the correct interference factors.

The use of modern digital computer equipment, together with simple superposition techniques, can greatly simplify the problems involved in obtaining the proper interference factors for models of arbitrary configuration. The first requirement is the existence of a theory which provides the interference at an arbitrary point in the tunnel occasioned by the presence of a vanishingly small model located in an arbitrary position in the tunnel. Several such theories exist (ref. 1), and these by themselves are easily programed for the computer. The remaining requirement is a simple program to select and sum the interferences at the proper positions for a general class of models. Subsequently, it is only necessary to specify a few general parameters and the interference factors are obtained promptly from the computer.

In the present paper, programs are developed for calculating the interference factors for a wide variety of configurations of V/STOL aircraft as well as conventional airplanes. These include swept wings, jet-lift systems, rotors, and lifting propellers. Since the emphasis is on V/STOL testing, the basic theory and the notation used are those of reference 2; however, with suitable change in notation, the same programs can be used with any other desired theory having a similar degree of completeness. Sample results are presented for a number of configurations in order to examine the relative magnitudes of effects caused by changes in certain parameters.

SYMBOLS

The selection of a single set of symbols and definitions for the wide variety of aerodynamic systems treated herein does not allow complete conformity with existing practice in all cases. The following list sets forth the terminology used herein. Positive directions are self-consistent; that is, all forces, directions, and velocities are positive when directed in the positive sense of the chosen axes (fig. 1). Similarly, all moments and angles are chosen as positive in the direction of the right-hand rule with the chosen axes. Certain unusual features result (i.e., a negative induced velocity w_0 results from a positive lift L). The reader should carefully consider the following definitions and make appropriate conversions for his own application.

A_m momentum area of lifting system

A_T cross-sectional area of test section

B	semiwidth of test section
b	distance from right-hand side of test section (viewed from behind) to origin of wake or model
D	drag
H	semiheight of test section
h	when unsubscripted, height of model or wake origin above floor of test section; when subscripted, height of element above origin at $\alpha = 0^{o}$
L	lift
L_N	relative lift factor of Nth element
l	distance of element behind origin at $\alpha = 0^{o}$
M,N	integers
R	radius of rotor
R_a,R_b	radii of equal load areas on rotor disk
s	semispan of wing
s_R	semispacing of laterally disposed rotors
u_0	mean, or momentum theory, value of model induced velocity along X-axis, positive rearward
w_0	mean, or momentum theory, value of model induced velocity along Z-axis, positive upward
X,Y,Z	Cartesian axes centered in model or at wake origin, parallel to tunnel axes, X positive rearward, Y positive to right when viewed from behind, Z positive upward

x,y,z	distances from origin along X, Y, and Z axes, positive when directed in positive direction of axes
x_R	distance behind center of rotation on longitudinal axis of rotor tip-path plane
α	angle of attack
β	sideslip angle, angle between longitudinal tunnel axis and longitudinal axis of model, positive to left side when viewed from above
γ	width-height ratio of tunnel, B/H
Δw	total vertical interference velocity
Δw_D	vertical interference velocity due to drag
Δw_L	vertical interference velocity due to lift
Δz	vertical distance through which model moves as a result of a change in angle of attack
δ	interference factor (general)
$\delta_{w,D}$	interference factor for vertical interference velocity due to drag, defined implicitly by $\Delta w_D = \delta_{w,D} \frac{A_m}{A_T} u_0$
$\delta_{w,L}$	interference factor for vertical interference velocity due to lift, defined implicitly by $\Delta w_L = \delta_{w,L} \frac{A_m}{A_T} w_0$
ζ	ratio of test-section semiheight to height of origin above floor, H/h
η	ratio of b to test-section semiwidth, b/B
θ	variable of integration
Λ	wing sweep angle, angle between lateral axis of model and lifting line, positive rearward

ρ	variable of integration
σ	span-width or diameter-width ratio, s/B or R/B
χ	effective wake skew angle, angle between center of rolled-up wake and negative Z-axis, positive rearward
ψ	azimuth angle in rotor measured from downstream position, positive when counterclockwise as viewed from above

Subscripts (unless otherwise defined above):

B	body
FR	front rotor
M	for Mth control point
max	maximum value
N	for Nth wake origin
N,M	to Mth control point from Nth wake origin
N,0	Nth wake origin at $\alpha = 0$
P	pivot point
R	rotor
RR	rear rotor
t	tail
w	wing

THEORY

General Procedure

The general procedure used in this paper is to distribute a number of elemental wakes (each of which is equivalent to the complete wake system of a vanishingly small model) in the tunnel in such a manner that the wake system of a more complex finite-size model is represented to a reasonable degree of approximation. A convenient reference origin is chosen, and its position in the wind tunnel is designated by $\eta = b/B$ and $\zeta = H/h$. The coordinates of the origin of each individual elemental wake, measured from the reference origin in the directions of the wind-tunnel X, Y, and Z axes, are $\left(\frac{x}{H}\right)_N$, $\left(\frac{y}{H}\right)_N$, and $\left(\frac{z}{H}\right)_N$. The values of η_N and ζ_N, the wind-tunnel positions of the origin of the Nth elemental wake, become

$$\left.\begin{aligned} \eta_N &= \frac{b - H\left(\frac{y}{H}\right)_N}{B} = \eta - \frac{1}{\gamma}\left(\frac{y}{H}\right)_N \\ \zeta_N &= \frac{H}{h + H\left(\frac{z}{H}\right)_N} = \frac{\zeta}{1 + \zeta\left(\frac{z}{H}\right)_N} \end{aligned}\right\} \tag{1}$$

At this stage, it is necessary to choose a number of control points at which the total interference of the complex model is to be evaluated. (Under certain circumstances, it will be convenient to choose points that coincide with the wake origins.) The coordinates of the Mth control points, measured in the same manner and from the same reference origin, are $\left(\frac{x}{H}\right)_M$, $\left(\frac{y}{H}\right)_M$, and $\left(\frac{z}{H}\right)_M$. Consequently, the coordinates of the Mth control point measured from the Nth elemental wake origin become

$$\left.\begin{aligned} \left(\frac{x}{H}\right)_{N,M} &= \left(\frac{x}{H}\right)_M - \left(\frac{x}{H}\right)_N \\ \left(\frac{y}{H}\right)_{N,M} &= \left(\frac{y}{H}\right)_M - \left(\frac{y}{H}\right)_N \\ \left(\frac{z}{H}\right)_{N,M} &= \left(\frac{z}{H}\right)_M - \left(\frac{z}{H}\right)_N \end{aligned}\right\} \tag{2}$$

The five values given by equations (1) and (2) are sufficient to determine the interference contributed at the Mth point by the presence of the Nth elemental wake. The total

interference at the Mth point is the sum of all the interferences contributed by the presence of all N elemental wakes. If the Nth wake represents a portion of the total aerodynamic force given by

$$\frac{L_N}{\sum_N L_N}$$

the total interference factor at the Mth point may be written as

$$\delta = \frac{1}{\sum_N L_N} \sum_N L_N \times \delta \quad \text{at} \begin{cases} \zeta_N = \zeta \Big/ \left[1 + \zeta \left(\frac{z}{H}\right)_N\right] \\ \eta_N = \eta - \frac{1}{\gamma}\left(\frac{y}{H}\right)_N \\ \left(\frac{x}{H}\right)_{N,M} = \left(\frac{x}{H}\right)_M - \left(\frac{x}{H}\right)_N \\ \left(\frac{y}{H}\right)_{N,M} = \left(\frac{y}{H}\right)_M - \left(\frac{y}{H}\right)_N \\ \left(\frac{z}{H}\right)_{N,M} = \left(\frac{z}{H}\right)_M - \left(\frac{z}{H}\right)_N \end{cases} \tag{3}$$

The average interference over the finite configuration is the average of the interference at all M control points; thus, the average interference factor may be written as

$$\delta = \frac{1}{M_{max} \sum_N L_N} \sum_M \sum_N L_N \times \delta \quad \text{at} \begin{cases} \zeta_N = \zeta \Big/ \left[1 + \zeta \left(\frac{z}{H}\right)_N\right] \\ \eta_N = \eta - \frac{1}{\gamma}\left(\frac{y}{H}\right)_N \\ \left(\frac{x}{H}\right)_{N,M} = \left(\frac{x}{H}\right)_M - \left(\frac{x}{H}\right)_N \\ \left(\frac{y}{H}\right)_{N,M} = \left(\frac{y}{H}\right)_M - \left(\frac{y}{H}\right)_N \\ \left(\frac{z}{H}\right)_{N,M} = \left(\frac{z}{H}\right)_M - \left(\frac{z}{H}\right)_N \end{cases} \tag{4}$$

The values of L_N may be chosen in such a manner as to represent any desired load distribution over the configuration. Alternatively, the values of L_N may be chosen as constant and the positions of the wake origins may be slightly redistributed to represent different load distributions. Both systems of representing different load distributions will be used in this paper. Note that if L_N is a constant it may be removed from under the summation sign, so that the initial factor on the right-hand side of equations (3) and (4) contains the term

$$\frac{L_N}{\sum L_N} = \frac{1}{N_{max}} \tag{5}$$

If the wall interference in the tunnel over some other member of the aircraft (such as a tail or an additional lifting element) caused by the presence of another member is required, it is only necessary to choose the control points M suitably disposed over that other member rather than over the original member which causes the wall interference.

The evaluation of equation (3) or (4) is extremely arduous if carried out manually since it may be necessary to evaluate several hundred interference factors for "vanishingly small" model cases in order to obtain the desired interference factor for the finite-span model. On the other hand, the use of modern automatic digital computing equipment reduces the evaluation of either equation (3) or (4) to a trivial expenditure of time and effort once a suitable computer program has been developed. In this regard, the largest part of the effort is involved in development of the basic "vanishingly small" model program. Once the initial program is in hand, relatively small modifications are needed to select the appropriate N elemental wake origins and M control points in order to proceed with the evaluation of equations (3) and (4) for a generalized class of model. Subsequently, the appropriate correction factors can be obtained by merely specifying a few input parameters describing the model being tested.

In the succeeding sections of this paper, equations (3) and (4) are evaluated for a variety of generalized configurations typical of those found in V/STOL aircraft. No one paper could possibly cover all V/STOL configurations; however, the examples provided herein should be adequate to provide guidance for configurations which are not treated explicitly.

In many cases, certain symmetries exist which may be used to reduce the computer time required to evaluate the interference factors. A number of these symmetries are noted in each case.

Swept Wings

Average interference.- For the present purposes, the wing, represented as a swept lifting line (fig. 2), is divided into 10 segments. An elemental wake is assumed to originate at the center of each segment. The origin, which corresponds to the assumed pivot point in pitch, is chosen to be at the apex of the lifting line. (Other pivot locations will be considered in later sections.) Note that the wing is represented strictly as a lifting line in the present report. No account is taken of induced camber or other finite-chord considerations. If the sweep angle is Λ and the ratio of wing span to the full test-section width is σ_w, then the coordinates of the origin of the Nth elemental wake are

$$\left.\begin{aligned}\left(\frac{x}{H}\right)_N &= \left|\frac{11 - 2N}{10}\right| \sigma_w \gamma \tan \Lambda \cos \alpha \\ \left(\frac{y}{H}\right)_N &= \frac{11 - 2N}{10} \sigma_w \gamma \\ \left(\frac{z}{H}\right)_N &= - \left|\frac{11 - 2N}{10}\right| \sigma_w \gamma \tan \Lambda \sin \alpha\end{aligned}\right\} \tag{6}$$

The factor corresponding to the average interference over the wing is obtained by substituting equations (6) into equation (4), with the M control points taken coincident with the N elemental wake origins, to yield

$$\delta = \frac{1}{10 \sum_{N=1}^{10} L_N} \sum_{M=1}^{10} \sum_{N=1}^{10} L_N \times \delta \quad \text{at} \left\{\begin{aligned}\zeta_N &= \frac{\zeta}{1 - \left|\frac{2N - 11}{10}\right| \sigma_w \gamma \zeta \tan \Lambda \sin \alpha} \\ \eta_N &= \eta + \frac{2N - 11}{10} \sigma_w \\ \left(\frac{x}{H}\right)_{N,M} &= \sigma_w \gamma \tan \Lambda \cos \alpha \left(\left|\frac{11 - 2M}{10}\right| - \left|\frac{11 - 2N}{10}\right|\right) \\ \left(\frac{y}{H}\right)_{N,M} &= \frac{1}{5} \sigma_w \gamma (N - M) \\ \left(\frac{z}{H}\right)_{N,M} &= \sigma_w \gamma \tan \Lambda \sin \alpha \left(\left|\frac{11 - 2N}{10}\right| - \left|\frac{11 - 2M}{10}\right|\right)\end{aligned}\right\} \tag{7}$$

Note that equation (7) requires the determination, summation, and averaging of 100 interference factors for the vanishingly small model case. If $\sigma_w = 0$, these factors will all be identical and expensive computer time will be wasted. Thus, for the case of

$\sigma_w = 0$, the computer program should be such that the calculation is made for only $N = M = 1$ and both the initial factor of 1/10 and the double summation are eliminated. Furthermore, if $\eta = 1$ (that is, if the model is centered laterally and the loads L_N are symmetrical), the interference flow will be completely symmetrical and the average interference values over each semispan will be identical. Thus, for the case of $\eta = 1$, computer time may be saved by summing on M from 1 to 5 only and changing the leading factor from $\dfrac{1}{10\sum_{N=1}^{10} L_N}$ to $\dfrac{1}{5\sum_{N=1}^{10} L_N}$. Some effort can be saved by building tables of L_N into the computer program for common loadings, say uniform and elliptical, so that the type of loading can be chosen by a single character on the input card.

Interference distribution.- The interference distribution over the wing may be obtained simply by substituting equations (6) into equation (4). Thus, for

$$\frac{y}{s} = \left(\frac{y}{H}\right)_M \frac{H}{B}\frac{2B}{2s} = \frac{11 - 2M}{10}\frac{\sigma_w\gamma}{\gamma\sigma_w} = \frac{11 - 2M}{10} \tag{8}$$

the interference factor is

$$\delta = \frac{1}{\sum_{N=1}^{10} L_N}\sum_{N=1}^{10} L_N \times \delta \quad \text{at} \quad \left\{\begin{array}{l} \zeta_N = \dfrac{\zeta}{1 - \left|\dfrac{2N - 11}{10}\right|\sigma_w\gamma\zeta\tan\Lambda\sin\alpha} \\ \eta_N = \eta + \dfrac{2N - 11}{10}\sigma_w \\ \left(\dfrac{x}{H}\right)_{N,M} = \sigma_w\gamma\tan\Lambda\cos\alpha\left(\left|\dfrac{11 - 2M}{10}\right| - \left|\dfrac{11 - 2N}{10}\right|\right) \\ \left(\dfrac{y}{H}\right)_{N,M} = \dfrac{1}{5}\sigma_w\gamma(N - M) \\ \left(\dfrac{z}{H}\right)_{N,M} = \sigma_w\gamma\tan\Lambda\sin\alpha\left(\left|\dfrac{11 - 2N}{10}\right| - \left|\dfrac{11 - 2M}{10}\right|\right) \end{array}\right\} \tag{9}$$

For $\sigma_w = 0$, the wing is vanishingly small and the interference is completely uniform in consequence of this small size. Thus, the calculation for the case $\sigma_w = 0$ should be made for only $N = M = 1$. Since the interference distribution will seldom be required unless the average interference has already been calculated, an alternative machine procedure is simply to reject any case with $\sigma_w = 0$. For $\eta = 1$ and

symmetrical L_N, the interference field is symmetrical, and the values of M (eq. (8)) for which equation (9) is evaluated should be limited to those corresponding to one half of the wing.

Interference at the tail.- The tail of an aircraft may have substantial sweep, dihedral, or anhedral. Since the tail span is generally substantially less than the wing span, these features are neglected herein in favor of the use of a mean tail positon which tends to average, to a degree, the effect of these features. In further consideration of the reduced span (as compared with the wing), only four control points are chosen (fig. 3) over which the interference of the wing is averaged. The forces produced by the tail are assumed to be small enough so that any interference due directly to the presence of the tail is negligible compared with the interference caused by the presence of the wing.

Under the foregoing assumptions, figure 3 shows that the coordinates of the Mth point on the tail, referred to the origin at the apex of the swept lifting line, are

$$\left.\begin{aligned} \left(\frac{x}{H}\right)_M &= \frac{l_t}{H}\cos\alpha + \frac{h_t}{H}\sin\alpha \\ \left(\frac{y}{H}\right)_M &= \frac{5 - 2M}{4}\sigma_t\gamma \\ \left(\frac{z}{H}\right)_M &= \frac{h_t}{H}\cos\alpha - \frac{l_t}{H}\sin\alpha \end{aligned}\right\} \tag{10}$$

Thus the interference factors at the tail are found by substituting equations (6) and (10) into equation (4), to yield

$$\delta = \frac{1}{4\sum_{N=1}^{10} L_N}\sum_{M=1}^{4}\sum_{N=1}^{10} L_N \times \delta \text{ at } \left\{\begin{aligned} \zeta_N &= \frac{\zeta}{1 - \left|\frac{2N - 11}{10}\right|\sigma_w\gamma\zeta\tan\Lambda\sin\alpha} \\ \eta_N &= \eta + \frac{2N - 11}{10}\sigma_w \\ \left(\frac{x}{H}\right)_{N,M} &= \frac{l_t}{H}\cos\alpha + \frac{h_t}{H}\sin\alpha - \sigma_w\gamma\tan\Lambda\cos\alpha\left|\frac{11 - 2N}{10}\right| \\ \left(\frac{y}{H}\right)_{N,M} &= \frac{5 - 2M}{4}\sigma_t\gamma - \frac{11 - 2N}{10}\sigma_w\gamma \\ \left(\frac{z}{H}\right)_{N,M} &= \frac{h_t}{H}\cos\alpha - \frac{l_t}{H}\sin\alpha + \sigma_w\gamma\tan\Lambda\sin\alpha\left|\frac{11 - 2N}{10}\right| \end{aligned}\right\} \tag{11}$$

Note that if σ_w and σ_t are both zero, it is sufficient to evaluate equation (11) for $M = N = 1$ only, eliminating both summations and the leading factor of 1/4. If only σ_t is zero, the summation with respect to N must be carried through; however, equation (11) need be evaluated for $M = 1$ only, eliminating the summation on M and the leading factor of 1/4. If only σ_w is zero, the summation with respect to M must be carried out; however, it is sufficient to set N equal to 1, eliminating the summation on N. If $\eta = 1$ and the loads L_N are symmetrical, the interference field is symmetrical, and the summation on M may be restricted to from 1 to 2 provided that the leading factor is altered from 1/4 to 1/2.

Jet-Lift Configurations

Average interference over a swept wing.- A winged jet-lift model will be affected by wall interference due to the presence of the wing within the wind-tunnel walls. The effect of the wing can be obtained from the equations given in the sections immediately preceding the present section. Furthermore, the presence of the lifting jets will cause additional interference at the wing. This and the succeeding sections are concerned solely with this additional interference.

Since in most cases the lift jets are supported independently of the balance system, the equations presented herein should be adequate to obtain all the interference components of interest. However, if the jets are on the balance, it is necessary to obtain the interference at the jets caused by both the wing and the jets themselves. Although these equations are not given explicitly herein, the general forms (eqs. (1) to (4)) and the cases which are treated should provide adequate guidance in setting up the required computer program.

It is assumed herein that all the jet exits are similarly oriented. This assumption is violated when both direct-lift and deflected cruise jets are present on the same model. In such cases, the jets should be divided into groups having the same nozzle inclination. The total interference will then be the sum of the interference velocities caused by each group of jets.

The representation of the wing and its origin is identical to that in the preceding sections (fig. 2). An arbitrary number of jets are assumed and the position of the Nth jet exit with respect to the origin at $\alpha = 0$ is given as $\left(\frac{x}{H}, \frac{y}{H}, \frac{z}{H}\right)_{N,0}$. The relative strength of each jet is L_N. For a given angle of attack, the coordinates of the Nth jet exit become

$$\left.\begin{aligned}\left(\frac{x}{H}\right)_N &= \left(\frac{x}{H}\right)_{N,0}\cos\alpha + \left(\frac{z}{H}\right)_{N,0}\sin\alpha \\ \left(\frac{y}{H}\right)_N &= \left(\frac{y}{H}\right)_{N,0} \\ \left(\frac{z}{H}\right)_N &= \left(\frac{z}{H}\right)_{N,0}\cos\alpha - \left(\frac{x}{H}\right)_{N,0}\sin\alpha\end{aligned}\right\} \tag{12}$$

The average interference at the wing is found by substituting equations (12) and (6) (for M) into equation (4), to yield

$$\delta = \frac{1}{10\sum_N L_N}\sum_{M=1}^{10}\sum_N L_N \times \delta \text{ at } \left\{\begin{aligned}\zeta_N &= \frac{\zeta}{1+\zeta\left[\left(\frac{z}{H}\right)_{N,0}\cos\alpha - \left(\frac{x}{H}\right)_{N,0}\sin\alpha\right]} \\ \eta_N &= \eta - \frac{1}{\gamma}\left(\frac{y}{H}\right)_{N,0} \\ \left(\frac{x}{H}\right)_{N,M} &= \left|\frac{11-2M}{10}\right|\sigma_w\gamma\tan\Lambda\cos\alpha - \left(\frac{x}{H}\right)_{N,0}\cos\alpha - \left(\frac{z}{H}\right)_{N,0}\sin\alpha \\ \left(\frac{y}{H}\right)_{N,M} &= \frac{11-2M}{10}\sigma_w\gamma - \left(\frac{y}{H}\right)_{N,0} \\ \left(\frac{z}{H}\right)_{N,M} &= -\left|\frac{11-2M}{10}\right|\sigma_w\gamma\tan\Lambda\sin\alpha - \left(\frac{z}{H}\right)_{N,0}\cos\alpha + \left(\frac{x}{H}\right)_{N,0}\sin\alpha\end{aligned}\right\} \tag{13}$$

Note that if $\sigma_w = 0$, it is sufficient to evaluate equation (13) at $M = 1$ only, thus eliminating both the summation with respect to M and the leading factor of 1/10. Jet configurations will generally be symmetrical; that is, $\left(\frac{y}{H}\right)_{N,0} = 0$ for some jets, and for each other jet of location $\left(\frac{x}{H}, \frac{y}{H}, \frac{z}{H}\right)_{N,0}$ and strength L_N, there is another with location $\left(\frac{x}{H}, -\frac{y}{H}, \frac{z}{H}\right)_{N,0}$, also of strength L_N. For such cases, when $\eta = 1.0$ the interference flow is symmetrical and it is adequate to sum over $1 < M < 5$ only, provided that the leading factor is changed from 1/10 to 1/5.

It should be noted that equation (13) yields only the interference due to the presence of the jets. In addition, there will be an interference on the wing due to its own presence in the tunnel. This term is given by equation (7).

Interference distribution over wing.- The interference distribution at the wing may be obtained by substituting equations (12) and (6) (for M) into equation (3). Thus, for

$$\frac{y}{s} = \frac{11-2M}{10} \tag{14}$$

the interference factor is

$$\delta = \frac{1}{\sum_N L_N} \sum_N L_N \times \delta \quad \text{at} \begin{cases} \zeta_N = \dfrac{\zeta}{1 + \zeta\left[\left(\frac{z}{H}\right)_{N,0} \cos\alpha - \left(\frac{x}{H}\right)_{N,0} \sin\alpha\right]} \\ \eta_N = \eta - \dfrac{1}{\gamma}\left(\dfrac{y}{H}\right)_{N,0} \\ \left(\dfrac{x}{H}\right)_{N,M} = \left|\dfrac{11 - 2M}{10}\right| \sigma_w \gamma \tan\Lambda \cos\alpha - \left(\dfrac{x}{H}\right)_{N,0} \cos\alpha - \left(\dfrac{z}{H}\right)_{N,0} \sin\alpha \\ \left(\dfrac{y}{H}\right)_{N,M} = \dfrac{11 - 2M}{10} \sigma_w \gamma - \left(\dfrac{y}{H}\right)_{N,0} \\ \left(\dfrac{z}{H}\right)_{N,M} = -\left|\dfrac{11 - 2M}{10}\right| \sigma_w \gamma \tan\Lambda \sin\alpha - \left(\dfrac{z}{H}\right)_{N,0} \cos\alpha + \left(\dfrac{x}{H}\right)_{N,0} \sin\alpha \end{cases} \tag{15}$$

For $\sigma_w = 0$ the distribution is uniform, and the values of the interference factor will be identical to that obtained from equation (13), which doubtless would be evaluated first. Thus, it is acceptable to merely reject $\sigma_w = 0$ cases from a program for the interference distribution. Note also that for symmetrical configurations (as previously defined) with $\eta = 1.0$, the interference field will be symmetrical; therefore, in such cases it is sufficient to evaluate equation (15) only for the values of M corresponding to one wing panel.

Average interference at the tail.- Under the same assumptions as were made for the case of interference at the tail behind a swept wing, the corresponding interference in the case of jet-lift configurations may be obtained by combining equations (4), (10), and (12) to yield

$$\delta = \frac{1}{4\sum_N L_N} \sum_{M=1}^{4} \sum_N L_N \times \delta \quad \text{at} \begin{cases} \zeta_N = \dfrac{\zeta}{1 + \zeta\left[\left(\frac{z}{H}\right)_{N,0} \cos\alpha - \left(\frac{x}{H}\right)_{N,0} \sin\alpha\right]} \\ \eta_N = \eta - \dfrac{1}{\gamma}\left(\dfrac{y}{H}\right)_{N,0} \\ \left(\dfrac{x}{H}\right)_N = \left[\dfrac{l_t}{H} - \left(\dfrac{x}{H}\right)_{N,0}\right] \cos\alpha + \left[\dfrac{h_t}{H} - \left(\dfrac{z}{H}\right)_{N,0}\right] \sin\alpha \\ \left(\dfrac{y}{H}\right)_N = \dfrac{5 - 2M}{4} \sigma_t \gamma - \left(\dfrac{y}{H}\right)_{N,0} \\ \left(\dfrac{z}{H}\right)_N = \left[\dfrac{h_t}{H} - \left(\dfrac{z}{H}\right)_{N,0}\right] \cos\alpha - \left[\dfrac{l_t}{H} - \left(\dfrac{x}{H}\right)_{N,0}\right] \sin\alpha \end{cases} \tag{16}$$

If $\sigma_t = 0$, it is sufficient to evaluate equation (16) for $M = 1$ only, thus eliminating both the summation with respect to M and the leading factor of 1/4. If the model is symmetrical and $\eta = 1.0$, it is adequate to evaluate equation (16) for $1 < M < 2$ only, provided that the leading factor is changed from 1/4 to 1/2.

Rotor or Propeller

Average interference.- Because of the similarity of rotors and lifting propellers, it is adequate to derive corrections for either one. In the present paper, the derivation is carried out for a rotor. The interference factors for the propeller are simply obtained from the present results by altering the propeller definition of angle of attack to correspond to the angle of attack as defined for the rotor.

Consider an axisymmetrically loaded rotor, as in figure 4, with origin at the rotor center. The total load is assumed to be divided into 20 equal segments, each with an elemental wake originating at (R_N, ψ_N), the centroid of load of each segment. (The disposition of the elements will be discussed in a later section; however, the use of symmetry to reduce the length of the calculations for the distributions will be facilitated by choosing symmetrically located points and by avoiding the longitudinal axis of the rotor.)

The location of each wake origin from the center of the rotor is given by

$$\left.\begin{aligned} \left(\frac{x}{H}\right)_N &= \frac{R_N}{R}\,\sigma_R\gamma\,\cos\psi_N\cos\alpha_R \\ \left(\frac{y}{H}\right)_N &= \frac{R_N}{R}\,\sigma_R\gamma\,\sin\psi_N \\ \left(\frac{z}{H}\right)_N &= -\frac{R_N}{R}\,\sigma_R\gamma\,\cos\psi_N\sin\alpha_R \end{aligned}\right\} \tag{17}$$

The average interference at the rotor is obtained by choosing control points M coincident with the wake origins N, and then substituting equations (5) and (17) into equation (4), to yield

$$\delta = \frac{1}{400} \sum_{M=1}^{20} \sum_{N=1}^{20} \delta \quad \text{at} \quad \left\{ \begin{array}{l} \zeta_N = \dfrac{\zeta}{1 - \dfrac{R_N}{R} \sigma_R \gamma \zeta \cos \psi_N \sin \alpha_R} \\ \\ \eta_N = \eta - \dfrac{R_N}{R} \sigma_R \sin \psi_N \\ \\ \left(\dfrac{x}{H}\right)_{N,M} = \sigma_R \gamma \cos \alpha_R \left(\dfrac{R_M}{R} \cos \psi_M - \dfrac{R_N}{R} \cos \psi_N\right) \\ \\ \left(\dfrac{y}{H}\right)_{N,M} = \sigma_R \gamma \left(\dfrac{R_M}{R} \sin \psi_M - \dfrac{R_N}{R} \sin \psi_N\right) \\ \\ \left(\dfrac{z}{H}\right)_{N,M} = -\sigma_R \gamma \sin \alpha_R \left(\dfrac{R_M}{R} \cos \psi_M - \dfrac{R_N}{R} \cos \psi_N\right) \end{array} \right\} \tag{18}$$

Again, when $\sigma_R = 0$ it is sufficient to evaluate equation (18) only once, for $M = N = 1$, thus eliminating both summations as well as the leading factor of $\frac{1}{400}$. When $\eta = 1.0$ the interference field is symmetrical; thus, if symmetrical locations of the N elemental wakes are used and no locations on the longitudinal axis have been chosen, substantial computer time may be saved by evaluating equation (18) for only those combinations of R_N and ψ_N for which $0 < \psi_N < \pi$ and, consequently, altering the leading factor of $\frac{1}{400}$ to $\frac{1}{200}$.

Lateral distribution of interference.- To obtain the lateral distributions of interference, the control points are chosen on that axis as

$$\left. \begin{array}{l} \left(\dfrac{x}{H}\right)_M = 0 \\ \\ \left(\dfrac{y}{H}\right)_M = \sigma_R \gamma (1.2 - 0.2M) \\ \\ \left(\dfrac{z}{H}\right)_M = 0 \end{array} \right\} \tag{19}$$

Substitution of equations (5), (17), and (19) into equation (3) yields

$$\delta = \frac{1}{20}\sum_{N=1}^{20} \delta \quad \text{at} \left\{ \begin{array}{l} \zeta_N = \dfrac{\zeta}{1 - \dfrac{R_N}{R}\sigma_R\gamma\zeta\cos\psi_N \sin\alpha_R} \\ \\ \eta_N = \eta - \dfrac{R_N}{R}\sigma_R \sin\psi_N \\ \\ \left(\dfrac{x}{H}\right)_{N,M} = -\sigma_R\gamma\dfrac{R_N}{R}\cos\alpha_R\cos\psi_N \\ \\ \left(\dfrac{y}{H}\right)_{N,M} = \sigma_R\gamma\left[(1.2 - 0.2M) - \dfrac{R_N}{R}\sin\psi_N\right] \\ \\ \left(\dfrac{z}{H}\right)_{N,M} = \sigma_R\gamma\dfrac{R_N}{R}\sin\alpha_R\cos\psi_N \end{array} \right\} \tag{20}$$

where, for a given M,

$$\frac{y}{R} = \left(\frac{y}{H}\right)_M \frac{H}{B}\frac{2B}{2R} = (1.2 - 0.2M) \tag{21}$$

If $\sigma_R = 0$, the calculation is unnecessary since the interference is uniform and equal to the average interference. The interference field is symmetrical for $\eta = 1.0$; therefore, in that case, it is necessary to evaluate equation (20) for the values of M on only one side of the rotor.

Longitudinal distribution of interference.- In contrast to the wings discussed earlier, a rotor has a large longitudinal extent in the tunnel. Thus, it will often be necessary to evaluate the distribution of interference along the longitudinal as well as the lateral axis. Control points on the longitudinal axis are chosen so that their coordinates are

$$\left. \begin{array}{l} \left(\dfrac{x}{H}\right)_M = \sigma_R\gamma(0.2M - 1.2)\cos\alpha_R \\ \\ \left(\dfrac{y}{H}\right)_M = 0 \\ \\ \left(\dfrac{z}{H}\right)_M = -\sigma_R\gamma(0.2M - 1.2)\sin\alpha_R \end{array} \right\} \tag{22}$$

Substitution of equations (5), (17), and (22) into equation (3) yields

$$\delta = \frac{1}{20}\sum_{N=1}^{20} \delta \quad \text{at} \left\{ \begin{array}{l} \zeta_N = \dfrac{\zeta}{1 - \dfrac{R_N}{R}\sigma_R \gamma \zeta \cos \psi_N \sin \alpha_R} \\ \eta_N = \eta - \dfrac{R_N}{R}\sigma_R \sin \psi_N \\ \left(\dfrac{x}{H}\right)_{N,M} = \sigma_R \gamma \cos \alpha_R \left[(0.2M - 1.2) - \dfrac{R_N}{R}\cos \psi_N\right] \\ \left(\dfrac{y}{H}\right)_{N,M} = -\sigma_R \gamma \dfrac{R_N}{R} \sin \psi_N \\ \left(\dfrac{z}{H}\right)_{N,M} = -\sigma_R \gamma \sin \alpha_R \left[(0.2M - 1.2) - \dfrac{R_N}{R}\cos \psi_N\right] \end{array} \right\} \tag{23}$$

where, for a given M,

$$\frac{x_R}{R} = (0.2M - 1.2) \tag{24}$$

Observe that x_R is measured in the plane of the rotor and not along the X-axis of the tunnel.

For $\sigma_R = 0$ the interference is, once again, uniform and equal to the average interference; thus the evaluation of equation (23) is unnecessary. For $\eta = 1.0$ the interference field is symmetrical and, provided that symmetrical elemental wake origins are chosen (and no wake origin is chosen on the longitudinal axis), it is sufficient to evaluate equation (23) for only those combinations of R_N and ψ_N for which $0 < \psi_N < \pi$, provided that the leading factor is changed from $\frac{1}{20}$ to $\frac{1}{10}$.

Average interference over tail behind rotor.- Because of flapping and built-in shaft tilt, the angle of attack of the fuselage which carries the tail may differ substantially from the angle of attack of the rotor tip-path plane. Thus, the present derivation allows for the use of two entirely different angles (fig. 5). Otherwise, the assumptions regarding the tail are identical to those used previously. At some fuselage angle of attack α_B, the coordinates of the control points on the tail are

$$\left.\begin{aligned}\left(\frac{x}{H}\right)_M &= \sigma_R\gamma\left(\frac{l_t}{R}\cos\alpha_B + \frac{h_t}{R}\sin\alpha_B\right)\\ \left(\frac{y}{H}\right)_M &= \sigma_R\gamma\,\frac{5-2M}{4}\,\frac{\sigma_t}{\sigma_R}\\ \left(\frac{z}{H}\right)_M &= \sigma_R\gamma\left(\frac{h_t}{R}\cos\alpha_B - \frac{l_t}{R}\sin\alpha_B\right)\end{aligned}\right\} \tag{25}$$

Substitution of equations (5), (17), and (25) into equation (4) yields

$$\delta = \frac{1}{80}\sum_{M=1}^{4}\sum_{N=1}^{20}\delta \quad \text{at}\left\{\begin{aligned}\zeta_N &= \frac{\zeta}{1 - \frac{R_N}{R}\sigma_R\gamma\zeta\cos\psi_N\sin\alpha_R}\\ \eta_N &= \eta - \frac{R_N}{R}\sigma_R\sin\psi_N\\ \left(\frac{x}{H}\right)_{N,M} &= \sigma_R\gamma\left(\frac{l_t}{R}\cos\alpha_B + \frac{h_t}{R}\sin\alpha_B - \frac{R_N}{R}\cos\alpha_R\cos\psi_N\right)\\ \left(\frac{y}{H}\right)_{N,M} &= -\sigma_R\gamma\left(\frac{2M-5}{4}\,\frac{\sigma_t}{\sigma_R} + \frac{R_N}{R}\sin\psi_N\right)\\ \left(\frac{z}{H}\right)_{N,M} &= \sigma_R\gamma\left(\frac{h_t}{R}\cos\alpha_B - \frac{l_t}{R}\sin\alpha_B + \frac{R_N}{R}\sin\alpha_R\cos\psi_N\right)\end{aligned}\right\} \tag{26}$$

If $\sigma_t = 0$ it is sufficient to evaluate equation (26) for $M = 1$ only, provided that the leading constant of 1/80 is altered to 1/20. If $\eta = 1.0$ the interference field is symmetrical, and it will suffice to evaluate equation (26) for $M = 1$ and 2 only, provided that the leading constant of 1/80 is changed to 1/40. Since the inputs to equation (26) are in terms of the radius, which is zero when $\sigma_R = 0$, such cases represent input errors and should be rejected.

Choice of (R_N,ψ_N) and (R_M,ψ_M).- The foregoing expressions have been developed by using 20 elemental wakes, since trial calculations indicated that this number of wakes yielded results essentially identical to those of the more elaborate (but also more restrictive) wake model of reference 3. As pointed out previously, it is advantageous to avoid the longitudinal axis and to choose symmetrical locations for the origins of the elemental wakes. The locations chosen for the program from which the sample calculations (to be discussed subsequently) were made are illustrated in figure 6. The angular positions of

the 20 elements are unaltered by the chosen load distribution; however, since no normalizing factor $\left(\text{such as } L_N\right)$ was employed, it is necessary to choose the radii appropriately in order to represent suitable axisymmetric disk-load distributions (ref. 4). The radii appropriate to two different disk-load distributions are derived herein. Appropriate tables of $\left(R_N, \psi_N\right)$ can be built into the computer program, and the table appropriate to a given load distribution can be selected by the use of a single input character.

Uniform disk-load distribution.- When the disk-load distribution is uniform, each of the elemental areas of figure 6 must be equal; thus

$$\frac{\pi}{8}\left[1 - \left(\frac{R_b}{R}\right)^2\right] = \frac{\pi}{8}\left[\left(\frac{R_b}{R}\right)^2 - \left(\frac{R_a}{R}\right)^2\right] = \frac{\pi}{4}\left(\frac{R_a}{R}\right)^2 \tag{27}$$

The solutions to equation (27) are

$$\left.\begin{aligned} \frac{R_a}{R} &= \sqrt{\frac{1}{5}} \approx 0.447 \\ \frac{R_b}{R} &= \sqrt{\frac{3}{5}} \approx 0.775 \end{aligned}\right\} \tag{28}$$

The centroid of each annular sector is found as

$$R_N = \frac{\int_{-\theta}^{\theta}\int_{R_i}^{R_o} \rho^2 d\rho\, d\theta}{\int_{-\theta}^{\theta}\int_{R_i}^{R_o} \rho\, d\rho\, d\theta} = \frac{2}{3}\frac{{R_o}^3 - {R_i}^3}{{R_o}^2 - {R_i}^2} \tag{29}$$

where R_i and R_o are the inner and outer radii of the sector. Substituting equations (28) into equation (29) yields

$$\left.\begin{aligned} \frac{R_N}{R} &= \frac{2}{3}\sqrt{\frac{1}{5}} \approx 0.298 && (1 \leqq N \leqq 4) \\ \frac{R_N}{R} &= \frac{3\sqrt{3} - 1}{3\sqrt{5}} \approx 0.625 && (5 \leqq N \leqq 12) \\ \frac{R_N}{R} &= \frac{5}{3}\sqrt{\frac{3}{5}} \approx 0.894 && (13 \leqq N \leqq 20) \end{aligned}\right\} \tag{30}$$

Triangular disk-load distribution.- An untapered untwisted rotor generally will have an average radial load distribution which approaches the triangular load distribution; that is, it increases essentially linearly with radius from zero at the hub. Analogous treatment of this case yields

$$\left.\begin{aligned} \frac{R_a}{R} &= \sqrt[3]{\frac{1}{5}} \approx 0.585 \\ \frac{R_b}{R} &= \sqrt[3]{\frac{3}{5}} \approx 0.845 \end{aligned}\right\} \tag{31}$$

and

$$\left.\begin{aligned} \frac{R_N}{R} &= \frac{3}{4}\sqrt[3]{\frac{1}{5}} \approx 0.439 && (1 \leqq N \leqq 4) \\ \frac{R_N}{R} &= \frac{3\left(3\sqrt[3]{3} - 1\right)}{8\sqrt[3]{5}} \approx 0.730 && (5 \leqq N \leqq 12) \\ \frac{R_N}{R} &= \frac{15}{8}\left(1 - \frac{3}{5}\sqrt[3]{\frac{3}{5}}\right) \approx 0.925 && (13 \leqq N \leqq 20) \end{aligned}\right\} \tag{32}$$

Tandem Rotors

Initial considerations.- The problem of wall interference encountered in tests of tandem rotors is generally similar to the problem of interference at a tail. The tandem-rotor interference is made significantly more complicated by several factors. First, the effect of the rear rotor on the overall interference level in the tunnel cannot be neglected (as is the interference caused by the presence of a tail) for the simple reason that the forces generated by the rear rotor are much larger than those generated by a tail. Secondly, the relative positions of the two rotors are affected by the angles of attack of the front rotor, rear rotor, and fuselage, which, in general, are all different and may vary with operating condition. Finally, the maximum cruise efficiency of a tandem-rotor helicopter generally occurs at substantial sideslip angles (on the order of 30°); therefore, it is necessary to test and to evaluate the interference at large sideslip angles.

Consider a tandem rotor system located in the wind tunnel as in figure 7. The origin is chosen at the center of the front rotor. The angle of attack is defined as the angle measured in the longitudinal plane of symmetry of the tandem rotor system. The sideslip angle β is defined as the angle measured in the X-Y plane. Each rotor is represented by 20 elemental wakes, as before, but with ψ measured from the longitudinal

plane of symmetry of the tandem rotor system. In accordance with usual practice, the radii of the two rotors are assumed to be equal. Under these definitions, the coordinates of the origin of the Nth elemental wake of the front rotor are

$$\left.\begin{aligned}\left(\frac{x}{H}\right)_N &= \frac{R_N}{R}\sigma_R\gamma\left(\cos\psi_N\cos\alpha_{FR}\cos\beta - \sin\psi_N\sin\beta\right)\\ \left(\frac{y}{H}\right)_N &= \frac{R_N}{R}\sigma_R\gamma\left(\sin\psi_N\cos\beta + \cos\psi_N\cos\alpha_{FR}\sin\beta\right)\\ \left(\frac{z}{H}\right)_N &= -\frac{R_N}{R}\sigma_R\gamma\cos\psi_N\sin\alpha_{FR}\end{aligned}\right\} \tag{33}$$

The corresponding coordinates of the Nth wake in the rear rotor are

$$\left.\begin{aligned}\left(\frac{x}{H}\right)_N &= \frac{R_N}{R}\sigma_R\gamma\left(\cos\psi_N\cos\alpha_{RR}\cos\beta - \sin\psi_N\sin\beta\right)\\ &\quad + \sigma_R\gamma\cos\beta\left(\frac{l_{RR}}{R}\cos\alpha_B + \frac{h_{RR}}{R}\sin\alpha_B\right)\\ \left(\frac{y}{H}\right)_N &= \frac{R_N}{R}\sigma_R\gamma\left(\sin\psi_N\cos\beta + \cos\psi_N\cos\alpha_{RR}\sin\beta\right)\\ &\quad + \sigma_R\gamma\sin\beta\left(\frac{l_{RR}}{R}\cos\alpha_B + \frac{h_{RR}}{R}\sin\alpha_B\right)\\ \left(\frac{z}{H}\right)_N &= -\sigma_R\gamma\left(\frac{R_N}{R}\cos\psi_N\sin\alpha_{RR} + \frac{l_{RR}}{R}\sin\alpha_B - \frac{h_{RR}}{R}\cos\alpha_B\right)\end{aligned}\right\} \tag{34}$$

Average interference over front rotor due to presence of front rotor.- The first interference component to be obtained is the average interference over the front rotor caused by its own presence in the tunnel. The control points are chosen to be identical to the wake origins. Then equations (5) and (33) are substituted into equation (4) to yield

$$\delta = \frac{1}{400}\sum_{M=1}^{20}\sum_{N=1}^{20}\delta \quad \text{at} \left\{ \begin{array}{l} \zeta_N = \dfrac{\zeta_{FR}}{1 - \dfrac{R_N}{R}\sigma_R\gamma\zeta_{FR}\cos\psi_N \sin\alpha_{FR}} \\ \\ \eta_N = \eta_{FR} - \dfrac{R_N}{R}\sigma_R\left(\sin\psi_N\cos\beta + \cos\psi_N\cos\alpha_{FR}\sin\beta\right) \\ \\ \left(\dfrac{x}{H}\right)_{N,M} = \sigma_R\gamma\left[\dfrac{R_M}{R}\left(\cos\psi_M\cos\alpha_{FR}\cos\beta - \sin\psi_M\sin\beta\right) - \dfrac{R_N}{R}\left(\cos\psi_N\cos\alpha_{FR}\cos\beta - \sin\psi_N\sin\beta\right)\right] \\ \\ \left(\dfrac{y}{H}\right)_{N,M} = \sigma_R\gamma\left[\dfrac{R_M}{R}\left(\sin\psi_M\cos\beta + \cos\psi_M\cos\alpha_{FR}\sin\beta\right) - \dfrac{R_N}{R}\left(\sin\psi_N\cos\beta + \cos\psi_N\cos\alpha_{FR}\sin\beta\right)\right] \\ \\ \left(\dfrac{z}{H}\right)_{N,M} = -\sigma_R\gamma\sin\alpha_{FR}\left(\dfrac{R_M}{R}\cos\psi_M - \dfrac{R_N}{R}\cos\psi_N\right) \end{array} \right\} \tag{35}$$

Observe that for $\beta = 0$, equation (35) is identical to equation (18), which was previously derived for the single rotor. At other yaw angles, equation (35) differs from equation (18) solely because the angle of attack is now defined in the plane of symmetry of the body rather than in the X-Z plane of the tunnel as in equation (18).

Average interference over front rotor due to presence of rear rotor.- Equation (35) does not represent the total interference at the front rotor. There is an additional interference because of the presence of the rear rotor. The factor for this interference is obtained by using the wake origins in the rear rotor and the control points in the front rotor. Thus, equations (5), (33) (for M), and (34) (for N) are combined with equation (4) to yield

$$\delta = \frac{1}{400}\sum_{M=1}^{20}\sum_{N=1}^{20}\delta \quad \text{at} \left\{ \begin{array}{l} \zeta_N = \dfrac{\zeta_{FR}}{1 - \sigma_R\gamma\zeta_{FR}\left(\dfrac{R_N}{R}\cos\psi_N \sin\alpha_{RR} + \dfrac{l_{RR}}{R}\sin\alpha_B - \dfrac{h_{RR}}{R}\cos\alpha_B\right)} \\ \\ \eta_N = \eta_{FR} - \dfrac{R_N}{R}\sigma_R\left(\sin\psi_N\cos\beta + \cos\psi_N\cos\alpha_{RR}\sin\beta\right) - \sigma_R\sin\beta\left(\dfrac{l_{RR}}{R}\cos\alpha_B + \dfrac{h_{RR}}{R}\sin\alpha_B\right) \\ \\ \left(\dfrac{x}{H}\right)_{N,M} = \sigma_R\gamma\left[\dfrac{R_M}{R}\left(\cos\psi_M\cos\alpha_{FR}\cos\beta - \sin\psi_M\sin\beta\right) - \dfrac{R_N}{R}\left(\cos\psi_N\cos\alpha_{RR}\cos\beta - \sin\psi_N\sin\beta\right)\right. \\ \qquad\qquad \left. - \cos\beta\left(\dfrac{l_{RR}}{R}\cos\alpha_B + \dfrac{h_{RR}}{R}\sin\alpha_B\right)\right] \\ \\ \left(\dfrac{y}{H}\right)_{N,M} = \sigma_R\gamma\left[\dfrac{R_M}{R}\left(\sin\psi_M\cos\beta + \cos\psi_M\cos\alpha_{FR}\sin\beta\right) - \dfrac{R_N}{R}\left(\sin\psi_N\cos\beta + \cos\psi_N\cos\alpha_{RR}\sin\beta\right)\right. \\ \qquad\qquad \left. - \sin\beta\left(\dfrac{l_{RR}}{R}\cos\alpha_B + \dfrac{h_{RR}}{R}\sin\alpha_B\right)\right] \\ \\ \left(\dfrac{z}{H}\right)_{N,M} = -\sigma_R\gamma\left(\dfrac{R_M}{R}\cos\psi_M \sin\alpha_{FR} - \dfrac{R_N}{R}\cos\psi_N \sin\alpha_{RR} - \dfrac{l_{RR}}{R}\sin\alpha_B + \dfrac{h_{RR}}{R}\cos\alpha_B\right) \end{array} \right\} \tag{36}$$

Average interference over rear rotor due to presence of rear rotor.- The initial component of interference at the rear rotor is caused by its own presence in the tunnel. The factor corresponding to this interference is developed by substituting equations (5) and (34) (for both M and N) into equation (4), to yield

$$\delta = \frac{1}{400}\sum_{M=1}^{20}\sum_{N=1}^{20}\delta \quad \text{at} \quad \left\{ \begin{array}{l} \zeta_N = \dfrac{\zeta_{FR}}{1 - \sigma_R\gamma\zeta_{FR}\left(\frac{R_N}{R}\cos\psi_N \sin\alpha_{RR} + \frac{l_{RR}}{R}\sin\alpha_B - \frac{h_{RR}}{R}\cos\alpha_B\right)} \\ \eta_N = \eta_{FR} - \frac{R_N}{R}\sigma_R\left(\sin\psi_N\cos\beta + \cos\psi_N\cos\alpha_{RR}\sin\beta\right) - \sigma_R\sin\beta\left(\frac{l_{RR}}{R}\cos\alpha_B + \frac{h_{RR}}{R}\sin\alpha_B\right) \\ \left(\frac{x}{H}\right)_{N,M} = \sigma_R\gamma\left[\frac{R_M}{R}\left(\cos\psi_M\cos\alpha_{RR}\cos\beta - \sin\psi_M\sin\beta\right) - \frac{R_N}{R}\left(\cos\psi_N\cos\alpha_{RR}\cos\beta - \sin\psi_N\sin\beta\right)\right] \\ \left(\frac{y}{H}\right)_{N,M} = \sigma_R\gamma\left[\frac{R_M}{R}\left(\sin\psi_M\cos\beta + \cos\psi_M\cos\alpha_{RR}\sin\beta\right) - \frac{R_N}{R}\left(\sin\psi_N\cos\beta + \cos\psi_N\cos\alpha_{RR}\sin\beta\right)\right] \\ \left(\frac{z}{H}\right)_{N,M} = -\sigma_R\gamma\sin\alpha_{RR}\left(\frac{R_M}{R}\cos\psi_M - \frac{R_N}{R}\cos\psi_N\right) \end{array} \right\} \tag{37}$$

Average interference over rear rotor due to presence of front rotor.- In addition to the interference resulting from its own presence, the rear rotor also experiences an interference due to the presence of the front rotor. Because of the manner in which wall interference increases with downstream position, this component of interference will often be the largest of the four components derived herein. The interference factor is developed by substituting equations (5), (33) (for N), and (34) (for M) into equation (4) to yield

$$\delta = \frac{1}{400}\sum_{M=1}^{20}\sum_{N=1}^{20}\delta \quad \text{at} \quad \left\{ \begin{array}{l} \zeta_N = \dfrac{\zeta_{FR}}{1 - \frac{R_N}{R}\sigma_R\gamma\zeta_{FR}\cos\psi_N\sin\alpha_{FR}} \\ \eta_N = \eta_{FR} - \frac{R_N}{R}\sigma_R\left(\sin\psi_N\cos\beta + \cos\psi_N\cos\alpha_{FR}\sin\beta\right) \\ \left(\frac{x}{H}\right)_{N,M} = \sigma_R\gamma\left[\frac{R_M}{R}\left(\cos\psi_M\cos\alpha_{RR}\cos\beta - \sin\psi_M\sin\beta\right) + \cos\beta\left(\frac{l_{RR}}{R}\cos\alpha_B + \frac{h_{RR}}{R}\sin\alpha_B\right)\right. \\ \qquad\qquad \left. - \frac{R_N}{R}\left(\cos\psi_N\cos\alpha_{FR}\cos\beta - \sin\psi_N\sin\beta\right)\right] \\ \left(\frac{y}{H}\right)_{N,M} = \sigma_R\gamma\left[\frac{R_M}{R}\left(\sin\psi_M\cos\beta + \cos\psi_M\cos\alpha_{RR}\sin\beta\right) + \sin\beta\left(\frac{l_{RR}}{R}\cos\alpha_B + \frac{h_{RR}}{R}\sin\alpha_B\right)\right. \\ \qquad\qquad \left. - \frac{R_N}{R}\left(\sin\psi_N\cos\beta + \cos\psi_N\cos\alpha_{FR}\sin\beta\right)\right] \\ \left(\frac{z}{H}\right)_{N,M} = -\sigma_R\gamma\left(\frac{R_M}{R}\cos\psi_M\sin\alpha_{RR} + \frac{l_{RR}}{R}\sin\alpha_B - \frac{h_{RR}}{R}\cos\alpha_B - \frac{R_N}{R}\cos\psi_N\sin\alpha_{FR}\right) \end{array} \right\} \tag{38}$$

Symmetry considerations.- For the tandem rotor system, symmetry exists only at zero yaw ($\beta = 0$) and when the model is centered in the tunnel ($\eta = 1.0$). If both these conditions are met, it is adequate to evaluate equations (35) to (38) for $1 < M < 10$ only, provided that the leading constant is altered from 1/400 to 1/200.

The rear rotor length and height in equations (34) to (38) are in terms of the rotor radius, which is zero when $\sigma_R = 0$. Such cases should be rejected in computer programs.

Additional considerations.- In applying interference calculations to the tandem rotor system, it will be observed that the total interference at either rotor is a function of the operating conditions of both rotors. Thus, in the notation of reference 2, where the vertical interference due to lift (or "lift interference") is expressed for a single rotor as

$$\Delta w_L = \delta_{w,L} \frac{A_m}{A_T} w_0 \tag{39}$$

the total interference at the front rotor of the tandem pair becomes

$$\Delta w_L = \frac{A_m}{A_T} \left[\underbrace{\delta_{w,L}}_{\substack{\text{from} \\ \text{eq. (35)}}} (w_0)_{FR} + \underbrace{\delta_{w,L}}_{\substack{\text{from} \\ \text{eq. (36)}}} (w_0)_{RR} \right] \tag{40}$$

and the total interference at the rear rotor of the tandem pair becomes

$$\Delta w_L = \frac{A_m}{A_T} \left[\underbrace{\delta_{w,L}}_{\substack{\text{from} \\ \text{eq. (37)}}} (w_0)_{RR} + \underbrace{\delta_{w,L}}_{\substack{\text{from} \\ \text{eq. (38)}}} (w_0)_{FR} \right] \tag{41}$$

where A_m in equations (39) to (41) is the momentum area of one rotor in all cases.

Examination of equations (40) and (41) indicates that the individual forces generated by each rotor while operating in tandem in the tunnel must be known. Otherwise, it is not possible to obtain the correct individual values of w_0. Estimation of the division of the overall forces between the rotors is unlikely to be adequate because of the large mutual interference between the rotors as well as their mutual effects on the wall interference. For cases such as the tandem-rotor system, it is necessary to provide auxiliary balances within the model so as to obtain the performance of the individual rotors in order to provide satisfactory wall corrections. Provision of such balances really is required in any event to insure that the actual model trim conditions are reasonably representative of a feasible steady-state operating condition in free air.

It should be understood that similar considerations apply in all multielement wall-interference calculations (although in many cases A_m may also be substantially different for the various elements). Thus auxiliary balances will, in general, be required in all such models.

The interference at the tail of a tandem rotor can be obtained as the sum of the interferences at the tail caused by the presence of both rotors. The derivation is not presented herein since current practice is to design such systems without a conventional horizontal tail.

Unloaded-Rotor Models

General considerations.- The nomenclature adopted for the unloaded-rotor configuration is illustrated in figure 8. The origin of the system is chosen at the center of the rotor. With this choice of origin, the interference at the rotor caused by its own presence may be obtained directly from equation (18). The interference at the tail caused by the presence of the rotor may be obtained directly from equation (26). The interference at the wing and at the tail due to the presence of the wing could be obtained directly from equations (7) and (11) by a suitable translation of origin and alterations in both tail length and height; however, these relations will be rederived herein in order to maintain a consistent nomenclature for the configuration. In addition, interference at the rotor due to the presence of the wing, as well as the interference at the wing due to the presence of the rotor, is required and will be derived herein.

Average interference at wing due to presence of rotor.- The values of the coordinates for the elemental wake origins in the rotor are given by equations (17). Referred to the present origin, the coordinates of the M control points on the wing are obtained from equations (6) by a simple translation of the origin, to yield

$$\left.\begin{aligned}
\left(\frac{x}{H}\right)_M &= \sigma_R\gamma\left(\left|\frac{11-2M}{10}\right|\frac{\sigma_w}{\sigma_R}\tan\Lambda\cos\alpha_B + \frac{l_w}{R}\cos\alpha_B + \frac{h_w}{R}\sin\alpha_B\right) \\
\left(\frac{y}{H}\right)_M &= \sigma_R\gamma\,\frac{11-2M}{10}\,\frac{\sigma_w}{\sigma_R} \\
\left(\frac{z}{H}\right)_M &= -\sigma_R\gamma\left(\left|\frac{11-2M}{10}\right|\frac{\sigma_w}{\sigma_R}\tan\Lambda\sin\alpha_B + \frac{l_w}{R}\sin\alpha_B - \frac{h_w}{R}\cos\alpha_B\right)
\end{aligned}\right\} \qquad (42)$$

The factor corresponding to the average interference over the wing caused by the presence of the rotor is obtained by combining equations (4), (5), (17), and (42) to yield

$$\delta = \frac{1}{200} \sum_{M=1}^{10} \sum_{N=1}^{20} \delta \quad \text{at} \quad \left\{ \begin{array}{l} \zeta_N = \dfrac{\zeta}{1 - \dfrac{R_N}{R} \sigma_R \gamma \zeta \cos \psi_N \sin \alpha_R} \\ \\ \eta_N = \eta - \dfrac{R_N}{R} \sigma_R \sin \psi_N \\ \\ \left(\dfrac{x}{H}\right)_{N,M} = \sigma_R \gamma \left(\left| \dfrac{11 - 2M}{10} \right| \dfrac{\sigma_w}{\sigma_R} \tan \Lambda \cos \alpha_B + \dfrac{l_w}{R} \cos \alpha_B + \dfrac{h_w}{R} \sin \alpha_B \right. \\ \qquad \left. - \dfrac{R_N}{R} \cos \alpha_R \cos \psi_N \right) \\ \\ \left(\dfrac{y}{H}\right)_{N,M} = \sigma_R \gamma \left(\dfrac{11 - 2M}{10} \dfrac{\sigma_w}{\sigma_R} - \dfrac{R_N}{R} \sin \psi_N \right) \\ \\ \left(\dfrac{z}{H}\right)_{N,M} = -\sigma_R \gamma \left(\left| \dfrac{11 - 2M}{10} \right| \dfrac{\sigma_w}{\sigma_R} \tan \Lambda \sin \alpha_B + \dfrac{l_w}{R} \sin \alpha_B - \dfrac{h_w}{R} \cos \alpha_B \right. \\ \qquad \left. - \dfrac{R_N}{R} \sin \alpha_R \cos \psi_N \right) \end{array} \right\} \tag{43}$$

When $\eta = 1.0$ this interference field is symmetrical, and it is satisfactory to evaluate equation (43) for $1 < M < 5$ only, provided that the leading factor is changed from 1/200 to 1/100.

Average interference over wing due to presence of wing.- The factor corresponding to the average interference over the wing due to its own presence can be obtained by combining equations (4) and (42), to obtain

$$\delta = \frac{1}{10 \sum_{N=1}^{10} L_N} \sum_{M=1}^{10} \sum_{N=1}^{10} L_N \times \delta \quad \text{at} \quad \left\{ \begin{array}{l} \zeta_N = \dfrac{\zeta}{1 - \sigma_R \gamma \zeta \left(\left| \dfrac{11 - 2N}{10} \right| \dfrac{\sigma_w}{\sigma_R} \tan \Lambda \sin \alpha_B + \dfrac{l_w}{R} \sin \alpha_B - \dfrac{h_w}{R} \cos \alpha_B \right)} \\ \\ \eta_N = \eta - \sigma_R \dfrac{11 - 2N}{10} \dfrac{\sigma_w}{\sigma_R} \\ \\ \left(\dfrac{x}{H}\right)_{N,M} = \sigma_R \dfrac{\sigma_w}{\sigma_R} \gamma \tan \Lambda \cos \alpha_B \left(\left| \dfrac{11 - 2M}{10} \right| - \left| \dfrac{11 - 2N}{10} \right| \right) \\ \\ \left(\dfrac{y}{H}\right)_{N,M} = \sigma_R \dfrac{\sigma_w}{\sigma_R} \gamma \dfrac{N - M}{5} \\ \\ \left(\dfrac{z}{H}\right)_{N,M} = -\sigma_R \dfrac{\sigma_w}{\sigma_R} \gamma \tan \Lambda \sin \alpha_B \left(\left| \dfrac{11 - 2M}{10} \right| - \left| \dfrac{11 - 2N}{10} \right| \right) \end{array} \right\} \tag{44}$$

When $\eta = 1$ the interference field is symmetrical, and it is satisfactory to evaluate equation (44) for only $1 < M < 5$, provided that the leading factor is changed from 1/10 to 1/5.

Average interference over rotor due to presence of wing.- The factor corresponding to this interference may be derived by combining equations (4), (17), and (42) to yield

$$\delta = \frac{1}{20\sum_{N=1}^{10} L_N} \sum_{M=1}^{20}\sum_{N=1}^{10} L_N \times \delta \quad \text{at} \quad \left\{ \begin{array}{l} \zeta_N = \dfrac{\zeta}{1 - \sigma_R\gamma\zeta\left(\left|\dfrac{2N-11}{10}\right|\dfrac{\sigma_w}{\sigma_R}\tan\Lambda\sin\alpha_B + \dfrac{l_w}{R}\sin\alpha_B - \dfrac{h_w}{R}\cos\alpha_B\right)} \\ \eta_N = \eta + \dfrac{2N-11}{10}\dfrac{\sigma_w}{\sigma_R} \\ \left(\dfrac{x}{H}\right)_{N,M} = \sigma_R\gamma\left(\dfrac{R_M}{R}\cos\alpha_R\cos\psi_M - \left|\dfrac{11-2N}{10}\right|\dfrac{\sigma_w}{\sigma_R}\tan\Lambda\cos\alpha_B - \dfrac{l_w}{R}\cos\alpha_B - \dfrac{h_w}{R}\sin\alpha_B\right) \\ \left(\dfrac{y}{H}\right)_{N,M} = \sigma_R\gamma\left(\dfrac{R_M}{R}\sin\psi_M - \dfrac{11-2N}{10}\dfrac{\sigma_w}{\sigma_R}\right) \\ \left(\dfrac{z}{H}\right)_{N,M} = -\sigma_R\gamma\left(\dfrac{R_M}{R}\sin\alpha_R\cos\psi_M - \left|\dfrac{11-2N}{10}\right|\dfrac{\sigma_w}{\sigma_R}\tan\Lambda\sin\alpha_B - \dfrac{l_w}{R}\sin\alpha_B + \dfrac{h_w}{R}\cos\alpha_B\right) \end{array} \right\} \tag{45}$$

When $\eta = 1$ the interference field is symmetrical (for symmetrical L_N), and it is sufficient to evaluate equation (45) for only the M points where $0 < \psi_M < \pi$, provided that the leading constant is changed from 1/20 to 1/10.

Average interference at tail due to presence of wing.- The coordinates of the control points on the tail are as given by equations (25). Combining equations (4), (25), and (42) yields

$$\delta = \frac{1}{4\sum_{N=1}^{10} L_N} \sum_{M=1}^{4}\sum_{N=1}^{10} L_N \times \delta \quad \text{at} \quad \left\{ \begin{array}{l} \zeta_N = \dfrac{\zeta}{1 - \sigma_R\gamma\zeta\left(\left|\dfrac{2N-11}{10}\right|\dfrac{\sigma_w}{\sigma_R}\tan\Lambda\sin\alpha_B + \dfrac{l_w}{R}\sin\alpha_B - \dfrac{h_w}{R}\cos\alpha_B\right)} \\ \eta_N = \eta + \dfrac{2N-11}{10}\sigma_R\dfrac{\sigma_w}{\sigma_R} \\ \left(\dfrac{x}{H}\right)_{N,M} = \sigma_R\gamma\left[\left(\dfrac{l_t}{R} - \dfrac{l_w}{R}\right)\cos\alpha_B + \left(\dfrac{h_t}{R} - \dfrac{h_w}{R}\right)\sin\alpha_B - \left|\dfrac{11-2N}{10}\right|\dfrac{\sigma_w}{\sigma_R}\tan\Lambda\cos\alpha_B\right] \\ \left(\dfrac{y}{H}\right)_{N,M} = \sigma_R\gamma\left(\dfrac{5-2M}{4}\dfrac{\sigma_t}{\sigma_R} - \dfrac{11-2N}{10}\dfrac{\sigma_w}{\sigma_R}\right) \\ \left(\dfrac{z}{H}\right)_{N,M} = -\sigma_R\gamma\left[\left(\dfrac{l_t}{R} - \dfrac{l_w}{R}\right)\sin\alpha_B - \left(\dfrac{h_t}{R} - \dfrac{h_w}{R}\right)\cos\alpha_B - \left|\dfrac{11-2N}{10}\right|\dfrac{\sigma_w}{\sigma_R}\tan\Lambda\sin\alpha_B\right] \end{array} \right\} \tag{46}$$

When $\eta = 1.0$ the interference field is symmetrical (for symmetrical L_N), and it is sufficient to evaluate equation (46) for $1 < M < 2$ only, provided that the leading constant is changed from 1/4 to 1/2.

Side-by-Side Rotors and Tilt Rotors

General considerations.- The two configurations treated in this section are similar in that a pair of rotors are laterally disposed. The tilt-rotor configuration supports and pivots the rotors from a wing. The side-by-side rotors of a helicopter are supported from a streamlined structure, essentially winglike, extending laterally from the fuselage. Both configurations, in general, use relatively conventional horizontal tails. The only significant difference between the two configurations (from the viewpoint of wall interference) is that the tilt-rotor configuration tilts the rotors forward during transition so that it flies essentially as a normal airplane in forward flight. This variable tilt of the rotors complicates the calculations somewhat since the relative positions of the wing and tail with respect to the rotors become a function of the tilt angle of the rotors.

For the present purposes, an origin is chosen midway between the two rotors. The remaining nomenclature is shown in figure 9.

Interference on right-hand rotor due to presence of right-hand rotor.- The interference factor corresponding to this interference is identical to that given by equation (18) except that the expression for η_N must be altered to

$$\eta_N = \eta - \frac{R_N}{R}\sigma_R \sin\psi_N - \frac{s_R}{R}\sigma_R \tag{47}$$

Note that the symmetries stated after equation (18) no longer apply, since at $\eta = 1$ the individual rotor is no longer in the center of the tunnel.

Interference on right-hand rotor due to presence of left-hand rotor.- The interference factor corresponding to this interference is identical to that given by equation (18) except that the expressions for η_N and $\left(\frac{v}{H}\right)_{N,M}$ must be altered to

$$\left.\begin{aligned} \eta_N &= \eta - \frac{R_N}{R}\sigma_R \sin\psi_N + \frac{s_R}{R}\sigma_R \\ \left(\frac{v}{H}\right)_{N,M} &= \sigma_R\gamma\left(\frac{R_M}{R}\sin\psi_M + 2\,\frac{s_R}{R} - \frac{R_N}{R}\sin\psi_N\right) \end{aligned}\right\} \tag{48}$$

Interference on right-hand rotor due to presence of wing.- The factor corresponding to this interference may be obtained directly from equation (45) provided that $\left(\frac{v}{H}\right)_{N,M}$ is altered to

$$\left(\frac{v}{H}\right)_{N,M} = \sigma_R\gamma\left(\frac{R_M}{R}\sin\psi_M + \frac{s_R}{R} - \frac{11 - 2N}{10}\,\frac{\sigma_w}{\sigma_R}\right) \tag{49}$$

Interference on left-hand rotor due to presence of left-hand rotor.- The factor corresponding to this interference may be obtained directly from equation (18) except that η_N must be altered to

$$\eta_N = \eta - \frac{R_N}{R}\sigma_R \sin \psi_N + \frac{s_R}{R}\sigma_R \tag{50}$$

Interference on left-hand rotor due to presence of right-hand rotor.- The factor corresponding to this interference may be obtained directly from equation (18) except that η_N and $\left(\frac{y}{H}\right)_{N,M}$ must be altered to

$$\left.\begin{aligned} \eta_N &= \eta - \frac{R_N}{R}\sigma_R \sin \psi_N - \frac{s_R}{R}\sigma_R \\ \left(\frac{y}{H}\right)_{N,M} &= \sigma_R \gamma \left(\frac{R_M}{R} \sin \psi_M - 2\frac{s_R}{R} - \frac{R_N}{R} \sin \psi_N\right) \end{aligned}\right\} \tag{51}$$

Interference on left-hand rotor due to presence of wing.- The interference factor corresponding to this interference may be obtained directly from equation (45) provided that $\left(\frac{y}{H}\right)_{N,M}$ is altered to

$$\left(\frac{y}{H}\right)_{N,M} = \sigma_R \gamma \left(\frac{R_M}{R} \sin \psi_M - \frac{s_R}{R} - \frac{11 - 2N}{10}\frac{\sigma_w}{\sigma_R}\right) \tag{52}$$

Interference on wing due to presence of wing.- The interference factor corresponding to this interference may be obtained directly from equation (44) without alteration. The symmetry provisions noted after equation (44) apply to this component of interference.

Interference on wing due to presence of right-hand rotor.- The interference factor corresponding to this interference may be obtained directly from equation (43) except that η_N and $\left(\frac{y}{H}\right)_{N,M}$ must be altered to

$$\left.\begin{aligned} \eta_N &= \eta - \frac{R_N}{R}\sigma_R \sin \psi_N - \frac{s_R}{R}\sigma_R \\ \left(\frac{y}{H}\right)_{N,M} &= \sigma_R \gamma \left(\frac{11 - 2M}{10}\frac{\sigma_w}{\sigma_R} - \frac{R_N}{R} \sin \psi_N - \frac{s_R}{R}\right) \end{aligned}\right\} \tag{53}$$

Interference on wing due to presence of left-hand rotor.- The interference factor corresponding to this interference may be obtained directly from equation (43) except that η_N and $\left(\frac{v}{H}\right)_{N,M}$ must be altered to

$$\left.\begin{aligned} \eta_N &= \eta - \frac{R_N}{R}\sigma_R \sin\psi_N + \frac{s_R}{R}\sigma_R \\ \left(\frac{v}{H}\right)_{N,M} &= \sigma_R\gamma\left(\frac{11 - 2M}{10}\frac{\sigma_w}{\sigma_R} - \frac{R_N}{R}\sin\psi_N + \frac{s_R}{R}\right) \end{aligned}\right\} \tag{54}$$

Interference on tail due to presence of right-hand rotor.- The interference factor corresponding to this interference may be found directly from equation (26) except that the expressions for η_N and $\left(\frac{v}{H}\right)_{N,M}$ must be altered to

$$\left.\begin{aligned} \eta_N &= \eta - \frac{R_N}{R}\sigma_R \sin\psi_N - \frac{s_R}{R}\sigma_R \\ \left(\frac{v}{H}\right)_{N,M} &= -\sigma_R\gamma\left(\frac{2M - 5}{4}\frac{\sigma_t}{\sigma_R} + \frac{R_N}{R}\sin\psi_N + \frac{s_R}{R}\right) \end{aligned}\right\} \tag{55}$$

Interference on tail due to presence of left-hand rotor.- The interference factor corresponding to this interference may be found directly from equation (26) except that the expressions for η_N and $\left(\frac{v}{H}\right)_{N,M}$ must be altered to

$$\left.\begin{aligned} \eta_N &= \eta - \frac{R_N}{R}\sigma_R \sin\psi_N + \frac{s_R}{R}\sigma_R \\ \left(\frac{v}{H}\right)_{N,M} &= -\sigma_R\gamma\left(\frac{2M - 5}{4}\frac{\sigma_t}{\sigma_R} + \frac{R_N}{R}\sin\psi_N - \frac{s_R}{R}\right) \end{aligned}\right\} \tag{56}$$

Interference on tail due to presence of wing.- The interference factor corresponding to this interference may be found directly from equation (46) without alteration. The symmetry provisions noted after equation (46) apply.

Symmetry considerations.- It will be noted that the symmetry conditions stated in earlier sections of the paper for $\eta = 1.0$ do not apply except in the case of the interferences at the wing and tail caused by the presence of the wing. The interference field is symmetrical, however, when $\eta = 1.0$. The total interference at one rotor will be the same as the total interference at the other rotor. Thus, it is only necessary to compute the three individual components at either one of the rotors. The interference caused at the wing and the tail by either rotor is also identical; therefore, these components need

be computed for only one of the rotors and then doubled to account for the presence of both. If the interference distribution over the wing and tail were being computed, rather than the average values, this latter symmetry could still be used by adding the values at $+y$ and $-y$ rather than simply doubling the result for one rotor.

Additional notes.- Examination and consideration of the input parameters for the case of side-by-side rotors and tilt rotors indicate that the program is extremely versatile. Proper selection of the appropriate angles of attack, span-width ratios, and lengths and heights will result in factors for tilt-wing aircraft, fan-in-wing aircraft, or cruise-fan aircraft. The only real limitation is that the configuration must have only two symmetrically located circular lifting elements.

Displaced Pivot Location

In all the foregoing derivations the model is assumed to be pivoted about a somewhat arbitrarily chosen origin when its angle of attack is varied in the tunnel. In practice, however, the actual pivot location, which may be either real or virtual, is determined by the available linkages and other physical restraints. This feature may be accounted for by treating the initial value of ζ as a function of angle of attack. If the dimensions h_P and l_P of the virtual pivot are measured from the origin as in figure 10 (when the model is at zero angle of attack), then the change in height of the origin at an angle of attack is

$$\Delta z = h_P(1 - \cos \alpha) + l_P \sin \alpha \tag{57}$$

Consequently, before use in the foregoing equations ζ must be altered to

$$\zeta = \frac{\zeta|_{\alpha=0}}{1 + \left[\frac{h_P}{H}(1 - \cos \alpha) + \frac{l_P}{H} \sin \alpha\right]\zeta|_{\alpha=0}} \tag{58}$$

A longitudinal motion also results from a displaced pivot; however, since the test section is considered herein to be infinitely long, this motion has no effect on the results. The values of $\left(\frac{x}{H}\right)_N$, $\left(\frac{y}{H}\right)_N$, and $\left(\frac{z}{H}\right)_N$ are unchanged since they are measured from the chosen origin. The value of η is unchanged because no lateral motion results from changing the angle of attack.

Availability of Computer Programs

All the cases treated herein have been programed in CDC FORTRAN, Version 2.1, to run on CDC 6000 Series computers with the SCOPE 3.0 operating system and library

tape. Only minor modifications should be necessary to run on IBM 7090 and 7094 computers with the IBSYS Version 13 operating system and library tape.

These programs use a common subroutine which calculates the interference factors for a vanishingly small model according to reference 2. Interference factors are computed for correcting from closed, closed-on-bottom-only, and open tunnels (as well as ground effect) to free air. In addition, interference factors are computed for correcting from closed and closed-on-bottom-only tunnels to ground effect.

Since the results of reference 2 are exactly equivalent to the results of classical theory when the wake is undeflected ($\chi = 90^{o}$), these programs can be used directly to obtain the classical correction factors. The only required modifications are to restrict one DO-loop to $K = 8,8$ rather than $K = 1,8$ and to multiply the factors by -1/4 to account for the different definitions of δ.

Because of the combined length of these programs, they have not been included in the present report. Instead, a technical memorandum (ref. 5) has been prepared giving the programs. The present report should provide adequate numerical values for check cases.

NUMERICAL RESULTS AND DISCUSSION

General Observations

The purpose of this portion of the paper is to utilize the hitherto developed equations to explore some of the variables that may affect the interference factors for a particular model. References 2, 3, and 6 have already shown that in certain cases, significant differences occur; however, the present study allows a more complete examination of many features than was presented in the reference papers.

The numerical results presented herein concern only the simpler cases studied earlier, since the number of configuration variables involved for the more complex configurations makes the generality of the results suspect in such cases. The basic theory used for the vanishingly small model is that of reference 2, since it is desired to focus attention particularly on V/STOL models. The results will be a function of the wake skew angle. Reference 2 coincides with classical undeflected-wake theory when the skew angle χ is 90^{o}. The interference factor $\delta_{w,L}$ of reference 2 corresponds to the classical "lift interference" factor; however, because of the unusual definition of $\delta_{w,L}$ (in terms of momentum area and mean induced velocity rather than wing area and lift coefficient), numerical values of $\delta_{w,L}$ must be divided by a factor of -4 in order to obtain

the corresponding conventional interference factor. Provided that the foregoing factor is applied, the effect of changing a variable in conventional wall-interference theory may be noted by examining the present results at $\chi = 90^{\circ}$. For skew angles other than 90°, the effective skew angle (ref. 6) is the correct skew angle to use.

In order to present a consistent set of correction factors for comparison purposes, virtually all the calculations are presented for a model centered in a closed wind tunnel with a width-height ratio of 1.5. It should be noted, however, that in certain cases it is necessary to define the exact meaning of "centered." In a few cases other mounting locations are used to illustrate specific points. In order to reduce the length of the presentation, in most cases only the interference factor for the vertical interference due to lift is presented. This single factor usually represents by far the largest portion of the overall wind-tunnel interference; however, it should be noted that changes of a comparable order of magnitude will result in the remaining factors.

The interference distributions are also studied in a number of cases. For consistency, and also to reduce the length of presentation, calculated results are presented for only two wake skew angles: 60° and 90°. The load distribution is assumed to be uniform in all cases unless otherwise noted.

Wings

Average interference for unswept wings.- Figure 11 presents the average values of $\delta_{w,L}$ for a series of rectangular wings of differing span-width ratio as computed from equation (7). (Note that no induced camber is considered herein.) Substantial effects of span are evident. For the test-section configuration used herein, increasing the span-width ratio decreases the interference at low skew angles. At the high skew angles, the initial effect of increasing span is to reduce the interference factors; however, the curve for the largest span-width ratio ($\sigma = 0.75$) indicates that for very large spans this trend is reversed.

Even though the interference factors are reduced as a result of increased span-width ratio, the interference velocities (or angles) are increased because the area ratio is increased. Note that for simple wings, where the momentum area is the area within a circle circumscribing the wing tips,

$$\Delta w_L = \delta_{w,L} \frac{A_M}{A_T} w_0 = \delta_{w,L} \frac{\pi s^2}{4BH} w_0 = \delta_{w,L} \frac{\pi}{4} \sigma_w{}^2 \gamma w_0 \tag{59}$$

It is obvious from figure 11 that the interference factors decrease far less rapidly than the square of the span-width ratio increases. Thus, the interference velocities increase with span-width ratio, but at a rate somewhat smaller than the area ratio would indicate.

Interference distribution over unswept wings.- The interference distribution across the span of the same unswept wings is shown in figure 12 as computed from equations (8) and (9). For most of the cases considered, the interference distribution is relatively uniform and decreases only slightly toward the wing tips. On the other hand, a large span ($\sigma = 0.75$) results in a substantial increase in interference toward the tips.

In practice, the wing operating condition may be corrected for the average interference velocities; however, correcting for spanwise interference distribution is difficult and is seldom attempted. It is obvious that nonuniform interference will affect measurements such as spanwise load distribution. Less obvious effects on the gross wing performance, particularly near stall, may also be observed. With an interference distribution such as that shown for $\sigma_w = 0.75$ in figure 12, the wing tips will be loaded more heavily relative to the wing root than they would be in free air. Thus, even after corrections based on the average interference, the stall angle of attack may be less in the tunnel than in free air if the wing has a basic tendency to stall initially at the tips. Conversely, if the wing tends to stall initially at the root, the stall angle in the tunnel may be greater than the stall angle in free air.

Effect of wing sweep on average interference.- Figure 13 shows the average interference factors for a series of swept wings at $\alpha = 0^\circ$. The span-width ratio is 0.5 in all cases. The interference varies as a function of sweep at the lower skew angles; however, the effect of sweep on the interference is small except when the sweep angle is extreme ($\Lambda = 75^\circ$).

At $\chi = 90^\circ$, when the wake is horizontal, wing sweep is found to have no effect upon the average interference. This result is in accord with Munk's stagger theorem (ref. 7). (See appendix.)

Effect of wing sweep on interference distribution.- In contrast to the small effect of sweep on the average interference, the effect of sweep on interference distribution is relatively large (fig. 14). The interference over the unswept wing ($\Lambda = 0$) decreases slightly toward the tips. The swept wings, however, all display interference distributions which increase toward the tip, the greatest nonuniformity being shown by the wings of greatest sweep. Since highly swept wings are generally prone to stall initially at the tip, the indicated interference distribution will generally result in a somewhat premature stall even after corrections based on the average interference.

An even more significant effect may be encountered as a result of nonuniform interference over a swept wing. When the wing is swept back, the wing tips are substantially farther rearward than the wing roots. Consequently, interference distributions such as those depicted in figure 14 may lead to a significant pitching moment. Furthermore, since the interference increases with lift coefficient, the pitching moment will increase with lift

coefficient. The result will be a direct effect upon the static margin of the aircraft as measured in the wind tunnel.

Effect of angle of attack on interference.- It will be observed from equation (7) that angle of attack has no effect upon the interference factors for an unswept wing. When the wing is swept, however, the relative vertical positions of the elements representing the wing become a function of angle of attack. The effect of a 20° angle of attack on the average interference factors of wings with 45° and 75° of sweep is shown in figure 15. The corresponding interference distributions are shown in figures 16 and 17. In all cases, equation (58) was used to maintain the position of the wing aerodynamic center at the center of the tunnel.

Figures 15 and 16 show that the effects of angle of attack on the average interference and the interference distributions are small even when the sweep angle is as great as 45°. When the wing sweep is extreme ($\Lambda = 75^{\circ}$), figures 15 and 17 indicate that reasonably significant effects occur. Note that for $\alpha = 20^{\circ}$ and $\Lambda = 75^{\circ}$, even the average interference at $\chi = 90^{\circ}$ is affected slightly.

Effect of load distribution on interference.- The actual load distribution on a wing generally tends toward being elliptical rather than uniform. Figure 18 shows a comparison of average interference factors for uniform and elliptically loaded unswept wings with a span-width ratio of 0.5. The interference is slightly higher for the elliptically loaded wing. Comparison with figure 11 shows that, as often assumed, the elliptically loaded wing is equivalent to a uniformly loaded wing of slightly smaller span-width ratio. If interference factors are calculated according to the procedures developed herein, it is no longer necessary to approximate the effects of load distribution by assumptions such as reduced span. Neither additional work nor additional computer time is required to obtain the appropriate interference factors for the desired load distribution.

Figure 19 shows the effect of load distribution on the interference distribution. Note that the interference is slightly more nonuniform for the elliptic load distribution than for the uniform load distribution. This result, which appears to contradict the usual practice of assuming elliptic loading to have the same effect as shortened span (see fig. 12), occurs because the distributions of figures 12 and 19 are presented in terms of the wing span rather than the tunnel dimensions. The trend of the distribution across the entire tunnel will be opposite to that of figures 12 and 19. Thus, to obtain results equivalent to figure 19 by using a shortened span it would be necessary to compute the distribution across the tunnel by using the reduced span and then convert the distribution to that across the wing by considering the full span of the wing.

Effect of pivot location on average interference of swept wings.- In the derivation of equations (6) to (56) the wing was assumed to pivot in angle of attack about the chosen

origin, which was the apex of the lifting line. If the wing did pivot about this origin, the average height of the wing above the floor would decrease (as a function of wing sweep) as the angle of attack increased. In computing the interference factors presented in the foregoing sections, this effect was negated by transferring the pivot (by eq. (58)) to the aerodynamic center of the wing.

Figure 20 compares, for swept wings, the interference factors obtained at an angle of attack of 20° when the wing pivots at the apex of the lifting line and when it pivots at the aerodynamic center. For an unswept wing no effect would be observed since the two points coincide. At a sweep angle of 45°, where the distance between the two points is equal to 3/8 of the tunnel semiheight, significant differences appear. At a sweep angle of 75°, where the distance between the two pivot locations is 1.40 times the tunnel semiheight, the choice of pivot location has far greater effect upon the interference factor than any other single parameter.

Although presented in figure 20 as a function of sweep, the effect under consideration is really the motion with angle of attack of the aerodynamic center of the model because of a pivot location that does not coincide with the aerodynamic center. Thus, similar effects may be observed for any arbitrary model.

In practice, the effective pivot center of a model in a given test usually will be determined by the physical considerations of model configuration, mounting system, and available angle-of-attack actuators. In many cases substantial offsets from the aerodynamic center and, consequently, significant effects upon wall interference may occur. Since the data report from a wind-tunnel test seldom specifies the actual effective pivot point of the model, it becomes extremely difficult to correct the data adequately subsequent to its publication.

In tunnels with width-height ratios similar to that for which the present results have been obtained, the interference factors generally increase in magnitude as the wake deflection from the horizontal increases. Since the wake deflection is a function of lift coefficient, which, in turn, depends at least partially upon angle of attack, some relief from the growth of interference factor with wake deflection can be obtained by a judicious choice of pivot location. If the pivot is chosen to be well behind the aerodynamic center, the model height will increase as angle of attack increases. The results of reference 2 indicate that the interference factors will be decreased at high lift by the resulting motion.

Interference at Tail Behind Wing

Effect of wing span-width ratio.- Since an aircraft tail is usually small and carries only small lift compared with the primary lifting system, the tail is usually assumed to incur no wall interference because of its own presence in the tunnel. (If these conditions

are not met, the treatment of tail interference should follow closely along the lines suggested in a later section entitled "Tandem Rotors.") Thus the total interference at the tail is considered to be caused entirely by the presence of the primary lifting system. For swept wings this interference is calculated by use of equation (11).

The interference at a zero-span tail located 1 tunnel semiheight behind unswept wings of various span-width ratios is presented in figure 21(a). Under these conditions, the interference factors decrease monotonically with increasing wing span-width ratio; however, the decrease in interference factor is again inadequate to overcome the increase in area ratio in determining the interference velocity.

In general, however, similar models have tail lengths in proportion to wing span. If the ratio of tail length to wing span is held constant, an entirely different result is obtained (fig. 21(b)). Under these circumstances the interference factor at the tail (except for the lowest wake skew angles) increases substantially with the span-width ratio of the wing. Thus the interference velocities at the tail will increase at a greater rate than the area of the lifting system. Since the corrections to pitching moment depend upon the differences in interference velocities at the lifting system and at the tail (ref. 8), and since the behavior of the interference factors at the wing (fig. 11) is opposite to that of figure 21(b), great caution must be exercised in choosing model size if exorbitantly large pitching-moment corrections are to be avoided.

Effect of angle of attack.- As the model is rotated to different angles of attack, the tail, because of its substantial lever arm, may move significantly up and down in the tunnel. This motion can have large effects on the interference at the tail. Figure 22 presents interference factors at a zero-span tail behind an unswept wing ($\sigma_w = 0.5$) at angles of attack of 0^o, 20^o, and -20^o. In general, substantial effects are evident; at very low wake skew angles the interference factors at $\alpha = 20^o$ (with the tail low) may be more than twice as great as those at $\alpha = -20^o$ (with the tail high). While this comparison has been made at constant wake angle, it should be noted that the wake angle will change with angle of attack as well, and may magnify the effects illustrated. Since the effect is mainly that of a different tail height above the floor, similar effects may be expected if the tail height of the model is significantly large.

When the wake is horizontal ($\chi = 90^o$), the effect of angle of attack is smaller and, as demanded by symmetry considerations, is the same for both positive and negative angles of attack. (See fig. 22.) If the wind-tunnel boundaries were not symmetrical this result would not be true. Figure 23 shows the corresponding interference factors in a tunnel which is closed on the bottom but open on the sides and ceiling. In this case, large effects of angle of attack are found even at $\chi = 90^o$.

Effect of wing sweep.- The effect of wing sweep on the interference at a zero-span tail is indicated in figure 24 for two angles of attack. Comparison with figure 13 shows that the effect of sweep on the interference at the tail is substantially greater than the effect on the average interference at the wing itself. The effect of sweep is relatively small for reasonable sweep angles, but becomes large when the sweep is extreme.

Effect of wing-load distribution.- The effect of wing-load distribution on the interference at a zero-span tail is demonstrated at $\alpha = 0^{\circ}$ for three different wing sweep angles in figure 25. Irrespective of the sweep angle, the elliptically loaded wing results in a slightly greater interference than the uniformly loaded wing. Comparison with figure 21(b) indicates that the effect of elliptic loading corresponds to the effect of shortening the wing span slightly.

Effect of tail span.- The effect of tail span on the average interference at the tail can be seen in figures 26 and 27 by comparing the interference factors for tails of zero span and of span equal to one-half the wing span ($\sigma_w = 0.5$, $\sigma_t = 0.25$) for different sweep angles and angles of attack. At least for the cases treated herein, a finite tail span slightly reduces the interference factors in all cases, indicating that the interference at the tail location decreases slightly to either side of the tunnel center line. Tail spans larger than half the wing span are not examined herein. If the tail span approaches sizes much larger than this, it would normally be expected that the tail lift forces would be comparatively large. If the tail forces are large, the treatment should be along the lines developed in a subsequent section on tandem rotors.

Single Rotors

Effect of diameter-width ratio on average interference factors.- Figure 28 presents the average interference factors according to equation (18) for a series of uniformly loaded rotors of various diameter-width ratios. As with wings, an increase in size reduces the interference factors, but not to the extent of overcoming the effect of the increasing area ratio. At $\chi = 90^{\circ}$, the interference factors for the rotors are the same as those for an elliptically loaded wing of the same span, since the average spanwise load distribution of a rotor with uniform disk-load distribution is elliptical. At lower skew angles, the interference factors may differ significantly from those for a wing. (Compare $\sigma_R = 0.50$ in fig. 28 with the elliptically loaded wing of fig. 18.)

Effect of diameter-width ratio on lateral distribution of interference factors.- Figure 29 presents the distribution of interference factors along the lateral axis of rotors of various diameter-width ratios. In general, the lateral distribution of interference factors is similar to that previously found for wings. The interference distribution becomes more nonuniform with increasing diameter-width ratio and, except for $\sigma_R = 0.75$,

decreases slightly toward the rotor tips. For $\sigma_R = 0.75$, where the tips are approaching the side walls, the interference increases again at the tips. This effect is greatest at wake skew angles near 90^o, which represent the high-speed conditions of a rotor. With a rotor of this large diameter-width ratio, retreating blade stall may be more extensive in the tunnel than in free air.

Effect of diameter-width ratio on the longitudinal distribution of interference.- As indicated in figure 30, the effect of increasing the diameter-width ratio is to increase rapidly the nonuniformity of the interference factor along the longitudinal axis of the rotor. The wall-induced upwash over the rearmost portions of the rotor disk will be substantially greater than the upwash over the forward portions of the disk. This effect is reinforced by the increasing area ratio of the model, which in this case is given by

$$\frac{A_m}{A_T} = \frac{\pi}{4} \sigma_R{}^2 \gamma \tag{60}$$

Figure 30 indicates that the slope of the interference velocities along the longitudinal axis of the rotor will increase approximately as the cube of the diameter-width ratio.

If the rotor flaps at its center of rotation, reference 9 indicates that the main effect of gradients such as those indicated in figure 30 would be to increase slightly the lateral tilt of the rotor plane. Under such conditions, the nonuniformities shown might still permit fairly large models to be used for gross performance measurements; however, measurements of the detailed blade load distributions might be severely affected if the rotor is large. On the other hand, if the rotor hub and blades are truly rigid, reference 10 indicates that similar gradients produce large and significant pitching moments. In such cases, the maximum permissible size of a rotor is severely restricted if reasonably small corrections to pitching moment are desired. If the rotor is submerged in a wing, as in a fan-in-wing design, no theory is available at present to predict the effect of gradients such as those indicated in figure 30. Since the effects of the gradient cannot be calculated, they cannot be removed from the data. In such cases, the model size must be chosen so that the longitudinal interference velocities are essentially uniform. Extremely small models may be required.

Effect of angle of attack on average interference.- The effect of angle of attack on the vertical interference due to lift is shown in figure 31(a). At low wake skew angles, a reasonably significant effect is found. It arises from the fact that the large longitudinal extent of the rotor results in substantial displacements from the center of the tunnel of the foremost and rearmost portions of the disk.

As noted earlier and in reference 2, the vertical interference due to lift is not the sole wall-induced interference present. In particular, there will also be a vertical

interference due to drag, given by

$$\Delta w_D = \delta_{w,D} \frac{A_m}{A_T} u_0 \tag{61}$$

From reference 11,

$$u_0 = \frac{D}{L} w_0 \tag{62}$$

The resultant force vector of a rotor, except at the most extreme operating conditions, is essentially normal to the rotor tip-path plane. Thus

$$\frac{D}{L} = \tan \alpha_R \tag{63}$$

Combining equations (61) to (63) yields

$$\Delta w_D = \delta_{w,D} \frac{A_m}{A_T} w_0 \tan \alpha_R \tag{64}$$

Finally, the total vertical interference velocity is the sum of the components due to lift and drag, so that

$$\Delta w = \left(\delta_{w,L} + \delta_{w,D} \tan \alpha_R\right) \frac{A_m}{A_T} w_0 \tag{65}$$

The effect of angle of attack on the sum $\delta_{w,L} + \delta_{w,D} \tan \alpha_R$ is presented in figure 31(b). It is obvious that the drag component substantially reinforces the effect of angle of attack on the vertical interference due to lift. While, in general, such effects have been omitted in this paper in the interest of brevity, figure 31(b) shows clearly that the drag effects can be large and should be considered when correcting wind-tunnel data.

Effect of angle of attack on distribution of interference.- Figure 32 shows the effect of angle of attack on the lateral distribution of interference over a rotor with a diameter-width ratio of 0.5. (In this and all succeeding figures in which angle of attack is varied, it should be noted that at $\chi = 90^\circ$ symmetry demands that the effect be the same for positive and negative angles of attack.) At $\chi = 90^\circ$, the effect of angle of attack on the lateral distribution of interference is essentially negligible. Even at a lower wake angle ($\chi = 60^\circ$) the effects of angle of attack are fairly small, with negative angles of attack slightly increasing the nonuniformity and positive angles slightly decreasing the nonuniformity.

As indicated by figure 33, angle of attack does not significantly influence the longitudinal distribution of interference at $\chi = 90^{\circ}$; however, reasonably large effects are noted at $\chi = 60^{\circ}$. At this wake angle, angle of attack produces the largest effects near the tips of the rotor. Because of the large moment arm, changes in interference at the rotor tips will have the greatest effect on pitching moment or lateral flapping.

Effect of disk-load distribution.- Because of the radial increase in local dynamic pressure, the disk-load distribution of a practical rotor will tend toward triangular loading (ref. 4) unless significant twist or taper is present. Figure 34 compares the average interference factors for similar rotors with uniform and triangular disk-load distributions. It is seen that the triangularly loaded rotor experiences a slightly smaller average interference than a uniformly loaded rotor. Comparison with figure 28 indicates that the effect of triangular loading is equivalent to the effect of a slightly increased diameter-width ratio. This result is not unexpected since the centroid of load is farther outboard for a triangular loading than for a uniform loading.

Figures 35 and 36 present the effect of load distribution on the lateral and longitudinal distribution of interference. At least for the case treated herein, the effect of load distribution is very small.

Tail Behind Rotor

Effect of rotor diameter-width ratio.- As indicated in figure 37(a), the effect of increasing the diameter-width ratio is to decrease the interference at a tail located at a fixed point in the tunnel. As was found for wings also, the trend is substantially different if the tail location is scaled geometrically with the rotor (fig. 37(b)). In such a case, the interference factors at the tail increase (over most of the wake skew-angle range) as the diameter-width ratio increases. Direct numerical comparison between figure 21 (for wings) and figure 37 (for rotors) should not be attempted. The tail locations are different in each case, being chosen to represent physically possible tail locations on plausible designs of each type.

Effect of angle of attack.- Figure 38 demonstrates the effect of angle of attack on the interference at the tail. This figure was prepared on the assumption that the angle of attack of the rotor was in all cases identical to the angle of attack of the body carrying the tail. As in the case of the wing (figs. 22 and 23), the effect of angle of attack on the interference at the tail is strong and occurs primarily because of the altered tail location in the tunnel. The lack of complete symmetry at $\chi = 90^{\circ}$ results from the chosen tail location, which is slightly below the plane of the rotor.

Despite the large interference factors at the tail, the effect of such interference may not be a powerful restriction on the size of rotor models as it is on the size of

winged airplane models. In many rotary-wing designs the tail is provided to stabilize only the fuselage rather than the entire aircraft. In these designs the major contributions to stability and control are provided by the rotor; thus, the forces and moments provided by the tail are minor, and contribute only slightly to the stability and control of the entire aircraft. In such cases, relatively large corrections to the tail contributions can be accepted; the critical sizing restrictions, as previously noted, result from the nonuniform longitudinal distribution of interference.

Effect of rotor disk-load distribution.- Figure 39 presents the effect of rotor disk-load distribution on the interference at the tail. The disk-load distribution has considerably more effect on the interference factors at the tail than on the average interference factors at the rotor itself (fig. 34). Comparison with figure 37(a) indicates that the effect of load distribution is such that the interference factors at a tail behind a triangularly loaded rotor are about the same as those for the same tail behind a somewhat larger uniformly loaded rotor.

Effect of tail span.- Figure 40 compares the average interference at the tail for a zero-span tail and for a tail with span equal to one-half the rotor span ($\sigma_R = 0.5$, $\sigma_t = 0.25$). The trend is similar to that indicated for a tail behind a wing (fig. 27) in that the average interference over the tail with large span is somewhat less than the interference over the zero-span tail.

Tandem Rotors

General comments.- Because of the wide disparity in wake deflections of the various lifting elements, as well as the large number of variables involved, it is not possible to present meaningful numerical interference factors for most of the more complex configurations studied in the earlier portions of this report unless particular test conditions are specified. Tandem rotors, under certain simplifying assumptions, are an exception. The following assumptions are made: the forces and wake skew angles produced by the two rotors are identical; the height of the rear rotor (see fig. 7) is zero; and the angles of attack of the front rotor, the rear rotor, and the body between them are all equal, so that the two rotors always lie in the same plane. These conditions will not, in general, be completely fulfilled in any particular test; however, deviations from these conditions would not be expected to cause changes in wall interference sufficient to invalidate the general conclusions.

Two rotor systems are studied. In the first, or nonoverlapped configuration, the rotor centers are separated by one full rotor diameter. In the second, or fully overlapped configuration, the rotor centers are separated by one rotor radius, this being the

minimum theoretical rotor spacing for which physical interference between rotors does not occur.

Only the longitudinal distribution of interference is considered, since it has previously been shown that longitudinal nonuniformity of interference has a limiting effect on the maximum permissible size of rotor models. The tunnel configuration is that of a closed tunnel with a width-height ratio of 1.5. The model is assumed to pivot about the center of the front rotor as the angle of attack is changed. The entire system is unyawed ($\beta = 0$). Under the assumptions and conditions outlined above, the longitudinal distribution of the system is obtained by use of equations (23), (24), and (58) together with suitable transpositions of the origin of x_R.

Contribution of each rotor to longitudinal distribution.- The contribution of the front rotor to the longitudinal distribution of interference factors is shown in figure 41. (Note that the scales used for the ordinate of this and subsequent figures differ substantially from those used earlier.) The interference factor becomes very much larger than at the origin as the distance downstream along and beyond the rotor longitudinal axis increases. When $\alpha = 0$, the interference produced by the front rotor in the region occupied by the rear rotor $\left(0 \leqq \frac{x}{R} \leqq 2 \quad \text{or} \quad 1 \leqq \frac{x}{R} \leqq 3, \text{ depending upon overlap}\right)$ is, on the average, two or three times the average value over the front rotor $\left(-1 \leqq \frac{x}{R} \leqq 1\right)$. Changing the angle of attack increases the interference over the rear rotor by perhaps 20 percent at $\chi = 90^\circ$; however, at $\chi = 60^\circ$, the angle of attack has extremely powerful effects, just as in the case of the tail behind a rotor (fig. 38). At negative angles of attack, where the rear rotor is high, the interference factors decrease to as little as one-half their value at $\alpha = 0$. At positive angles of attack, where the rear rotor is low, the interference for certain locations may be more than three times the value at $\alpha = 0$. It is evident from figure 41 that the interference at the rear rotor will be powerfully affected by the presence of the front rotor in the tunnel; furthermore, the interference caused at the rear rotor by the presence of the front rotor will be very sensitive to the angle of attack of the entire rotor system.

The contribution of the rear rotor to the interference distribution of the system is shown in figure 42 for the nonoverlapped system and in figure 43 for the overlapped system. At zero angle of attack, the contribution of the rear rotor is identical to that of the front rotor except for a transposition of the origin. At any other angle of attack, the rear rotor is either higher or lower in the tunnel; that is, its pivot point is located at the center of the front rotor. At both wake angles (60° and 90°) the average interference at the front rotor due to the presence of the rear rotor is very small, and only a small increase in nonuniformity will be noted at the front rotor. The rear rotor does, however, contribute substantially to the interference over itself. Furthermore, the vertical motion of the rear rotor as a function of angle of attack can increase this interference considerably.

Interference distribution over complete tandem system.- The total interference over the tandem system is, of course, the sum of the effects of the front and rear rotors. Under the assumptions of equality of forces and skew angles, the total interference factors based on the area of one rotor are obtained by direct addition.

Figures 44 to 46 present the total interference distribution over nonoverlapped tandem rotor systems with diameter-width ratios of 0.5, 0.375, and 0.25. Figures 47 to 49 present the corresponding distributions over fully overlapped systems. It is evident in all cases that the total interference at the front rotor is not affected to a large degree by the presence of the rear rotor. On the other hand, in all cases the interference over the rear rotor is substantially worsened, both in overall magnitude and in nonuniformity, by the presence of the front rotor. (Compare with fig. 30.) The interference at the rear rotor is significantly affected by angle of attack and may become impossibly large in some cases of low wake skew angle and large positive angle of attack. For example, equation (60) shows that for $\chi = 60^{\circ}$ and $\alpha = 20^{\circ}$, the local interference velocities near the trailing edge of the rear rotor (when $\sigma_R = 0.5$) are more than $2\frac{1}{2}$ times the basic mean induced velocity of the rotor. Such wind-tunnel interferences are clearly excessive; the validity of data obtained under such conditions is extremely doubtful.

Maximum permissible size of tandem rotors.- The maximum permissible size of a rotor for a wind-tunnel test is largely a function of the type and accuracy of the data that are required. Thus a maximum size cannot be stated explicitly in terms of an absolute value. On the other hand, if the maximum-size rotor that is satisfactory for a similar test is already known, it is possible to draw conclusions as to the relative rotor size that will produce equivalent results in tests of a tandem-rotor system.

Equation (60) has been used to convert the interference factors presented herein to the form $\Delta w_L/w_0$, thereby including the effect of rotor size on the interference velocities. Figures 50 to 53 present the distributions of interference velocity over the rear rotor and compare these distributions with the equivalent distributions for a single rotor. Examination of these figures indicates that, in general, in order to maintain the mean interference velocity and its nonuniformity over the rear rotor at the same levels as would be present in tests of a single rotor, the radii of the rotors comprising the tandem system must be reduced to about one-half to two-thirds of the radius of an acceptable single rotor. Even so, it should be noted that because of the difference in interference between the two rotors (figs. 44 to 49), pitching-moment corrections will still be larger for the tandem system than for the single rotor. Because of the pitching moments, tandem-rotor radii should preferably be chosen at the low end of the aforementioned range; that is, one-half the radius of an acceptable single-rotor model.

CONCLUDING REMARKS

This report presents a superposition method which may be used in conjunction with digital computing equipment to extend, to arbitrary finite configurations, wall interference theories for vanishingly small models, provided that the basic theory is suitable for obtaining the interference at an arbitrary point in the tunnel near an arbitrarily located model. A variety of specific configurations are treated.

Sample numerical results indicate that, aside from the wind-tunnel configuration and proportions, a large number of variables may individually or collectively produce substantial effects on wind-tunnel interference. Items that should be considered are configuration, wake deflection, model location, span of wing and tail, load distribution, wing sweep, angle of attack, pivot location, and tail length and height.

In many complex configurations it may be necessary to install auxiliary balances to measure the forces produced by the individual components in order to correct the data. Inconsistencies, particularly with respect to pitching moments, may still result if available theories are not adequate to evaluate the effect of nonuniformities in wall interference on the characteristics of the model.

The rear rotor of a tandem-rotor system experiences significantly greater interference and nonuniformity of interference than a single rotor. To achieve results for tandem systems equivalent to those for a single rotor, the diameter of the rotors making up the tandem system should be about half the diameter of an acceptable single rotor.

Langley Research Center,
National Aeronautics and Space Administration,
Langley Station, Hampton, Va., September 4, 1968,
721-01-00-20-23.

APPENDIX

PROOF THAT AVERAGE INTERFERENCE OVER A WING IS INDEPENDENT OF WING SWEEP

In linearized theory, to the extent that a wing may be represented as a lifting line, the wing may be represented either as a swept bound vortex with trailing vortices (sketch (a)) or as an assemblage of small rectilinear horseshoe vortices (sketch (b)). The exactitude of the latter representation depends only upon the number of elemental rectilinear vortices chosen; a one-to-one correspondence is obtained when an infinite number of rectilinear vortices of zero span is used.

Consider the latter representation when the angle of attack is zero and the wake is undeflected (that is, the wake passes directly rearward). The assemblage of rectilinear horseshoe vortices comprising the swept wing can equally well be considered as a fixed

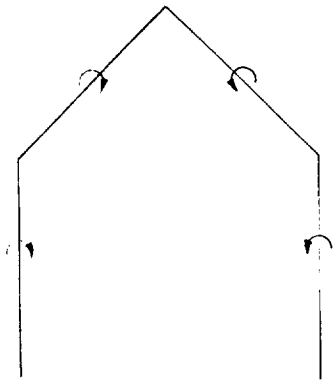

Sketch (a)

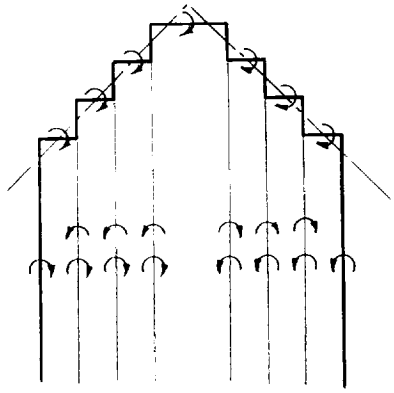

Sketch (b)

formation of independent wings flying together. Provided only that the load distribution between the wings remains fixed, Munk (ref. 7) has already shown that the total power (or induced velocity) is independent of the streamwise location of the many small wings. Thus, the first result is that the total induced velocity of the system in free air is independent of sweep.

Now assume that the wind-tunnel walls can be completely represented by an image system external to the walls (sketch (c)) and that a finite solution exists for the interference occasioned by the walls. It is observed that the total induced velocity of the entire image system, including the real model, is (by Munk's stagger theorem) independent of wing sweep. Furthermore, since the repetition pattern of the images is infinite in both directions, the total induced velocity over any image is identical to that over any other image, is finite (or the assumed solution would not exist), and is independent of sweep.

(Or, if images of opposite sense exist, all images of the same sense have the same interference, independent of sweep.)

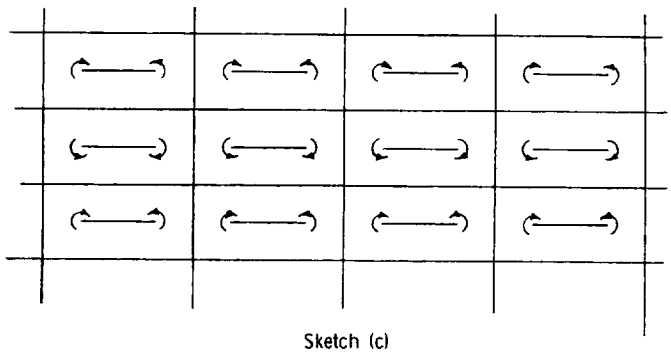

Sketch (c)

The wall interference is the difference between the induced velocity of the wing in the tunnel (which is identical to any one of the images) and the induced velocity in free air. Since both of these induced velocities are independent of wing sweep, the wall-induced interference velocity is also independent of wing sweep.

Consider now some angle of attack other than zero, but with the wake still passing directly rearward. The lifting lines for various swept wings, which are the loci of the rectilinear elements comprising the wing, appear as in sketch (d) when viewed from behind. Note that the vertical position of any point on the wing has become a function of the sweep angle so that Munk's stagger theorem, which does not allow vertical translation of the elements, does not apply. On the other hand, provided that the product $(\sin \alpha)(\tan \Lambda)$ is constant, the wings will have the same streamwise projection. Thus, if $(\sin \alpha)(\tan \Lambda)$ is constant, the wall interference will be independent of sweep.

If the wake is deflected downward, the wake in the tunnel and the image directly beneath the tunnel appear as in sketch (e). Note that the vertical heights of the elements in planes transverse to the stream will vary with the downstream location of the plane. Thus, Munk's theorem cannot be used to prove independence of sweep under such conditions.

It should be noted that complete representation by an external image system is required for the proof. Certain tunnels, such as the circular tunnel, can only be satisfactorily represented by an external image system in the Trefftz plane (ref. 12). Such cases are excluded from the present proof.

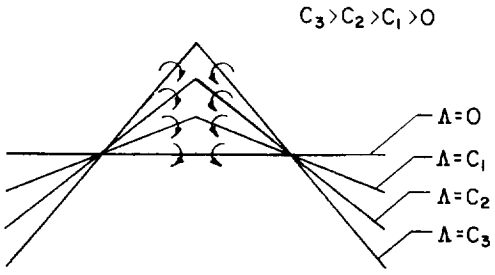

Sketch (d)

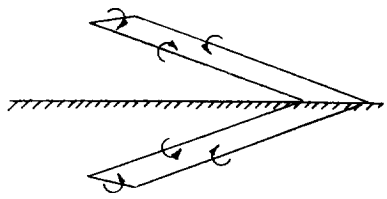

Sketch (e)

APPENDIX

Slotted wind tunnels cannot, in general, be represented by external image systems. On the other hand, reference 13 shows that under certain restrictive assumptions the interference in a slotted tunnel can be represented as a combination of the interferences with the walls both completely closed and completely open. Thus it might be surmised that the interference in slotted tunnels is at least relatively independent of sweep.

It should be emphasized that Munk's stagger theorem refers only to the total or the average interference. It cannot be extended to the distribution of interference or to the interference at an arbitrary point such as at a tail. Indeed, the numerical results presented in the body of this paper indicate significant differences caused by wing sweep.

REFERENCES

1. Garner, H. C.; Rogers, E. W. E.; Acum, W. E. A.; and Maskell, E. C.: Subsonic Wind Tunnel Wall Corrections. AGARDograph 109, 1966.

2. Heyson, Harry H.: Linearized Theory of Wind-Tunnel Jet-Boundary Corrections and Ground Effect for VTOL-STOL Aircraft. NASA TR R-124, 1962.

3. Heyson, Harry H.: Jet-Boundary Corrections for Lifting Rotors Centered in Rectangular Wind Tunnels. NASA TR R-71, 1960.

4. Heyson, Harry H.; and Katzoff, S.: Induced Velocities Near A Lifting Rotor With Nonuniform Disk Loading. NACA Rep. 1319, 1957. (Supersedes NACA TN 3690 by Heyson and Katzoff and TN 3691 by Heyson.)

5. Heyson, Harry H.: FORTRAN Programs for Calculating Wind-Tunnel Boundary Interference. NASA TM X-1740, 1969.

6. Heyson, Harry H.; and Grunwald, Kalman, Jr.: Wind-Tunnel Boundary Interference for V/STOL Testing. Conference on V/STOL and STOL Aircraft, NASA SP-116, 1966, pp. 409-434.

7. Munk, Max M.: The Minimum Induced Drag of Aerofoils. NACA Rep. 121, 1921.

8. Heyson, Harry H.: Equations for the Application of Wind-Tunnel Wall Corrections to Pitching Moments Caused by the Tail of an Aircraft Model. NASA TN D-3738, 1966.

9. Wheatley, John B.: An Aerodynamic Analysis of the Autogiro Rotor With a Comparison Between Calculated and Experimental Results. NACA Rep. 487, 1934.

10. Sweet, George E.: Static-Stability Measurements of a Stand-On Type Helicopter With Rigid Blades, Including a Comparison With Theory. NASA TN D-189, 1960.

11. Heyson, Harry H.: Nomographic Solution of the Momentum Equation for VTOL-STOL Aircraft. NASA TN D-814, 1961. (Also available as "V/STOL Momentum Equation," Space/Aeron., vol. 38, no. 2, July 1962, pp. B-18 – B-20.)

12. Lotz, Irmgard: Correction of Downwash in Wind Tunnels of Circular and Elliptic Sections. NACA TM 801, 1936.

13. Davis, Don D., Jr.; and Moore, Dewey: Analytical Study of Blockage- and Lift-Interference Corrections for Slotted Tunnels Obtained by the Substitution of an Equivalent Homogeneous Boundary for the Discrete Slots. NACA RM L53E07b, 1953.

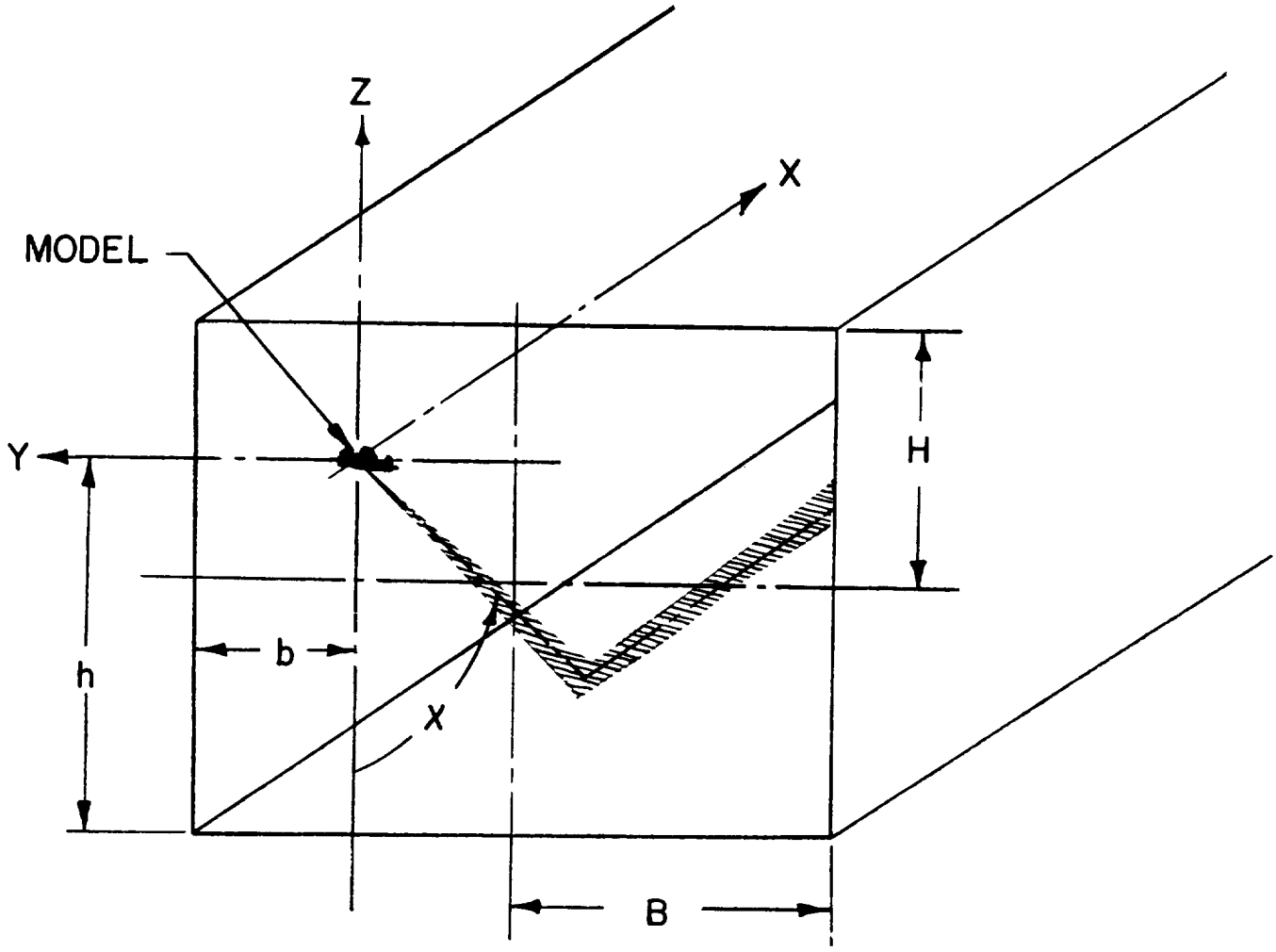

Figure 1.- Geometric arrangement of vanishingly small model (or elemental wake) in wind tunnel.

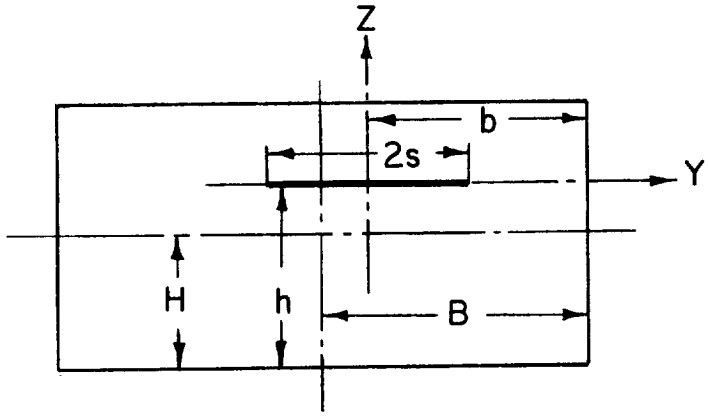

(a) View upstream in tunnel.

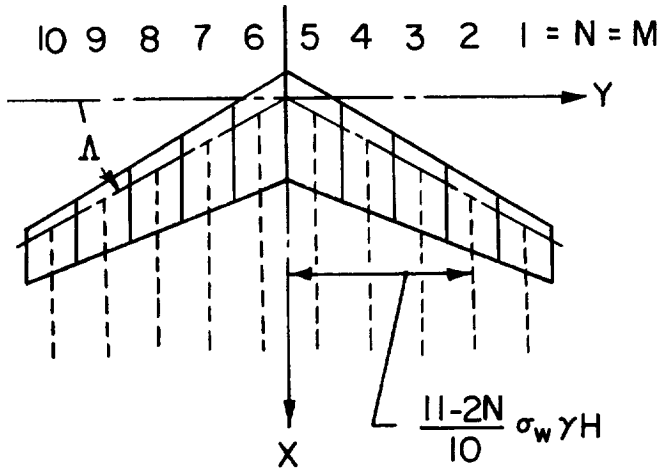

(b) Plan view.

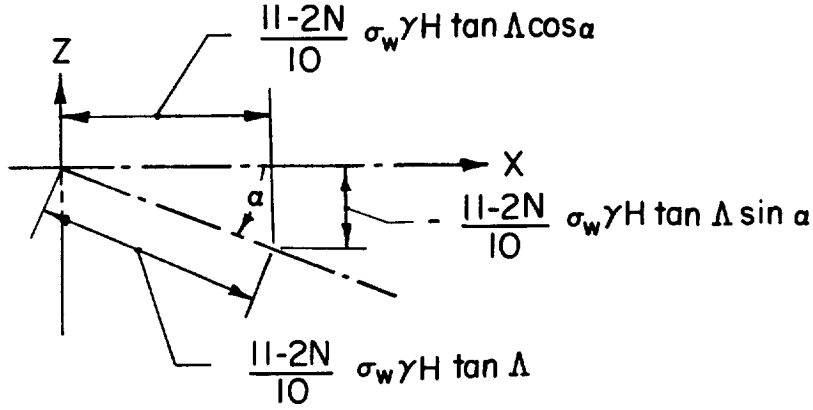

(c) Side view.

Figure 2.- Geometric arrangement of swept wing. Note that wing is represented only by the lifting line.

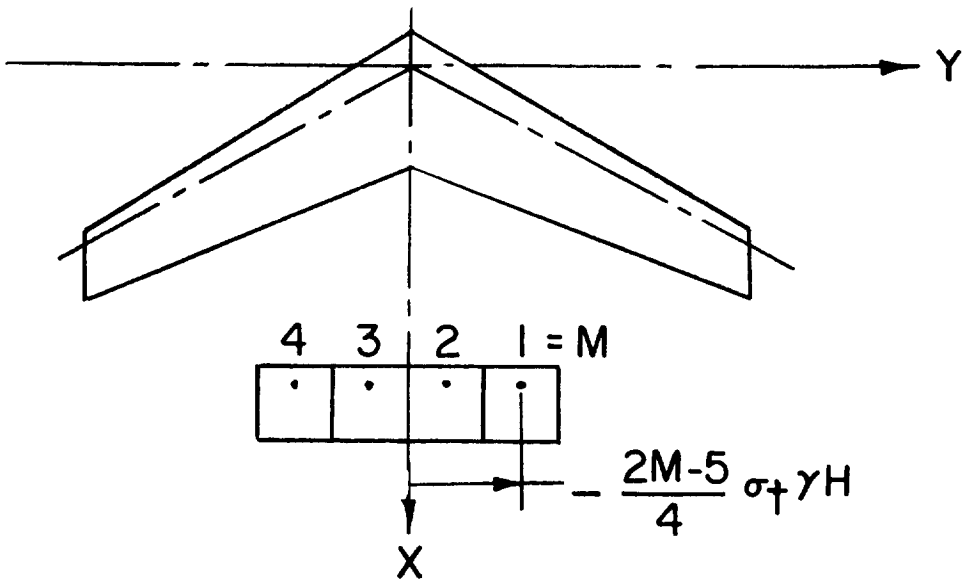

(a) Plan view.

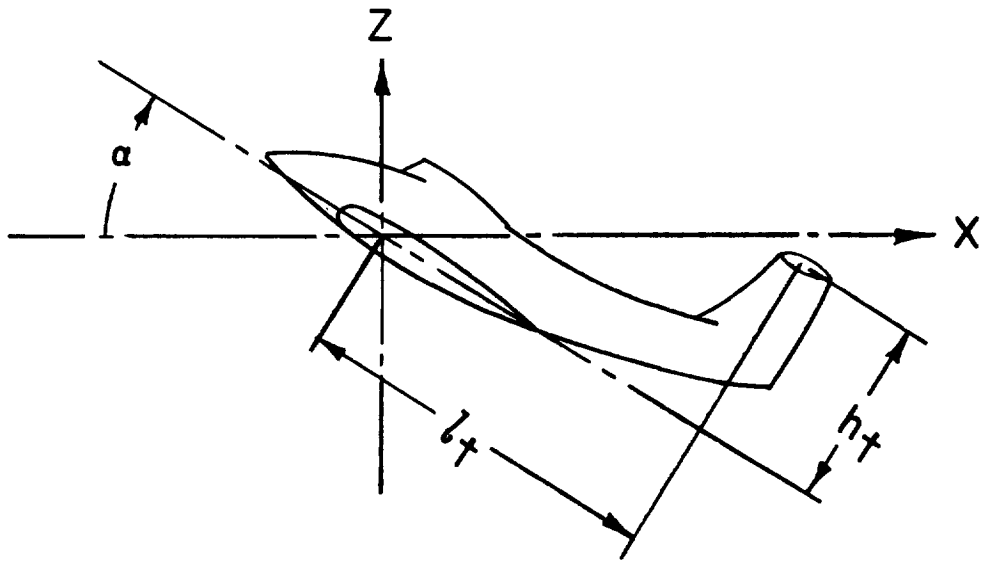

(b) Side view.

Figure 3.- Geometric arrangement of tail behind swept wing.

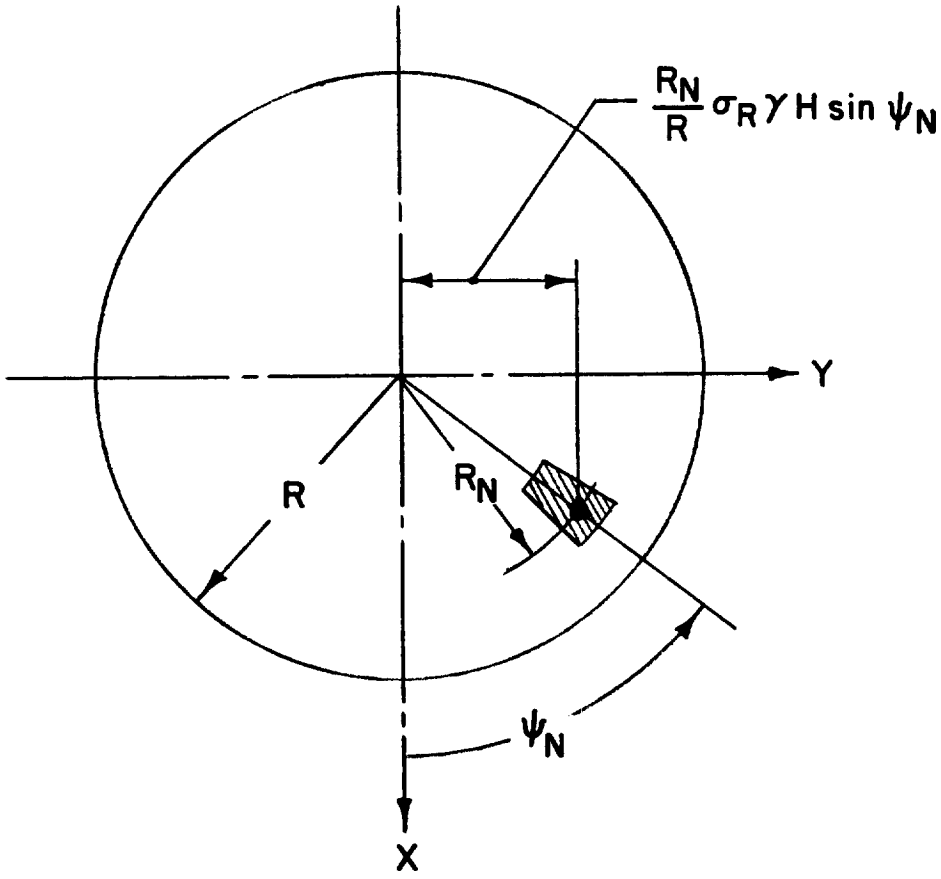

(a) Plan view.

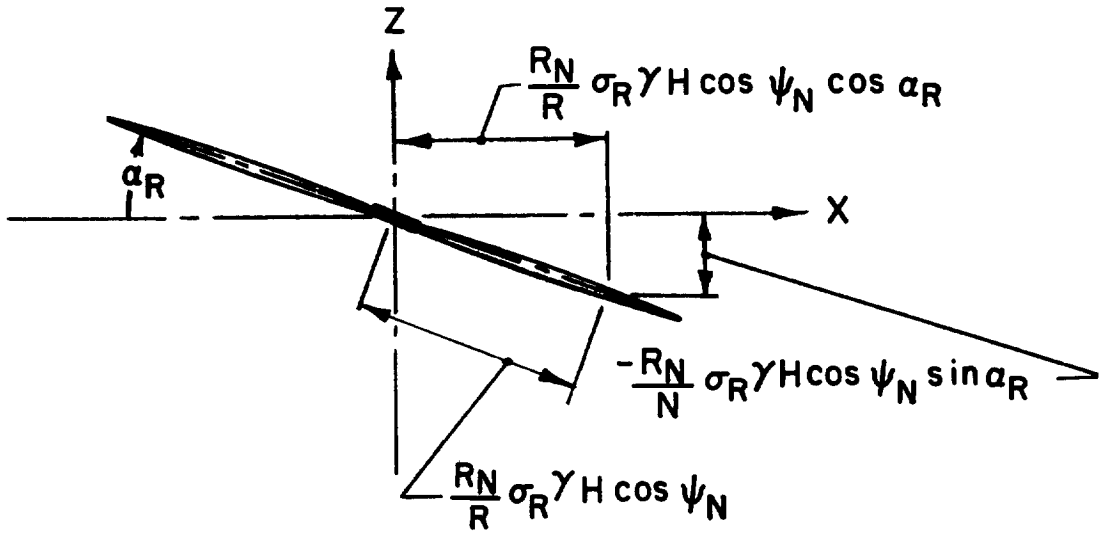

(b) Side view.

Figure 4.- Geometric arrangement of rotor or propeller.

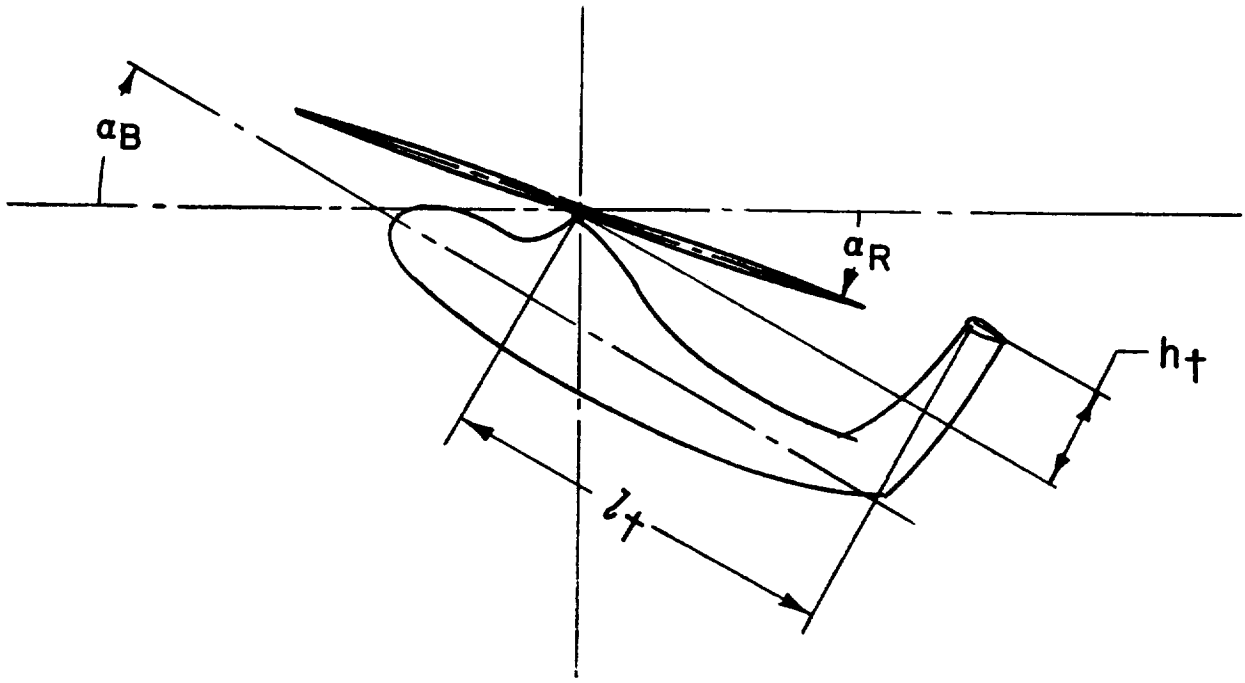

Figure 5.- Geometric arrangement of tail behind rotor.

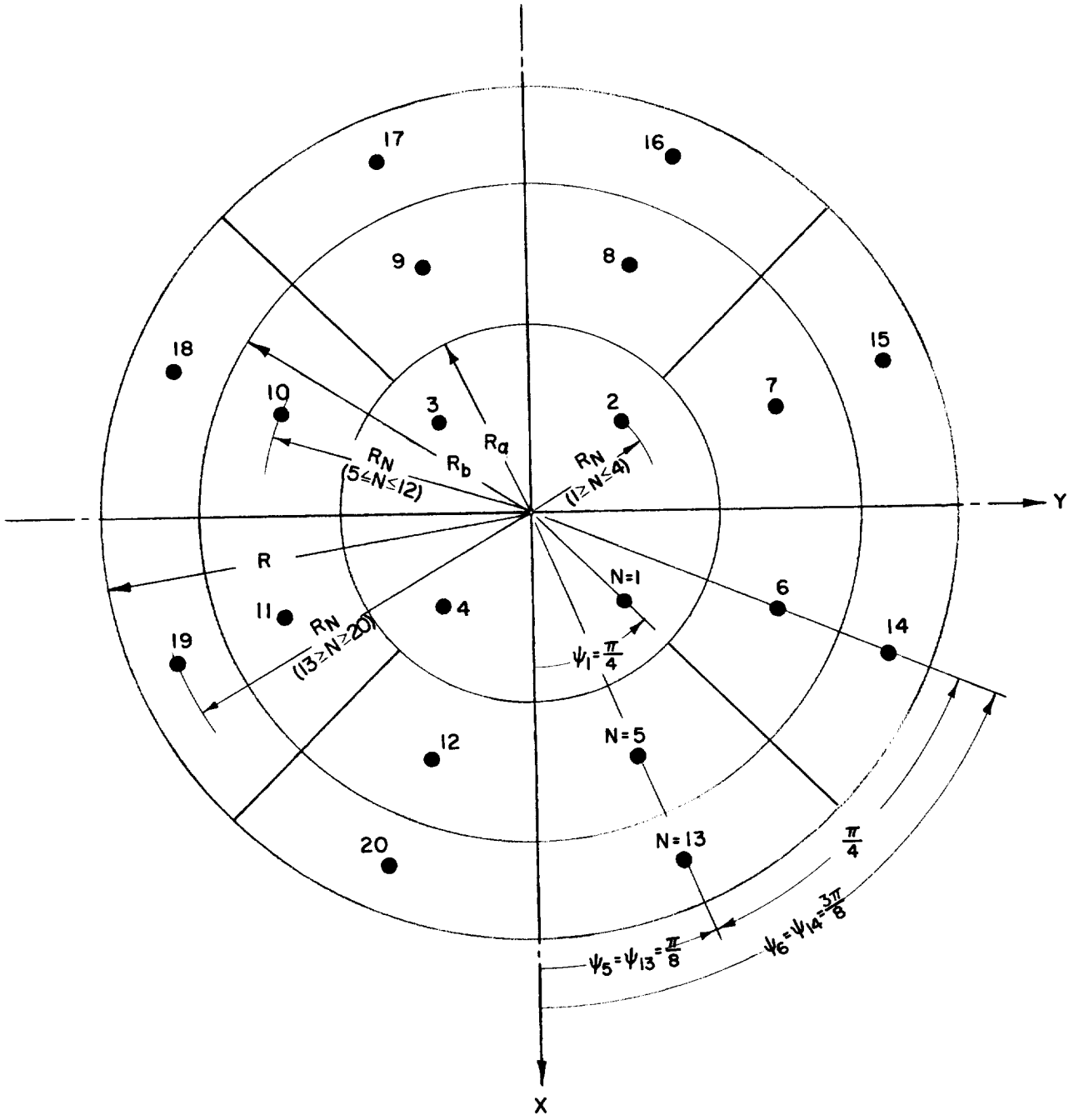

Figure 6.- Sketch illustrating selection and distribution of wake origins and control points for rotor.

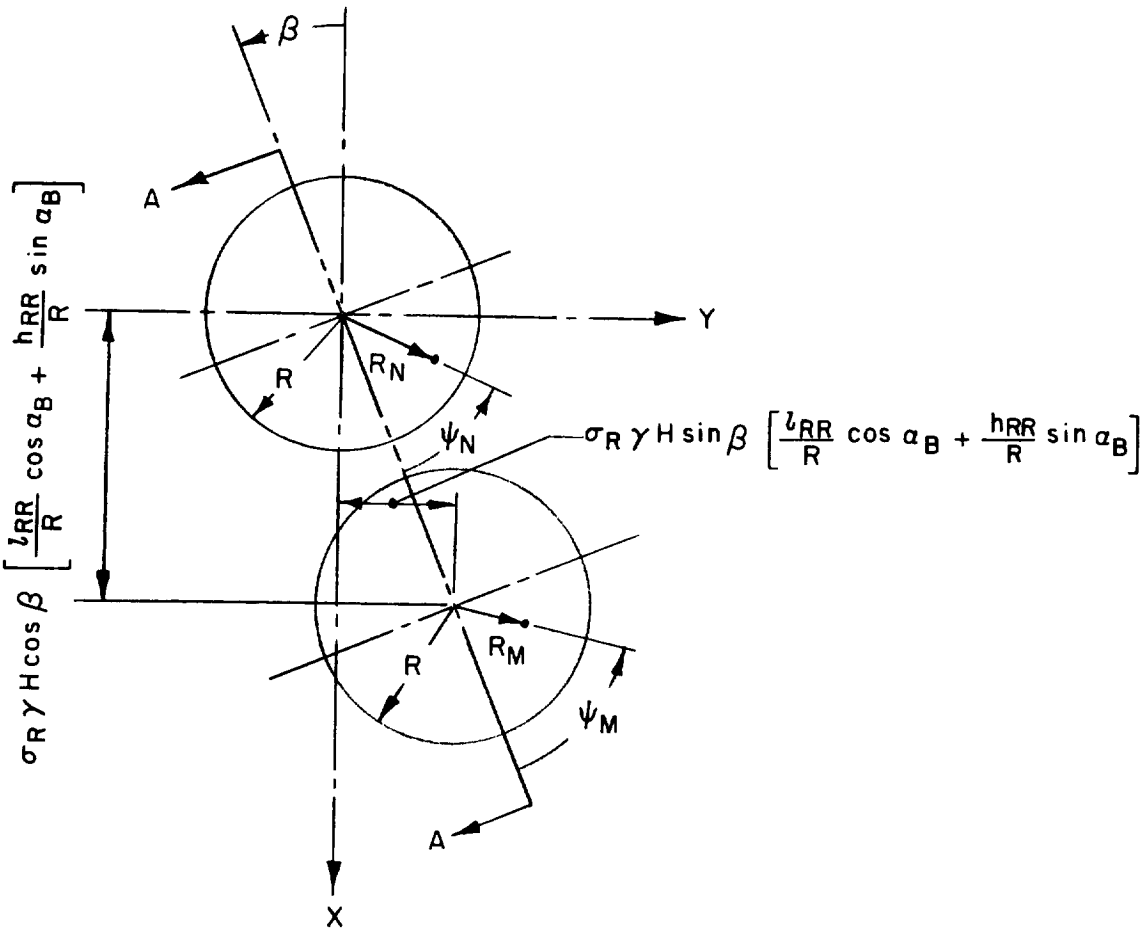

(a) Plan view.

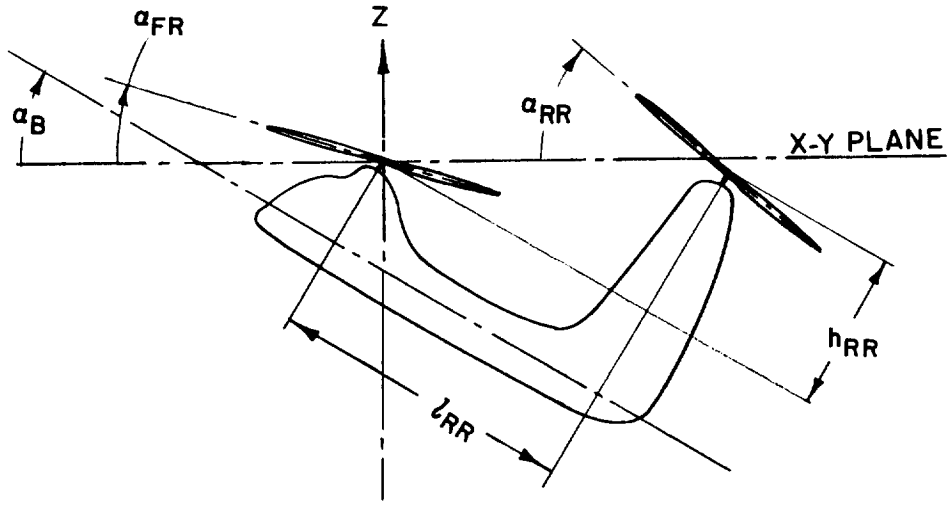

(b) View A-A.

Figure 7.- Geometric arrangement of yawed tandem-rotor system.

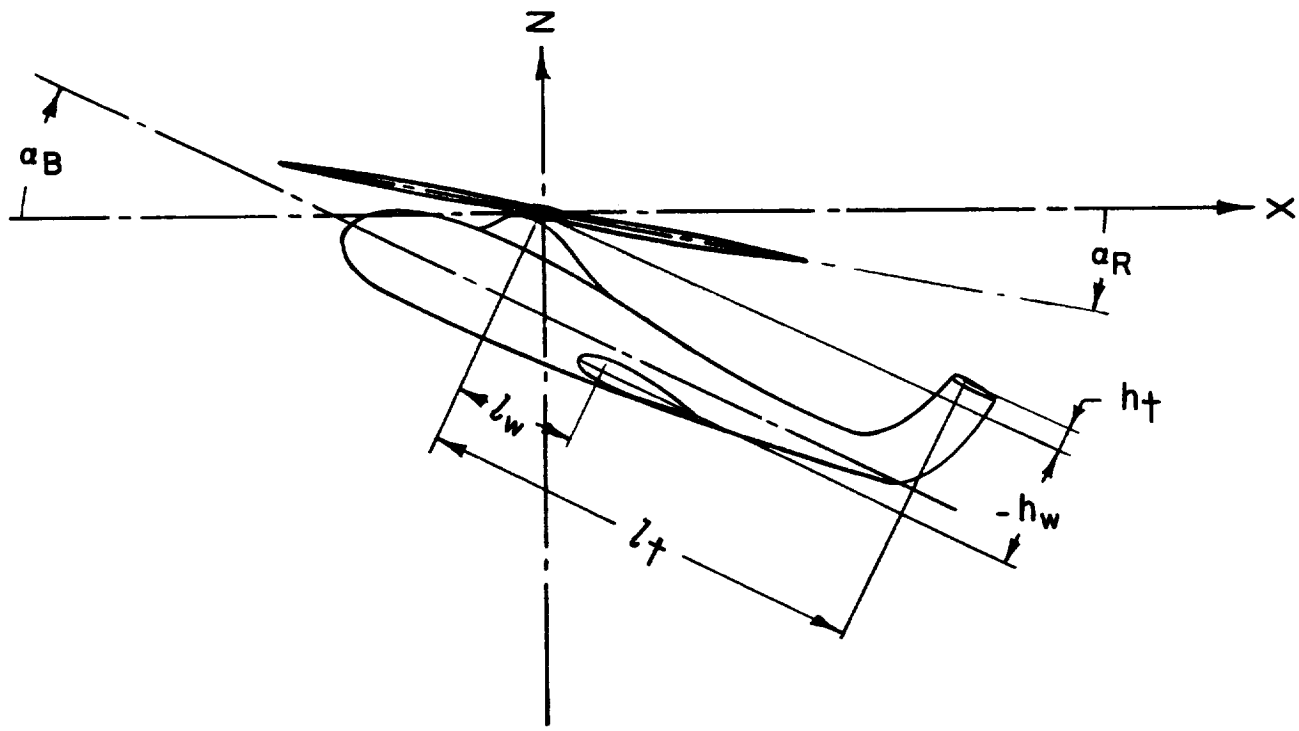

Figure 8.- Geometric arrangement of unloaded-rotor system.

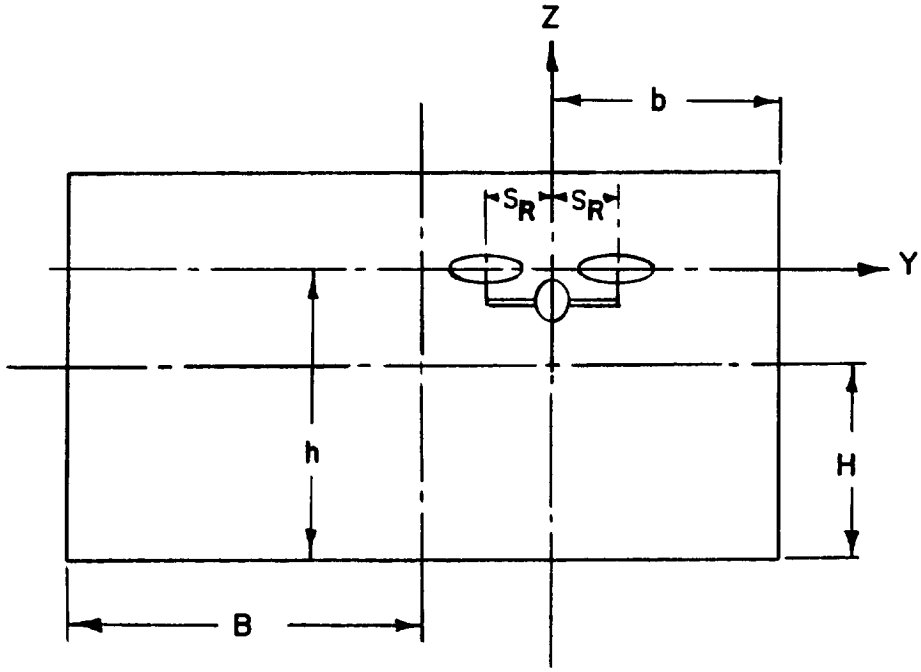

(a) Upstream view in tunnel.

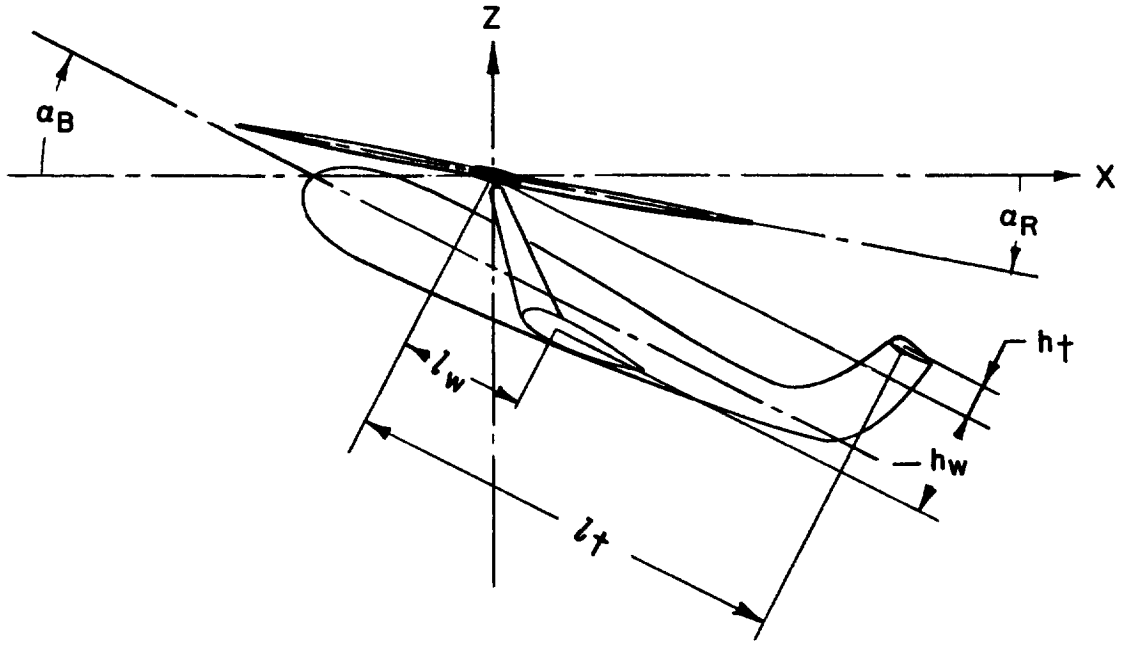

(b) Side view.

Figure 9.- Geometric arrangement of side-by-side and tilt rotor configurations.

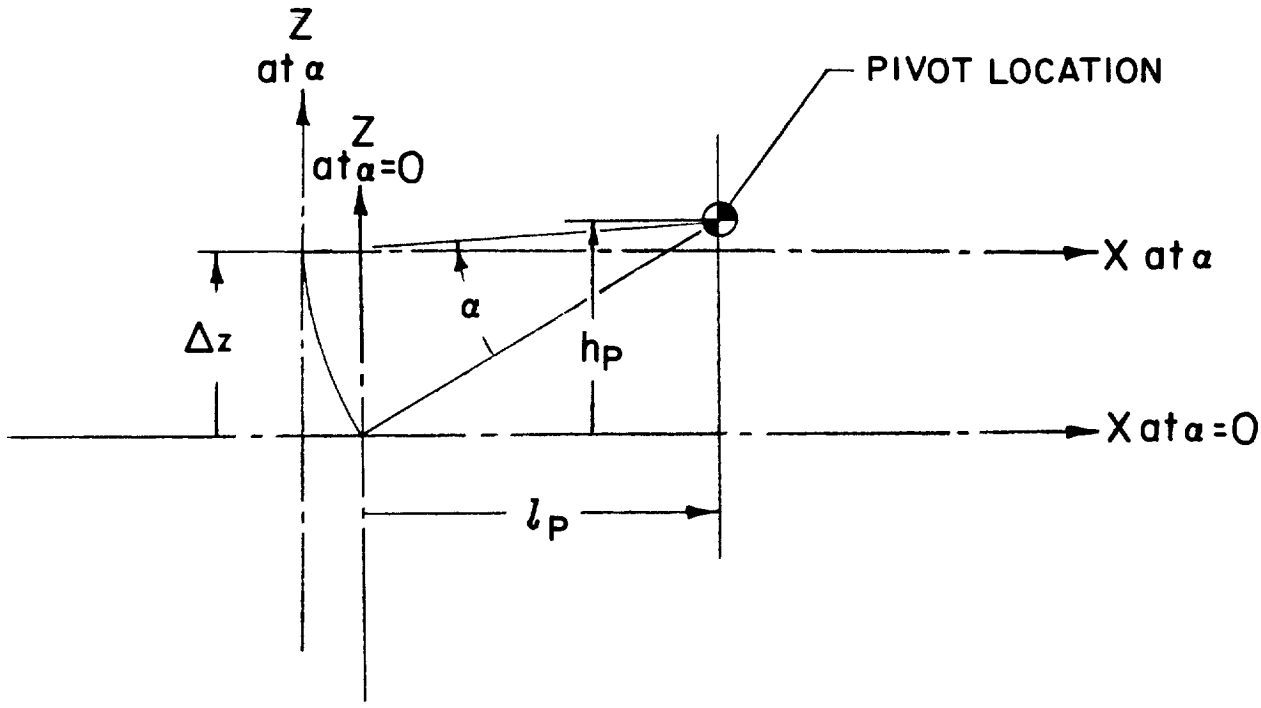

Figure 10.- Sketch for determining effect of pivot location when displaced from nominal origin.

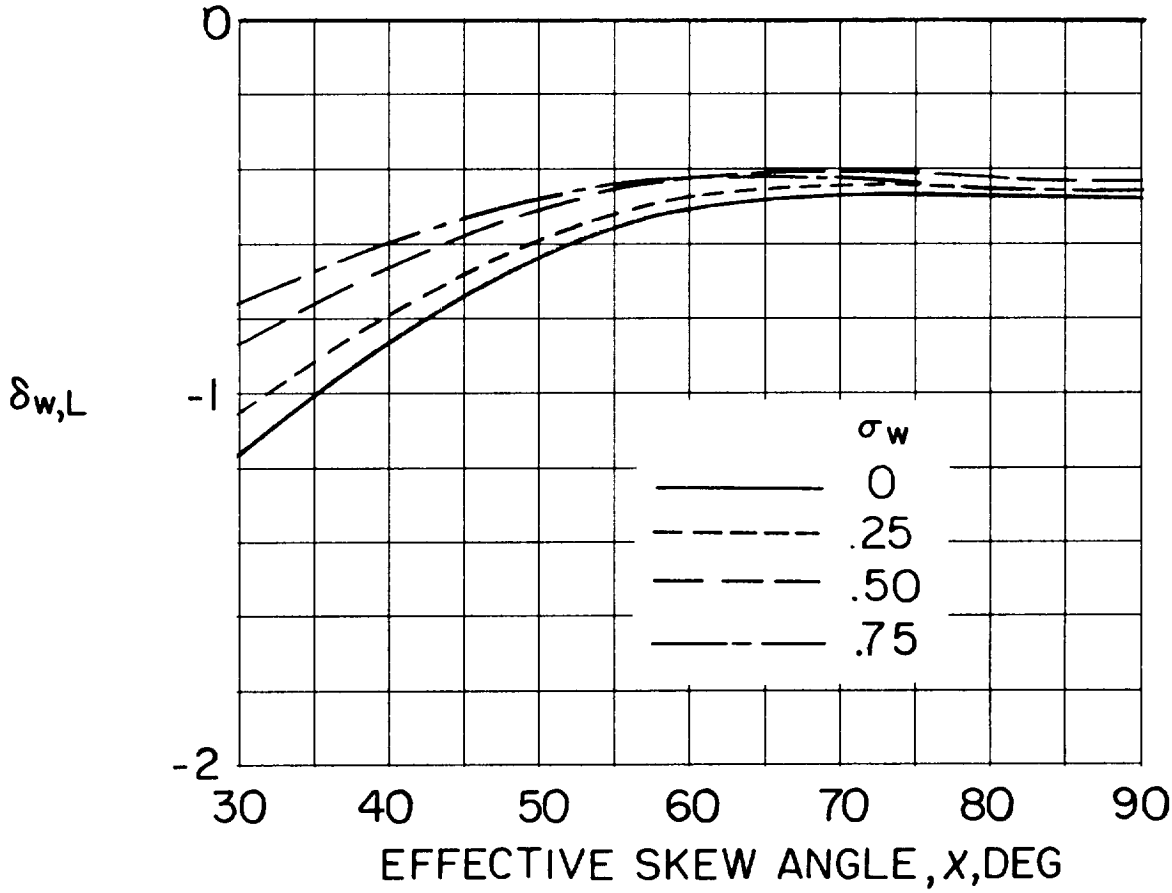

Figure 11.- Effect of span-width ratio on average interference factor for unswept wings centered in a closed tunnel. $\gamma = 1.5$; uniform load distribution.

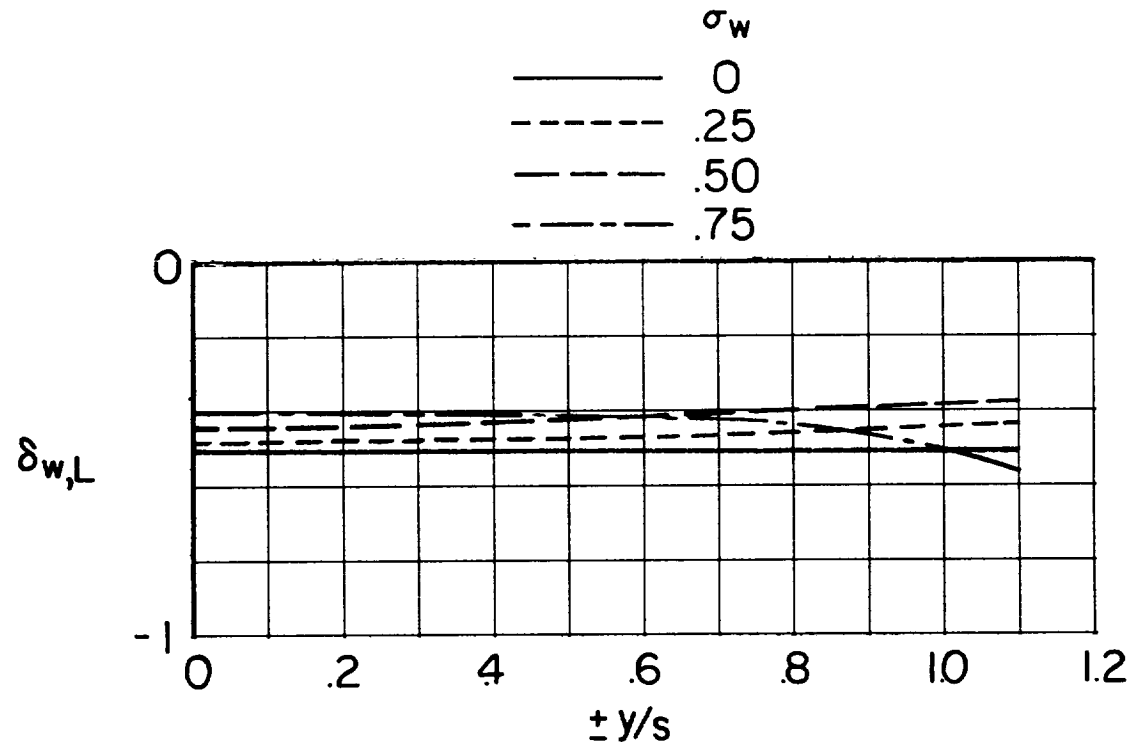

(a) $\chi = 60^0$.

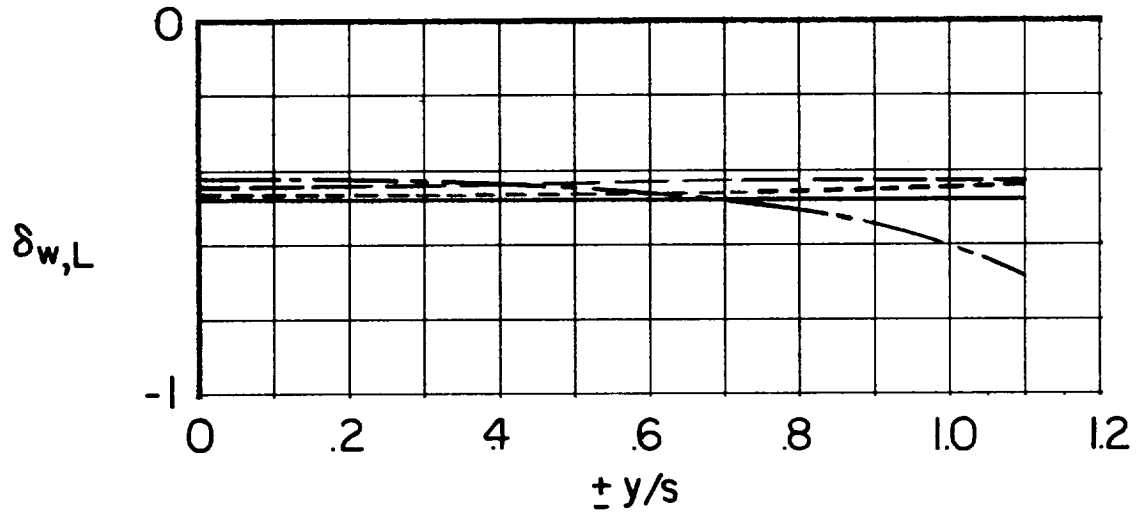

(b) $\chi = 90^0$.

Figure 12.- Effect of span-width ratio on distribution of interference factor over unswept wings centered in a closed tunnel. $\gamma = 1.5$; uniform load distribution.

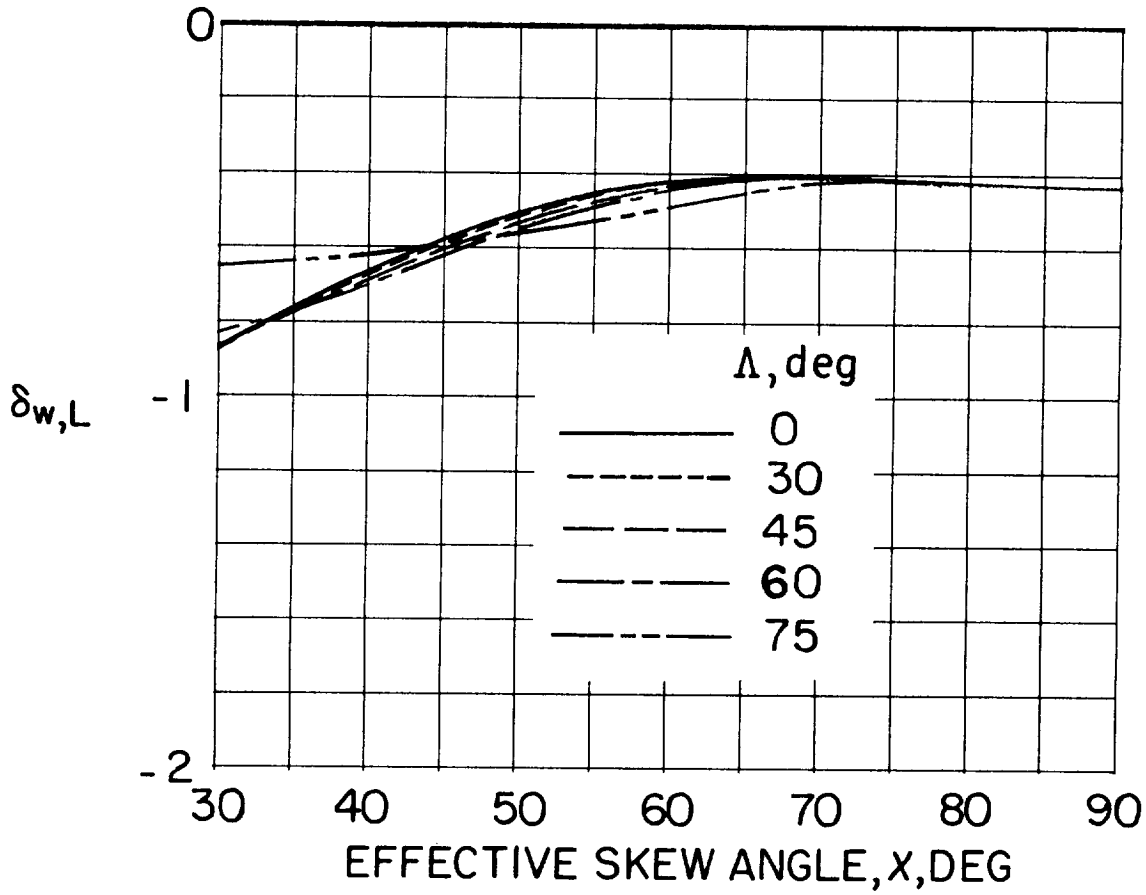

Figure 13.- Effect of wing sweep on average interference factor for wings with aerodynamic center at center of closed tunnel. $\gamma = 1.5$; $\sigma_w = 0.5$; $\alpha = 0^0$; uniform load distribution.

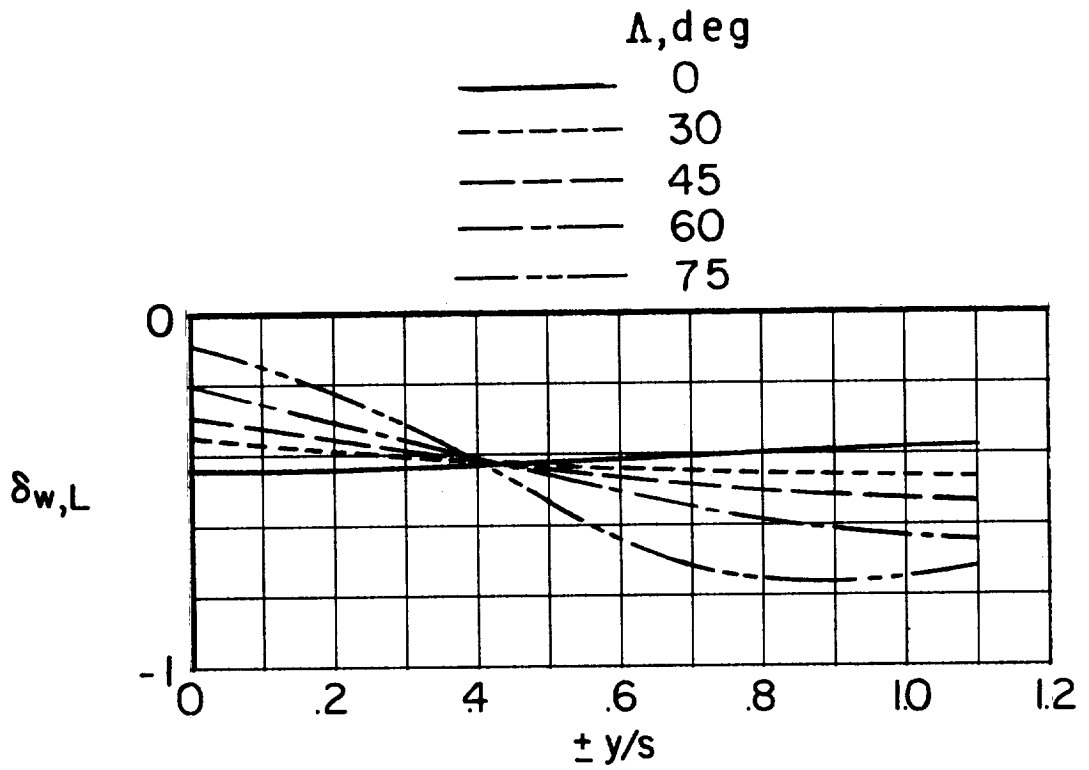

(a) $\chi = 60^0$.

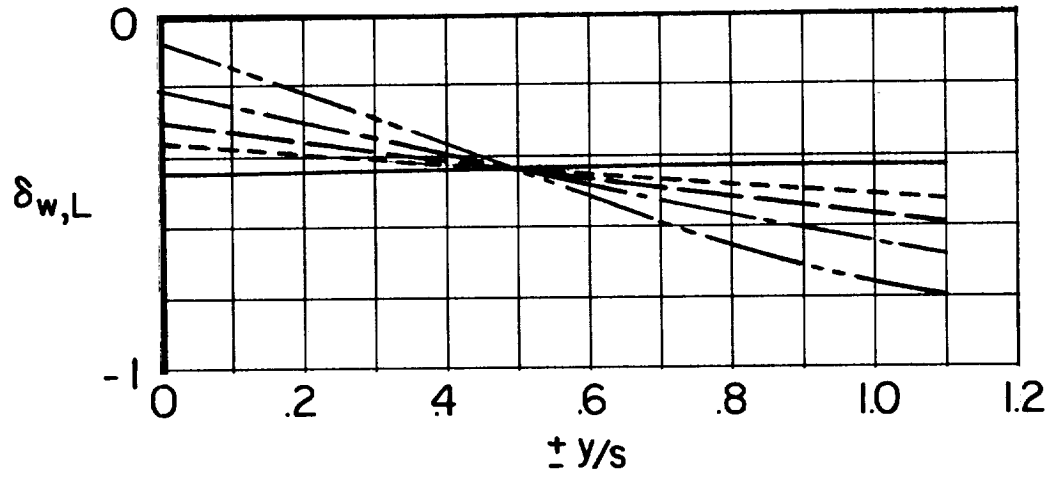

(b) $\chi = 90^0$.

Figure 14.- Effect of wing sweep on distribution of interference factor over wings with aerodynamic center at center of closed tunnel. $\gamma = 1.5$; $\sigma_w = 0.5$; $\alpha = 0^0$; uniform load distribution.

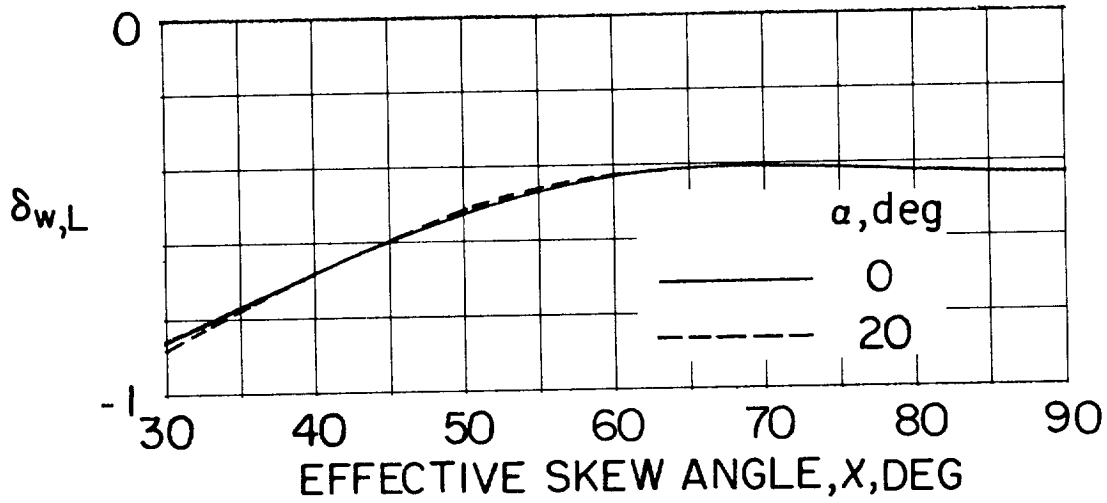

(a) $\Lambda = 45^0$.

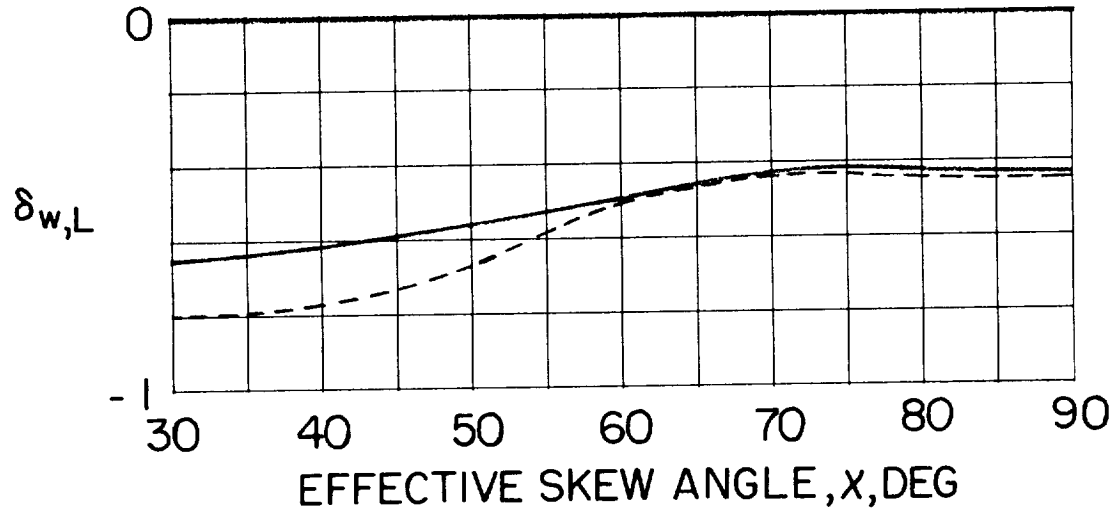

(b) $\Lambda = 75^0$.

Figure 15.- Effect of angle of attack on average interference factor for wings with aerodynamic center at center of closed tunnel. (Angle of attack has no effect on the average interference over unswept ($\Lambda = 0^0$) wings.) $\gamma = 1.5$; $\sigma_w = 0.5$; uniform load distribution.

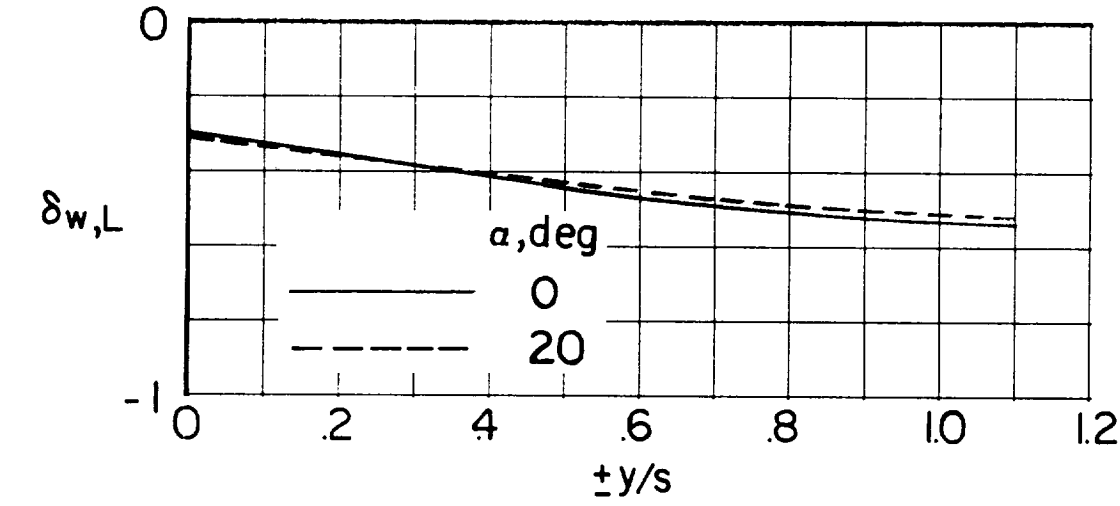

(a) $\chi = 60^0$.

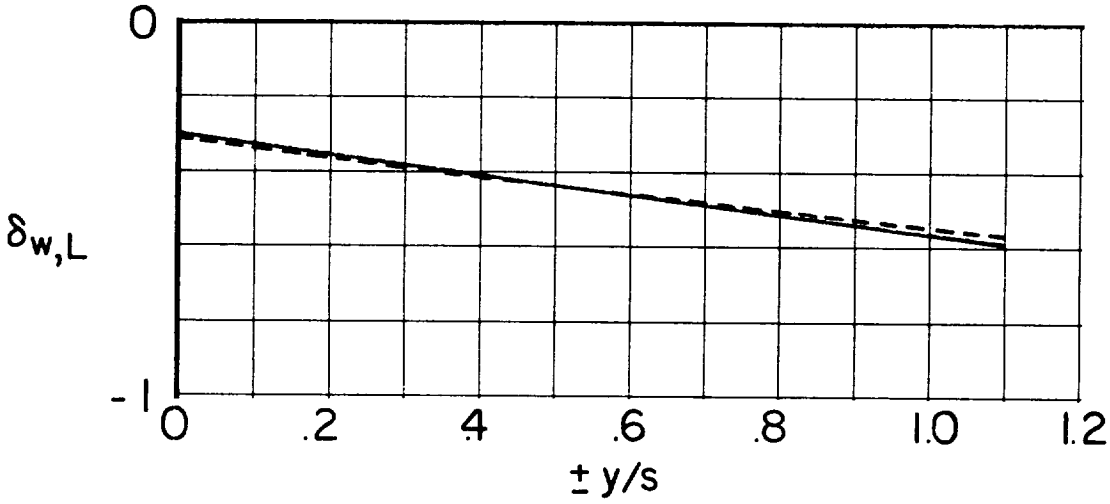

(b) $\chi = 90^0$.

Figure 16.- Effect of angle of attack on distribution of interference factor over a 45^0 swept wing with aerodynamic center at center of closed tunnel. (Angle of attack has no effect on distribution of interference over unswept ($\Lambda = 0^0$) wings.) $\gamma = 1.5$; $\sigma_w = 0.5$; uniform load distribution.

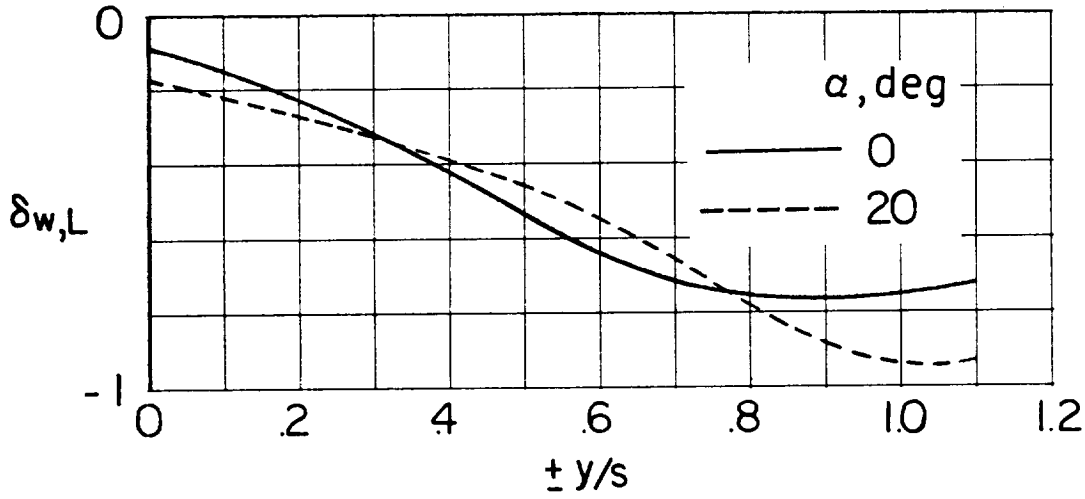

(a) $\chi = 60^0$.

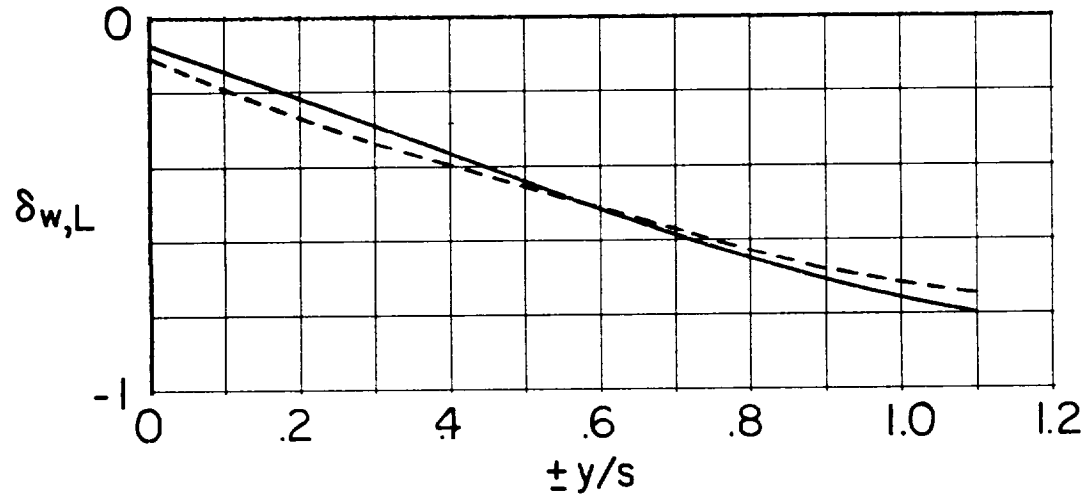

(b) $\chi = 90^0$.

Figure 17.- Effect of angle of attack on distribution of interference factor over a 75^0 swept wing with aerodynamic center at center of closed tunnel. $\gamma = 1.5$; $\alpha_w = 0.5$; uniform load distribution.

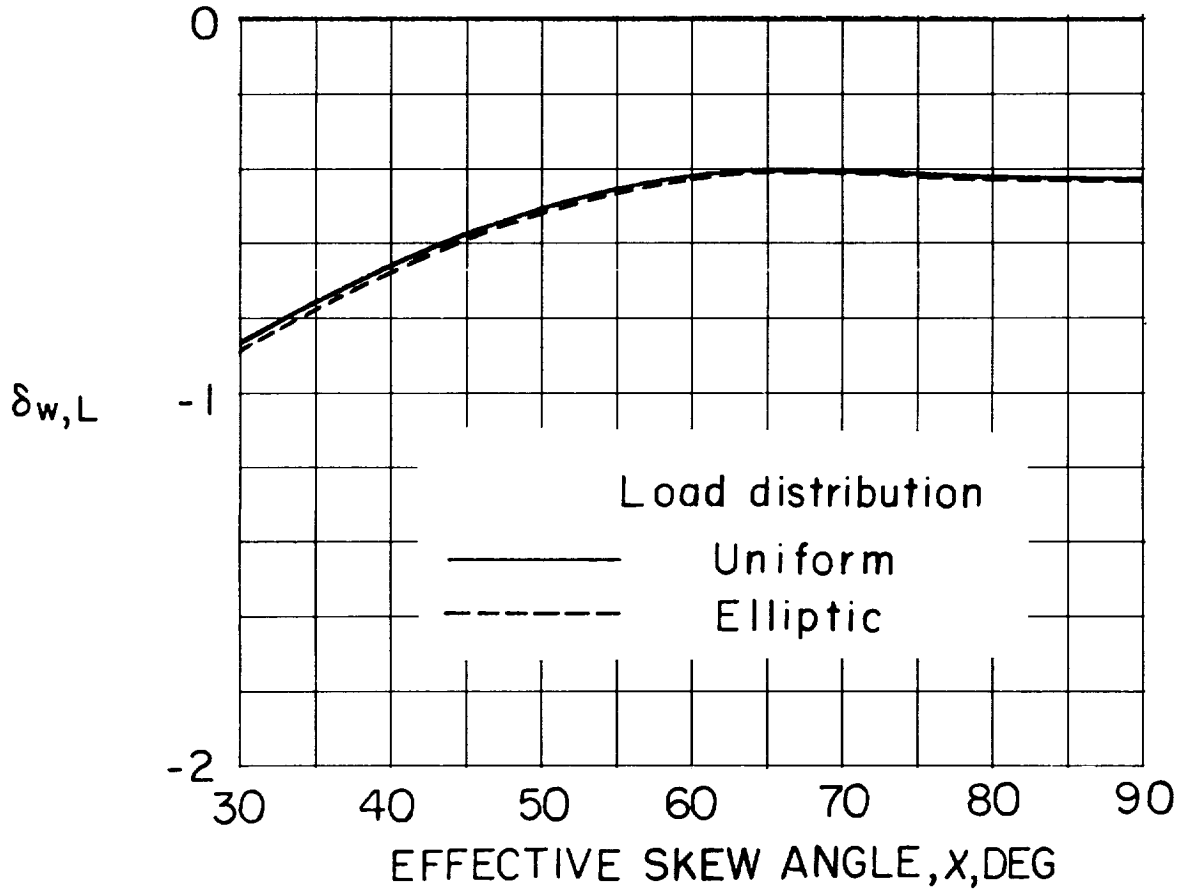

Figure 18.- Effect of load distribution on average interference factor for an unswept wing centered in closed tunnel. $\gamma = 1.5$; $\alpha_w = 0.5$.

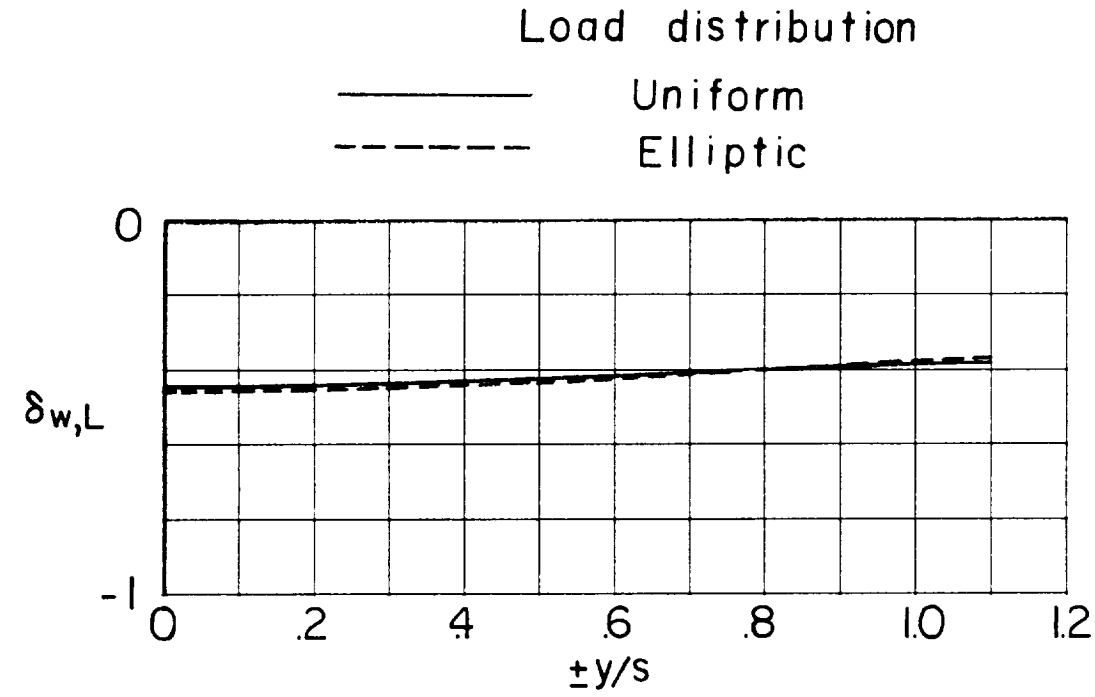

(a) $\chi = 60^0$.

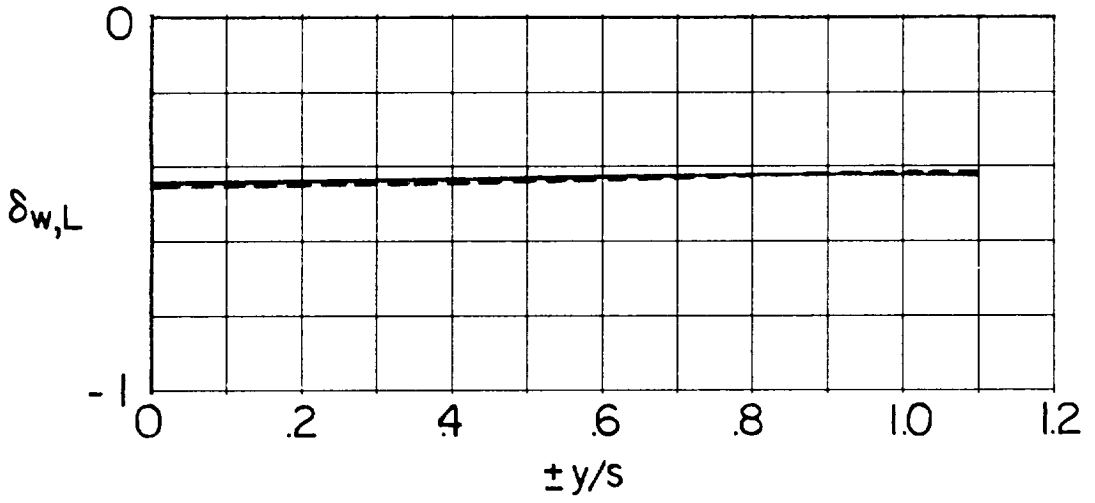

(b) $\chi = 90^0$.

Figure 19.- Effect of load distribution on distribution of interference factors over an unswept wing centered in a closed tunnel. $\gamma = 1.5$; $\sigma_w = 0.5$.

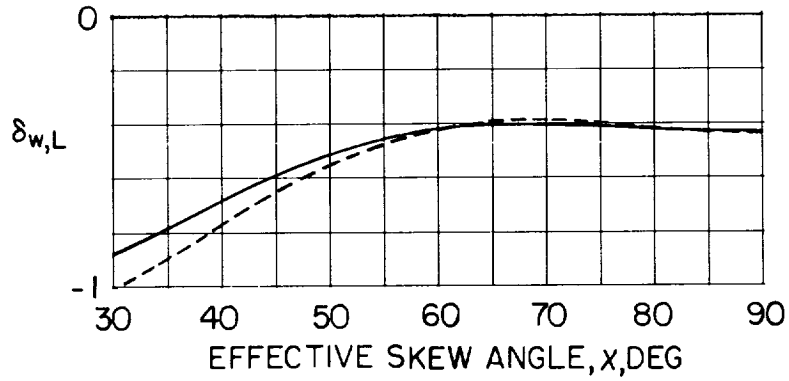

(a) $\Lambda = 45^0$.

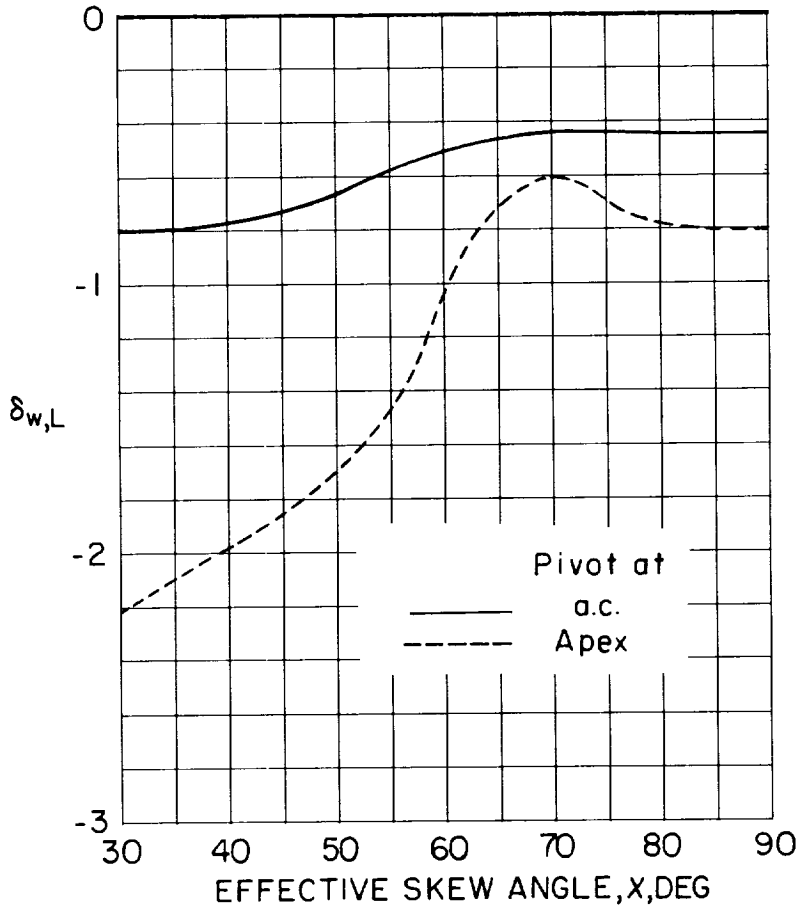

(b) $\Lambda = 75^0$.

Figure 20.- Effect of pivot-point location on average interference factor for swept wings with different pivot points. Pivot is at center of closed tunnel. $\gamma = 1.5$; $\sigma_w = 0.5$; $\alpha = 20^0$; uniform load distribution.

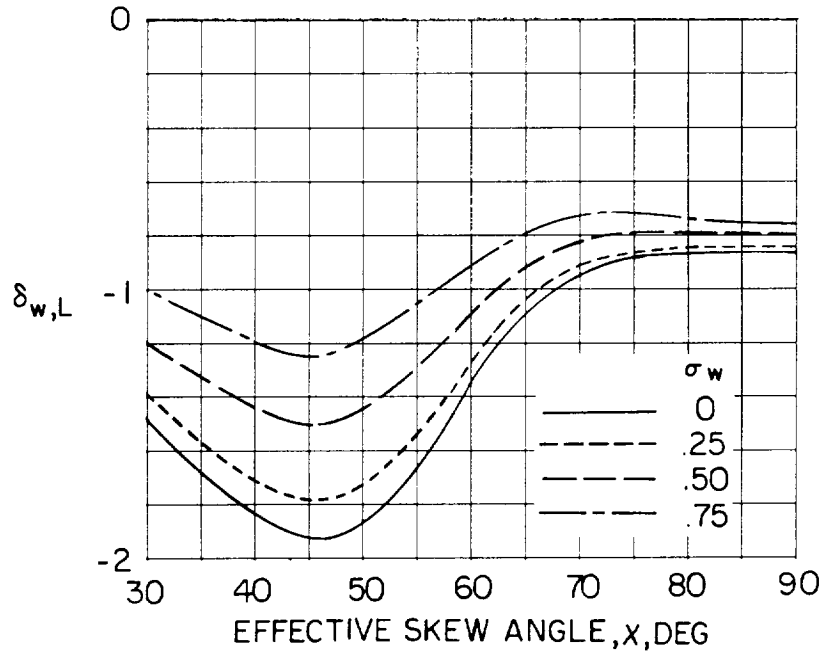

(a) $\frac{l_t}{H} = 1.0$.

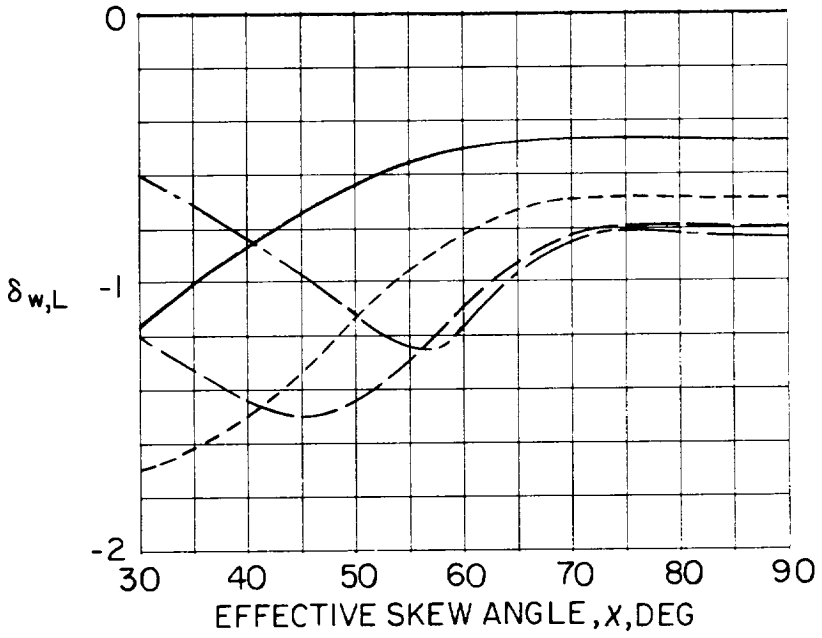

(b) $\frac{l_t}{2s} = \frac{2}{3}$.

Figure 21.- Effect of span-width ratio of wing on interference factor at a zero-span tail. Wing centered in closed tunnel; $\gamma = 1.5$; $\Lambda = 0^0$; $\alpha = 0^0$; $\frac{h_t}{H} = 0$; uniform wing-load distribution.

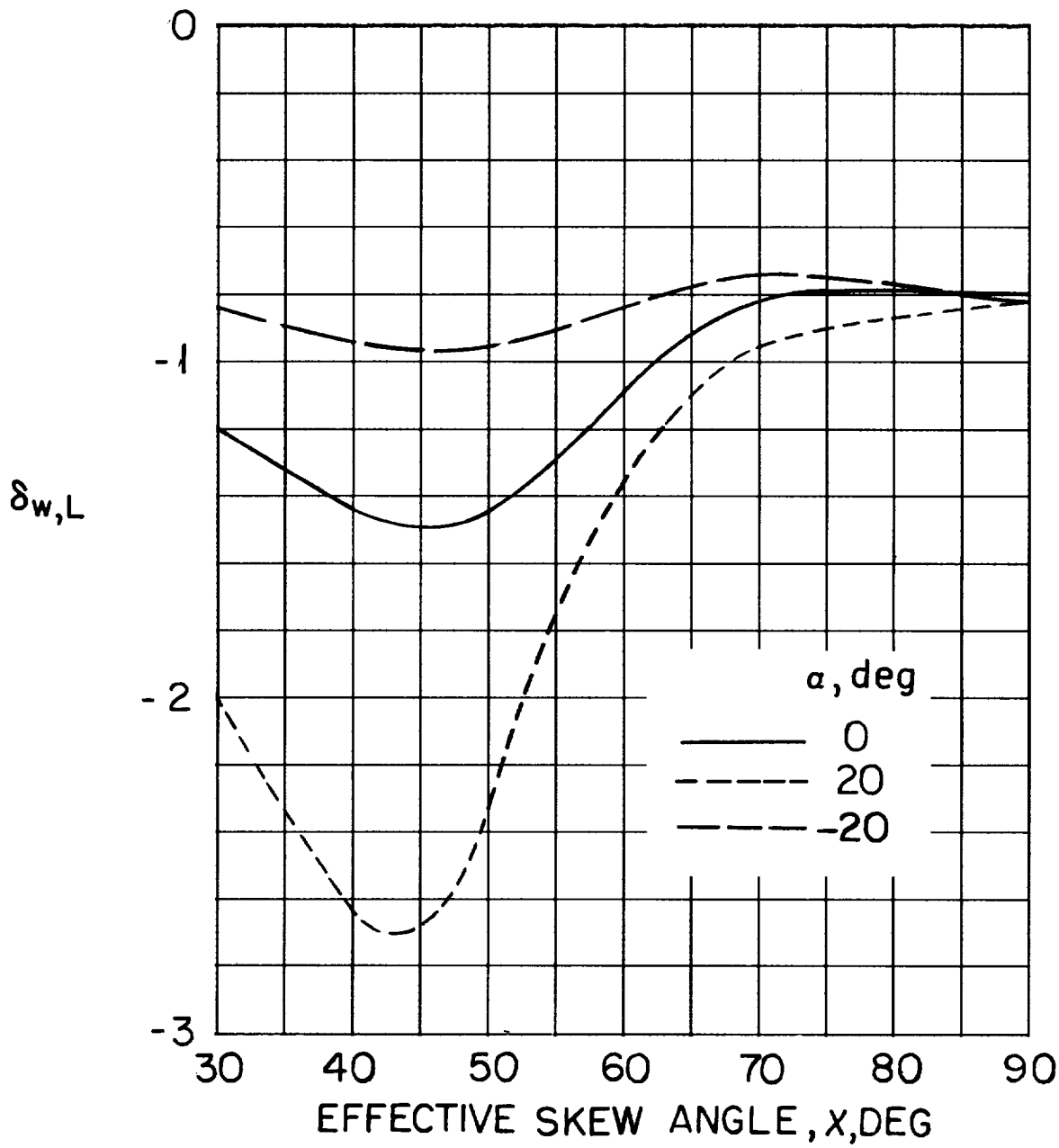

Figure 22.- Effect of angle of attack on interference factor at a zero-span tail. Unswept wing centered in closed tunnel; $\gamma = 1.5$; $\sigma_w = 0.5$; $\frac{l_t}{H} = 1.0$ $\left(\frac{l_t}{2s} = \frac{2}{3}\right)$; $\frac{h_t}{H} = 0$; uniform wing-load distribution.

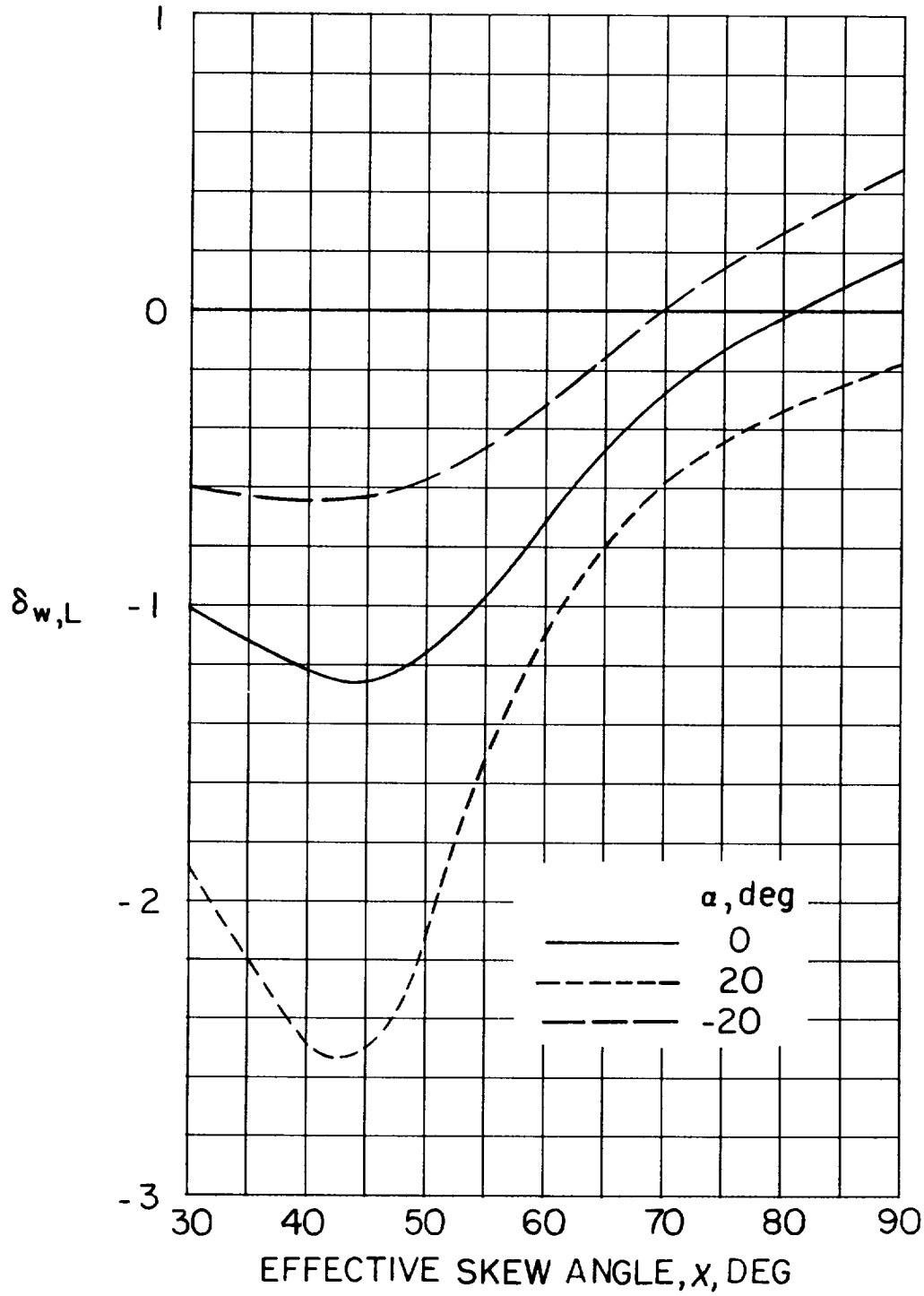

Figure 23.- Effect of angle of attack on interference factor at a zero-span tail. Unswept wing centered in closed-on-bottom-only tunnel; $\gamma = 1.5$; $\sigma_w = 0.5$; $\frac{l_t}{H} = 1.0 \left(\frac{l_t}{2s} = \frac{2}{3}\right)$; $\frac{h_t}{H} = 0$; uniform wing-load distribution.

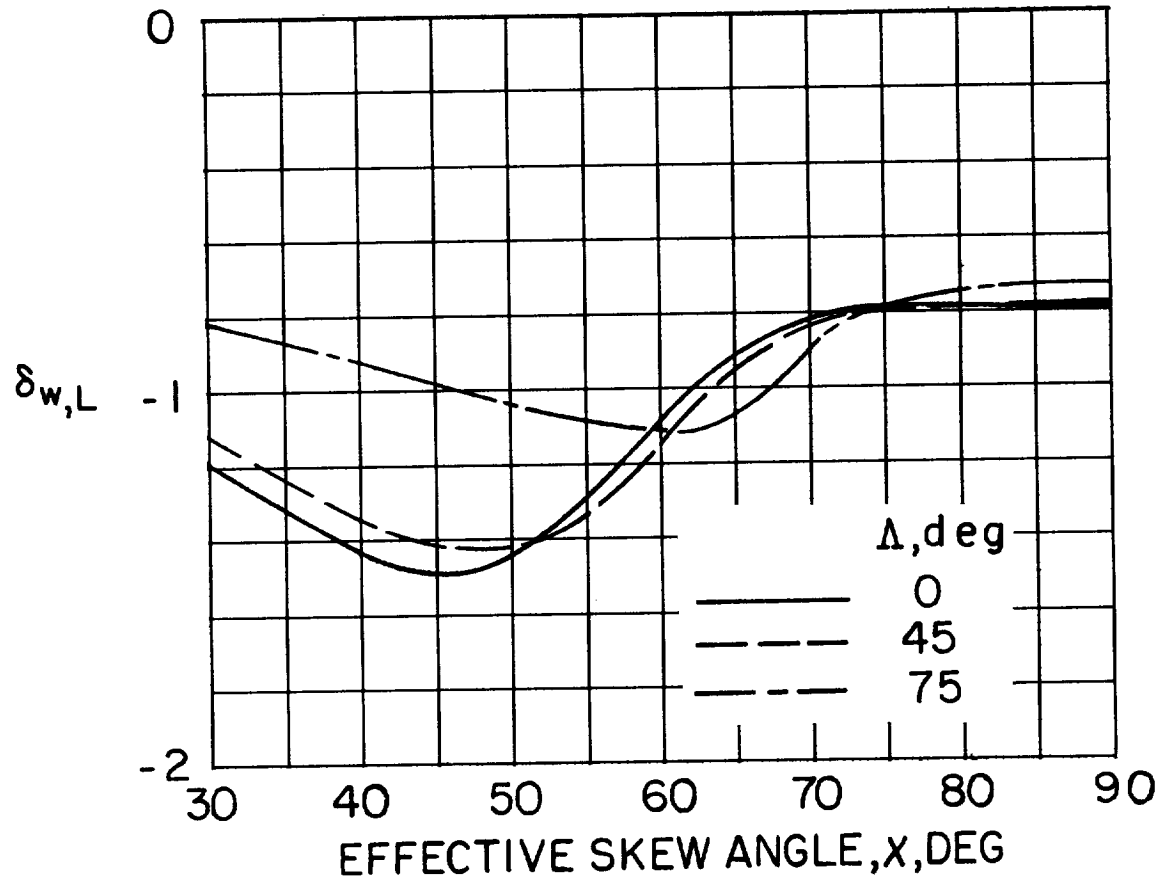

(a) $\alpha = 0^0$.

Figure 24.- Effect of wing sweep on interference factor at a zero-span tail. Aerodynamic center of wing is at center of closed tunnel; tail is located 2/3 of wing span behind aerodynamic center. $\gamma = 1.5$; $\alpha_w = 0.5$; $\frac{h_t}{H} = 0$; uniform wing-load distribution.

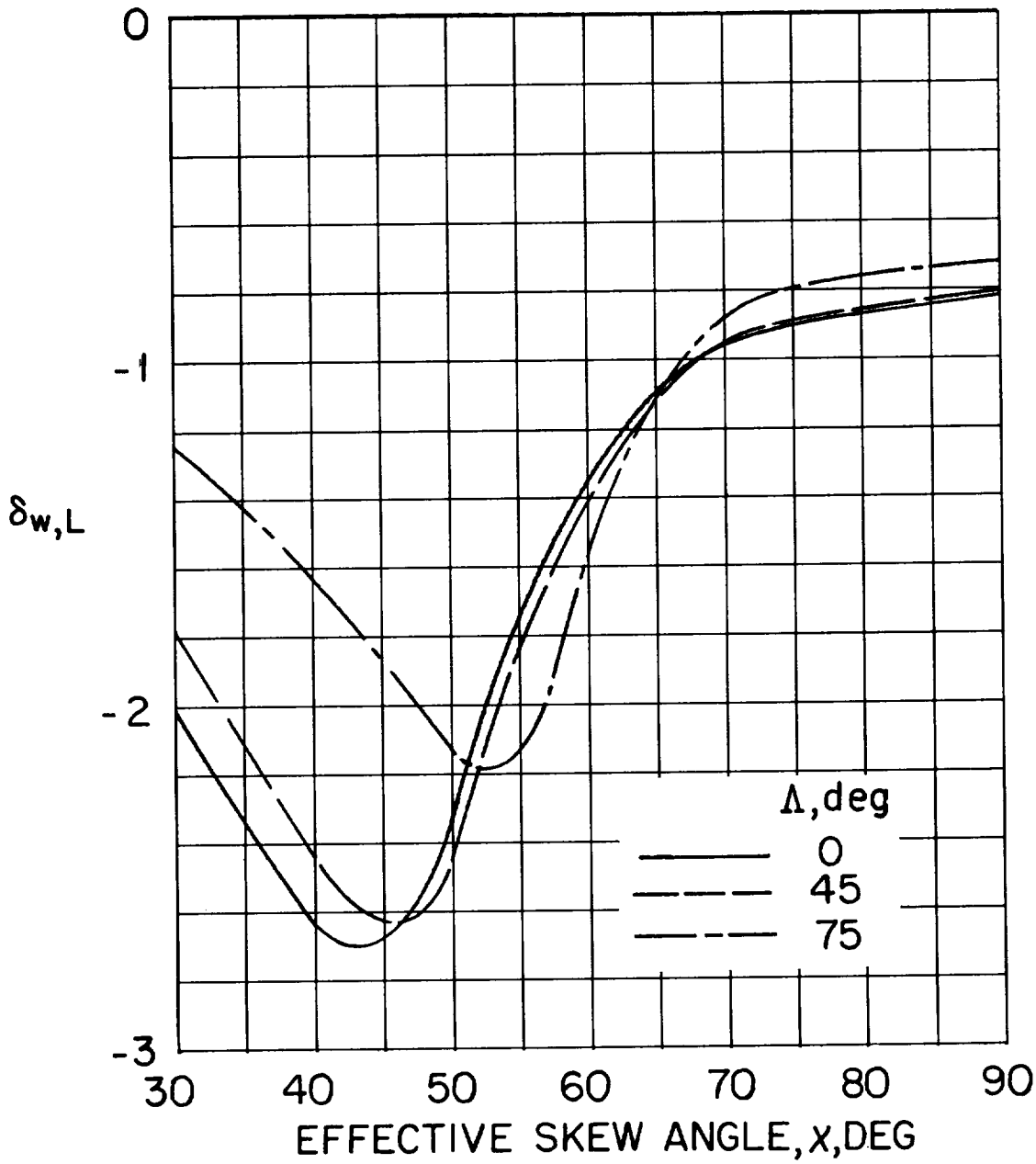

(b) $\alpha = 20^0$.

Figure 24.- Concluded.

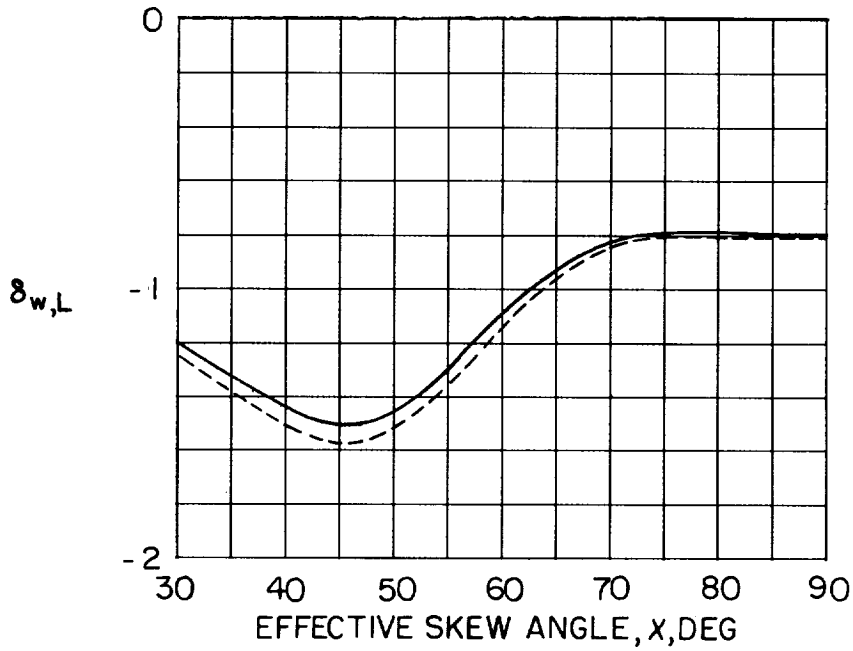

(a) $\Lambda = 0^{o}$.

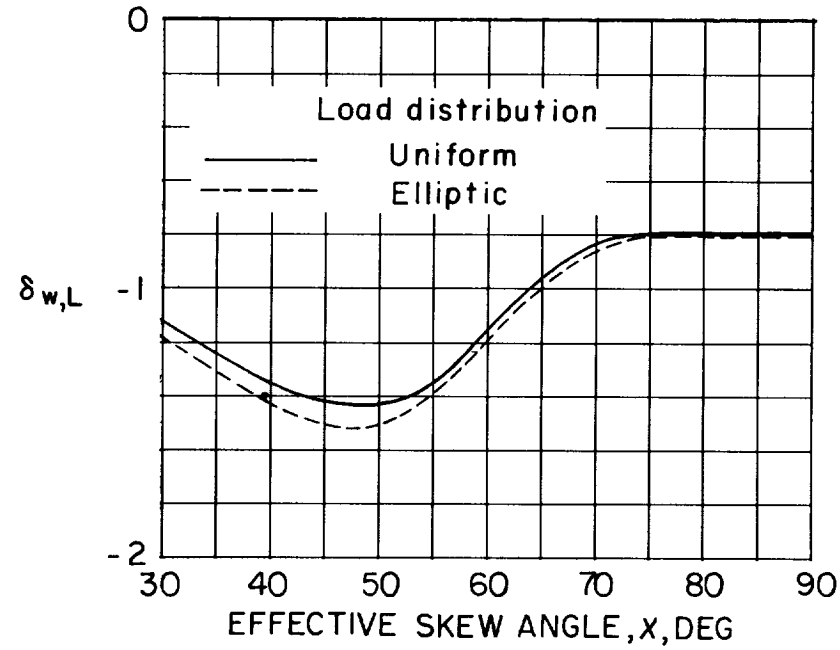

(b) $\Lambda = 45^{o}$.

Figure 25.- Effect of wing-load distribution on the interference factor at a zero-span tail. Aerodynamic center of wing is at center of closed tunnel; tail is located 2/3 of wing span behind aerodynamic center. $\gamma = 1.5$; $\alpha_w = 0$; $\frac{h_t}{H} = 0$; $\alpha = 0^{o}$.

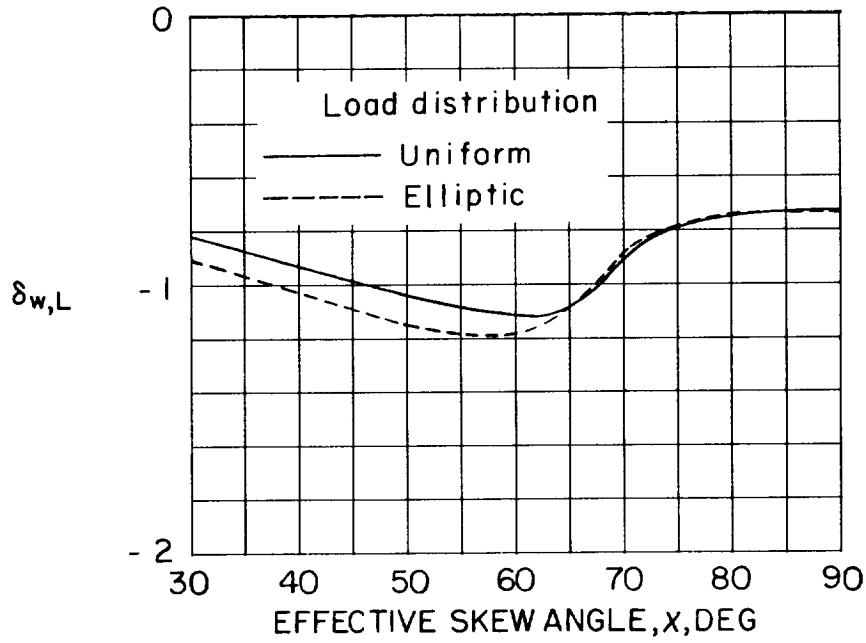

(c) $\Lambda = 75^{o}$.

Figure 25.- Concluded.

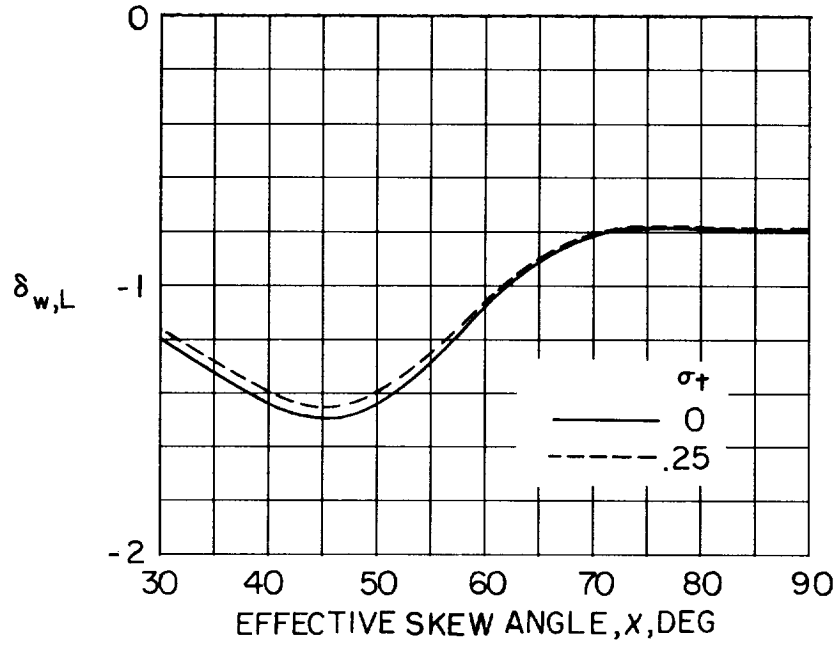

(a) $\Lambda = 0^0$.

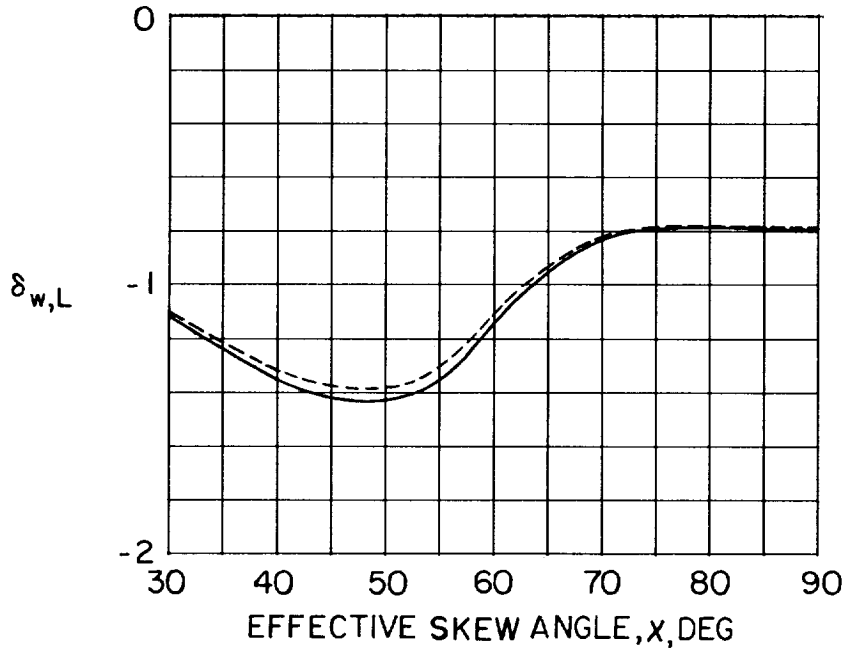

(b) $\Lambda = 45^0$.

Figure 26.- Effect of tail span on interference factor at a tail behind a wing with aerodynamic center at center of closed tunnel. Tail is located 2/3 of wing span behind aerodynamic center. $\gamma = 1.5$; $\sigma_w = 0.5$; $\frac{h_t}{H} = 0$; $\alpha = 0^0$; uniform wing-load distribution.

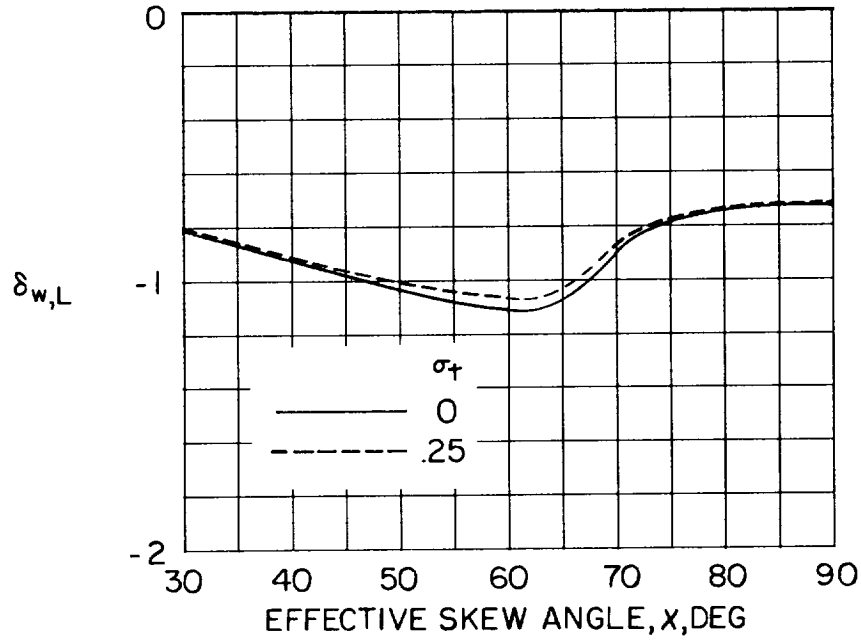

(c) $\Lambda = 75^0$.

Figure 26.- Concluded.

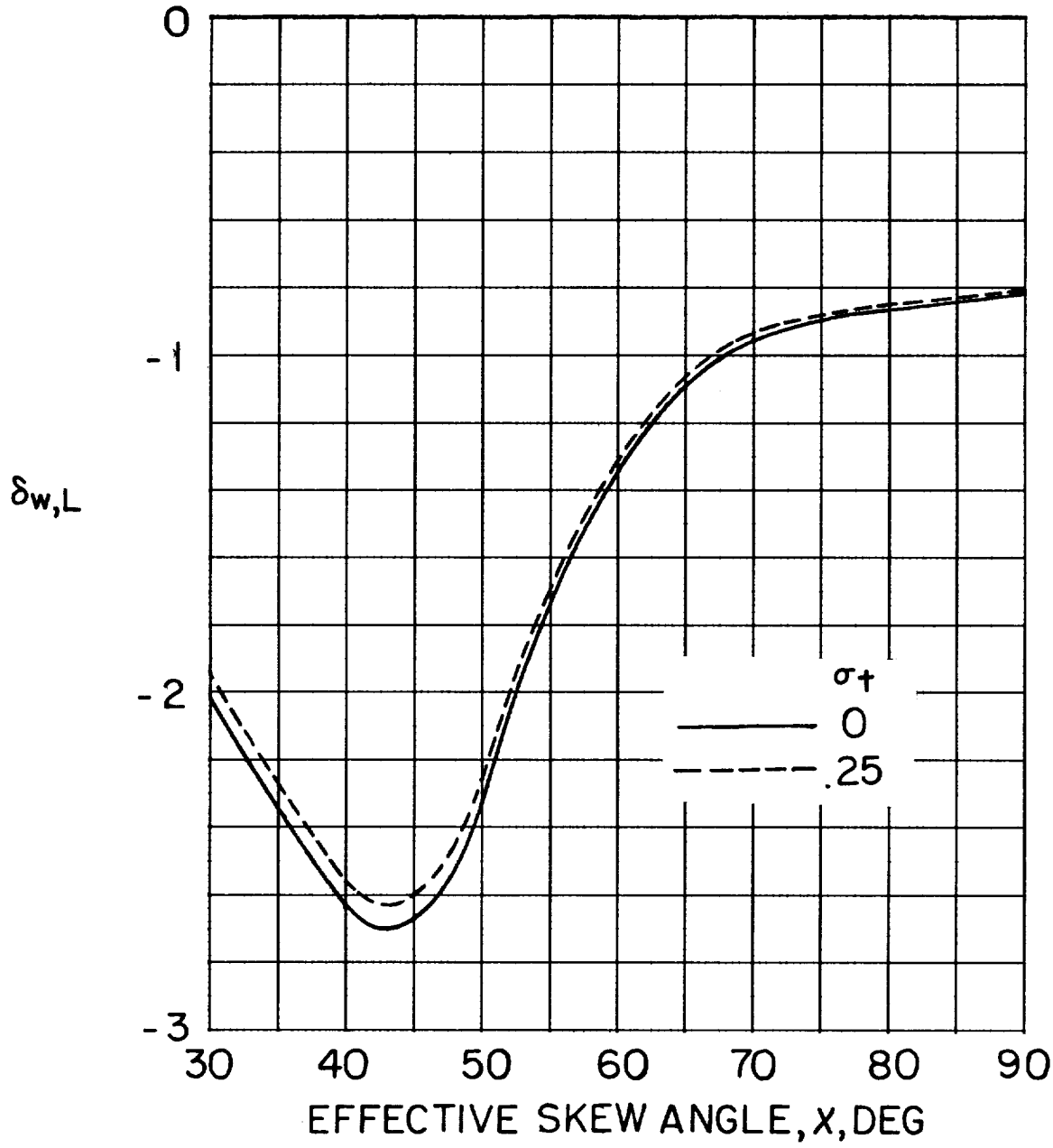

(a) $\Lambda = 0^0$.

Figure 27.- Effect of tail span on interference factors at a tail behind a wing with aerodynamic center at center of a closed tunnel. Tail is located 2/3 of wing span behind aerodynamic center. $\gamma = 1.5$; $\sigma_w = 0.5$; $\frac{h_t}{H} = 0$; $\alpha = 20^0$; uniform wing-load distribution.

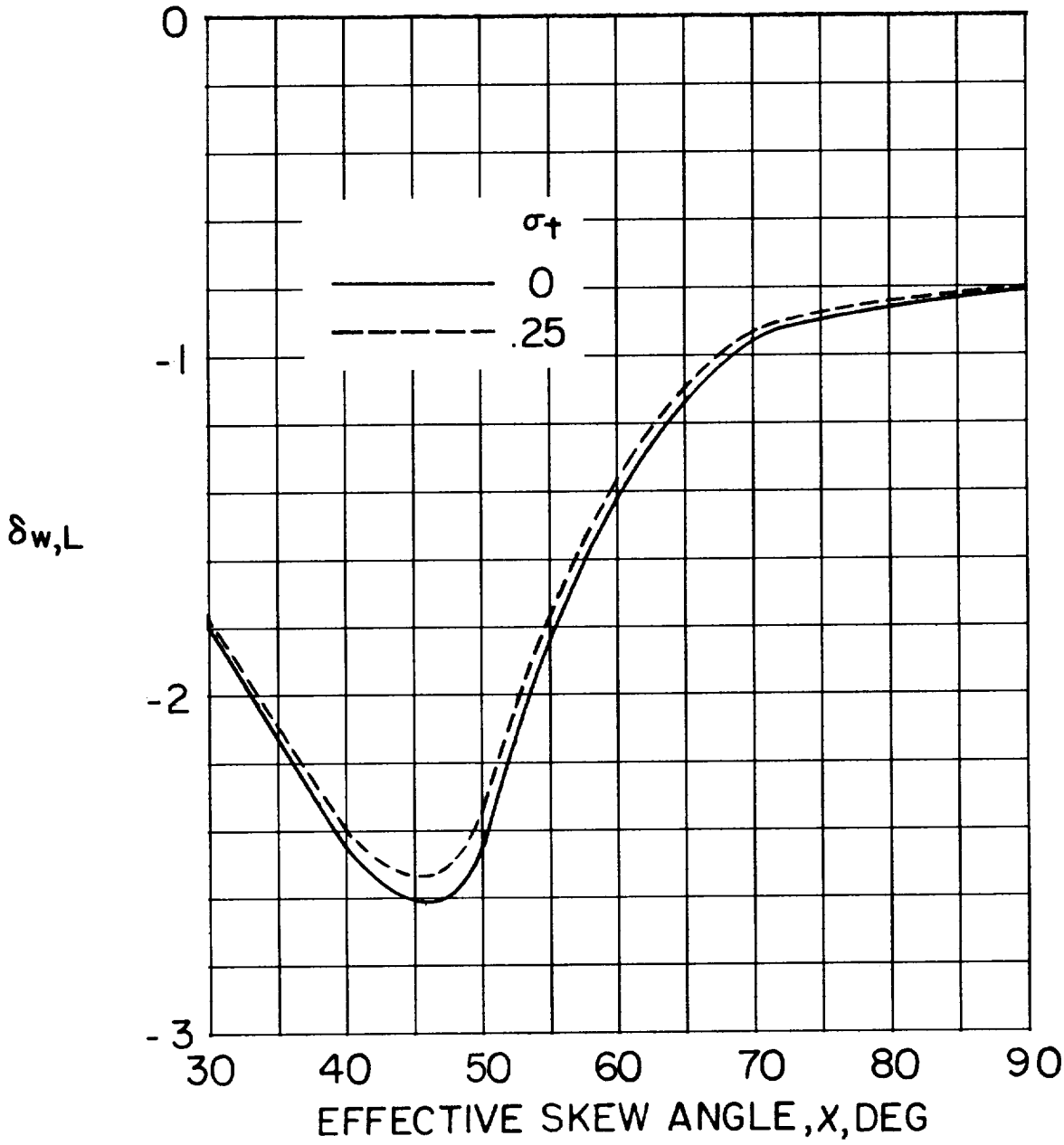

(b) $\Lambda = 45^0$.

Figure 27.- Continued.

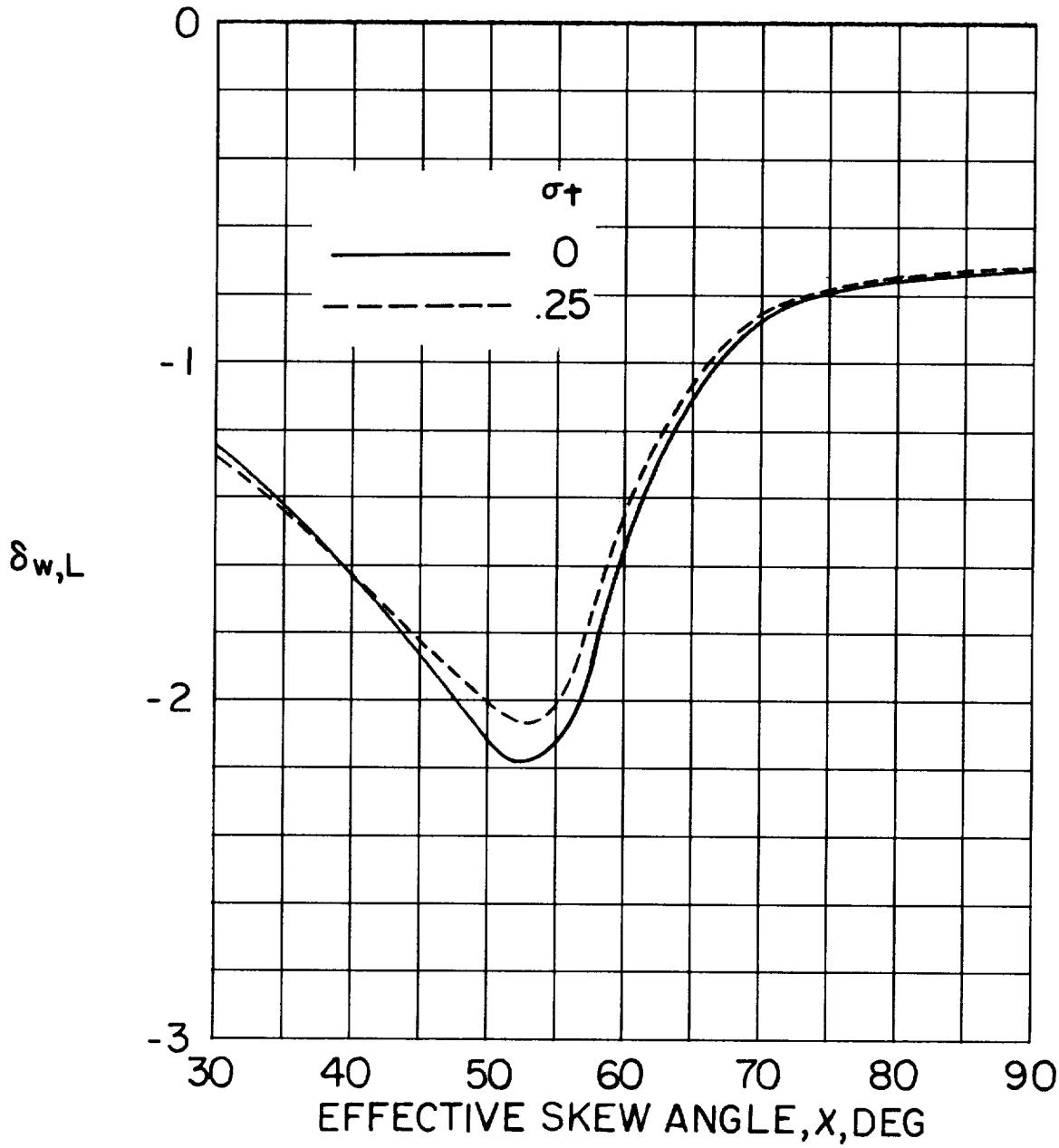

(c) $\Lambda = 75^0$.

Figure 27.- Concluded.

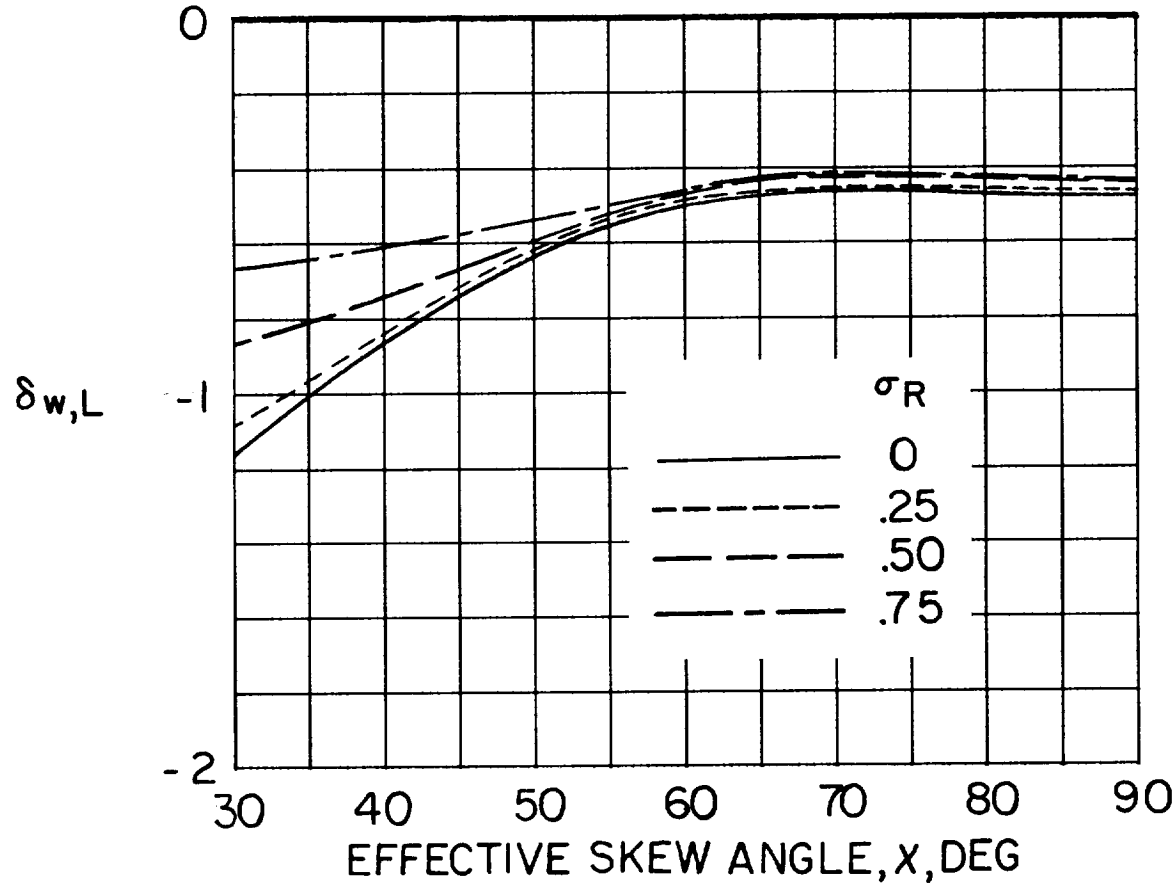

Figure 28.- Effect of diameter-width ratio on average interference factor for uniformly loaded rotor centered in closed tunnel. $\gamma = 1.5$; $\alpha_R = 0^o$.

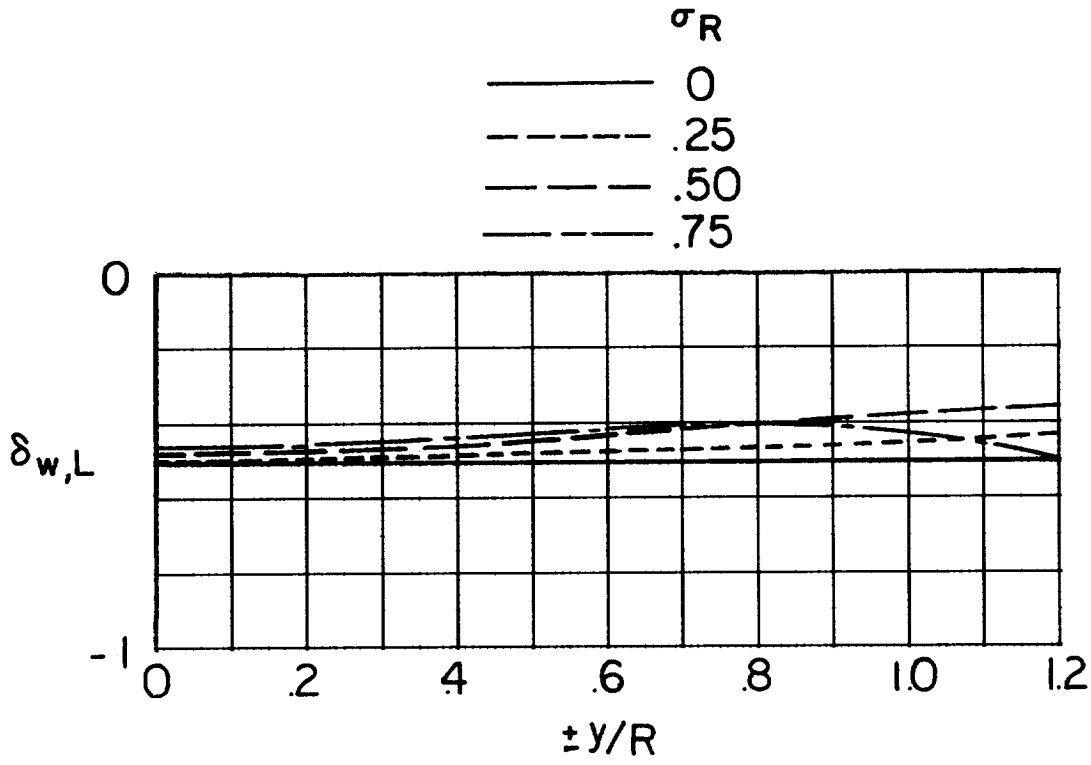

(a) $\chi = 60^0$.

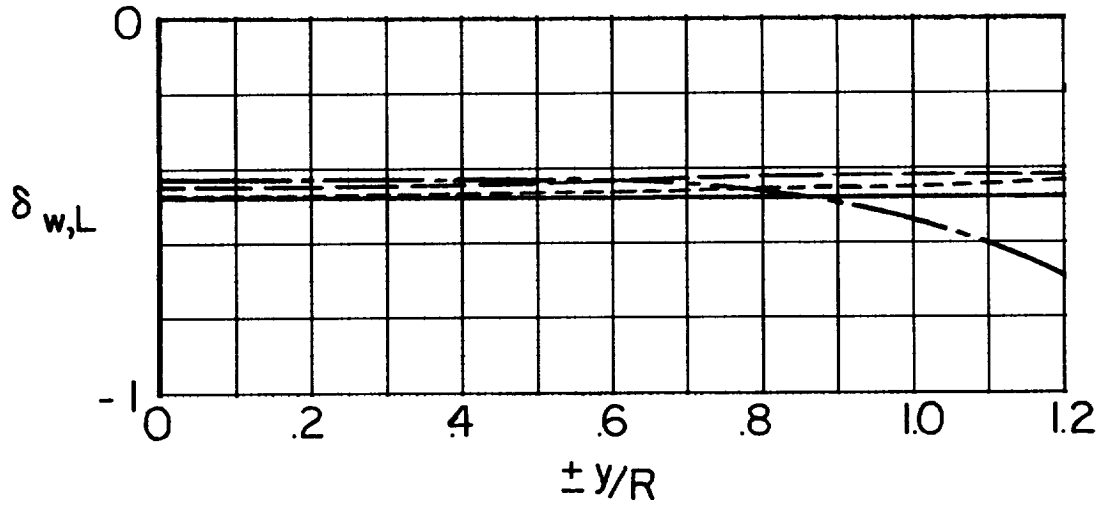

(b) $\chi = 90^0$.

Figure 29.- Effect of diameter-width ratio on distribution of interference factor on lateral axis of uniformly loaded rotor centered in closed tunnel. $\gamma = 1.5$; $\alpha_R = 0^0$.

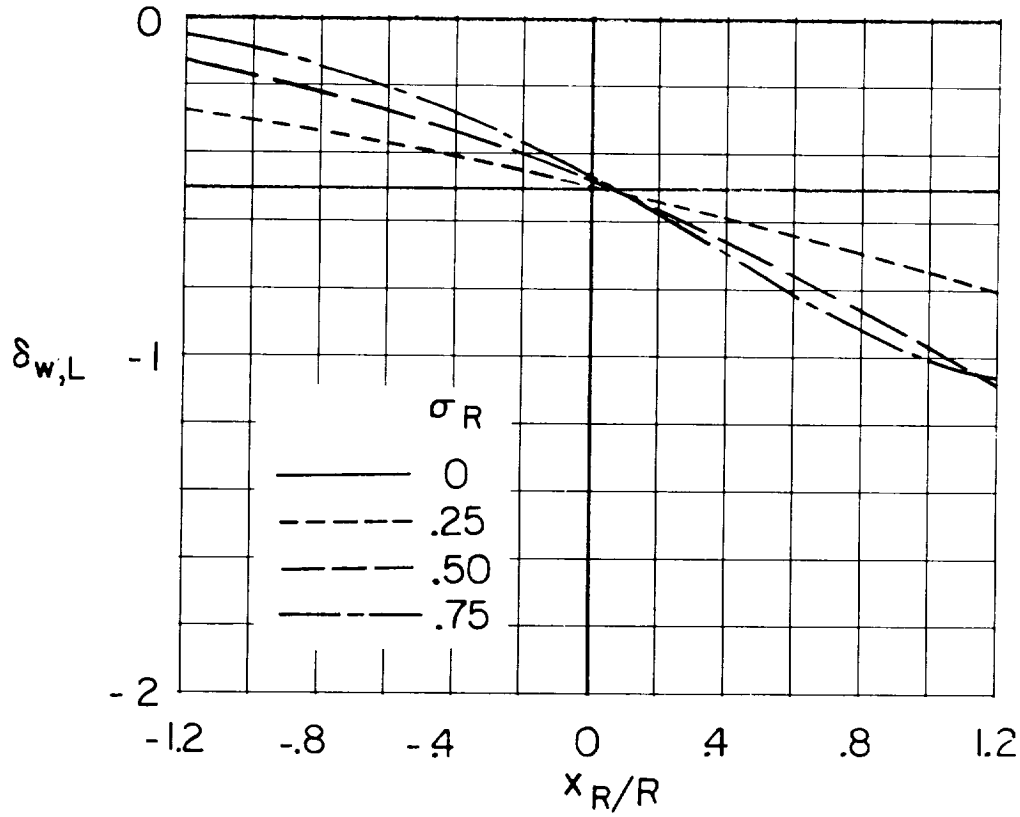

(a) $\chi = 60^0$.

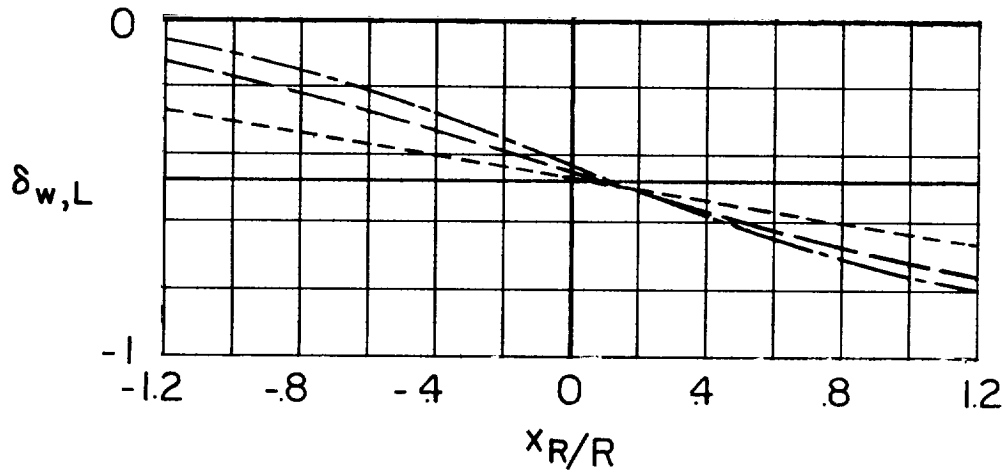

(b) $\chi = 90^0$.

Figure 30.- Effect of diameter-width ratio on distribution of interference factor on longitudinal axis of uniformly loaded rotor centered in closed tunnel. $\gamma = 1.5$; $\alpha_R = 0^0$.

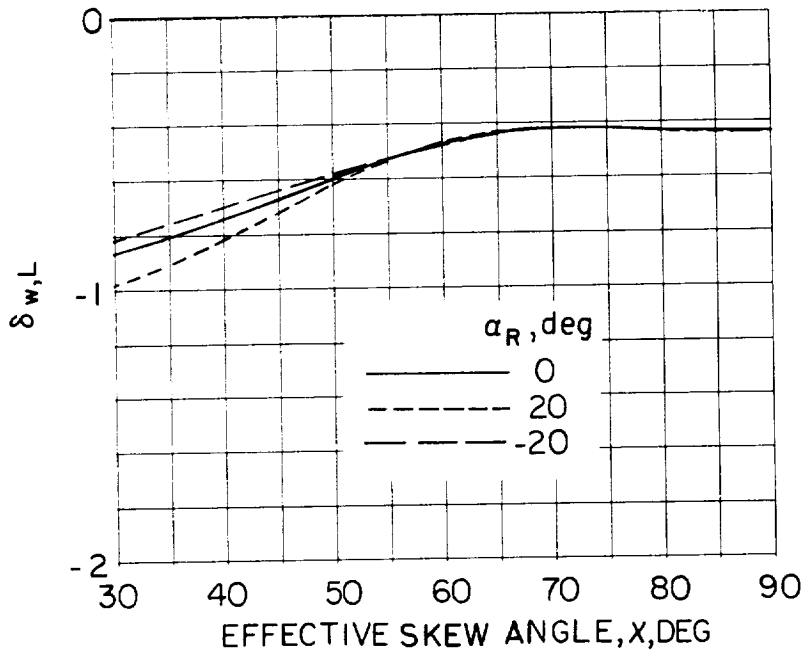

(a) Excluding drag effects.

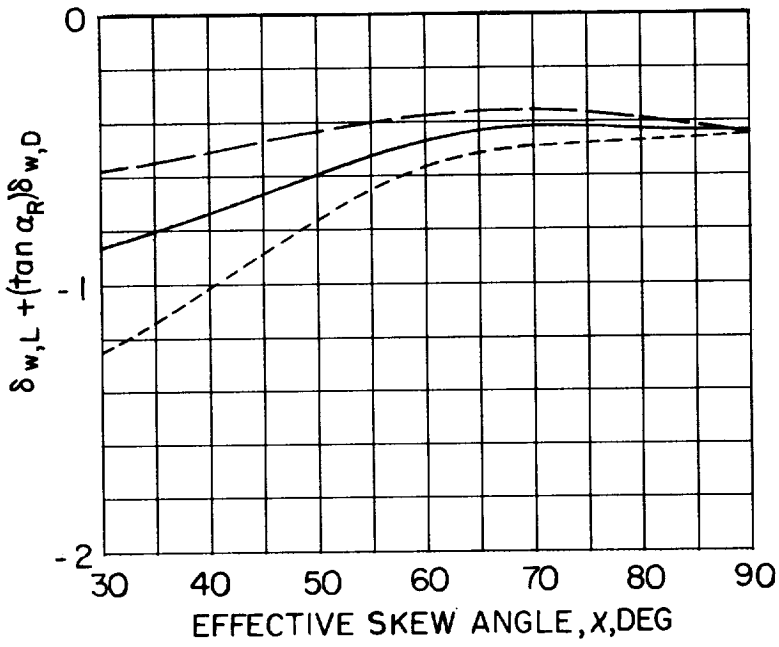

(b) Including drag effects.

Figure 31.- Effect of angle of attack on average interference factor for uniformly loaded rotor centered in closed tunnel. $\gamma = 1.5$; $\sigma_R = 0.5$.

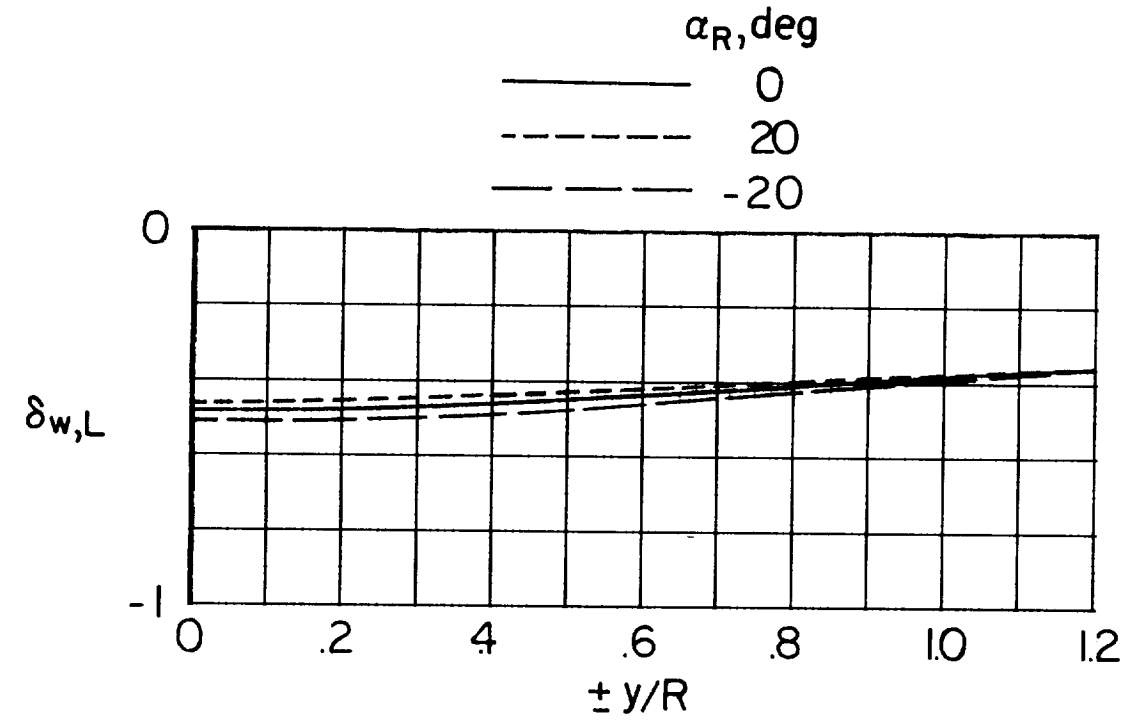

(a) $\chi = 60^0$.

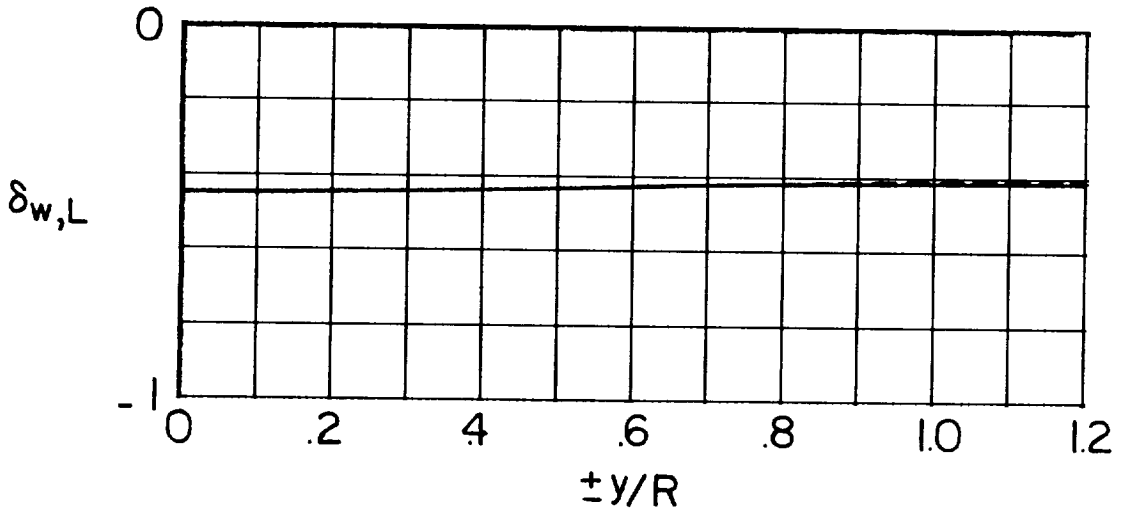

(b) $\chi = 90^0$.

Figure 32.- Effect of angle of attack on distribution of interference factors on lateral axis of uniformly loaded rotor centered in closed tunnel. $\gamma = 1.5$; $\sigma_R = 0.5$. At $\chi = 90^0$, interference factors are symmetrical about $\alpha_R = 0^0$.

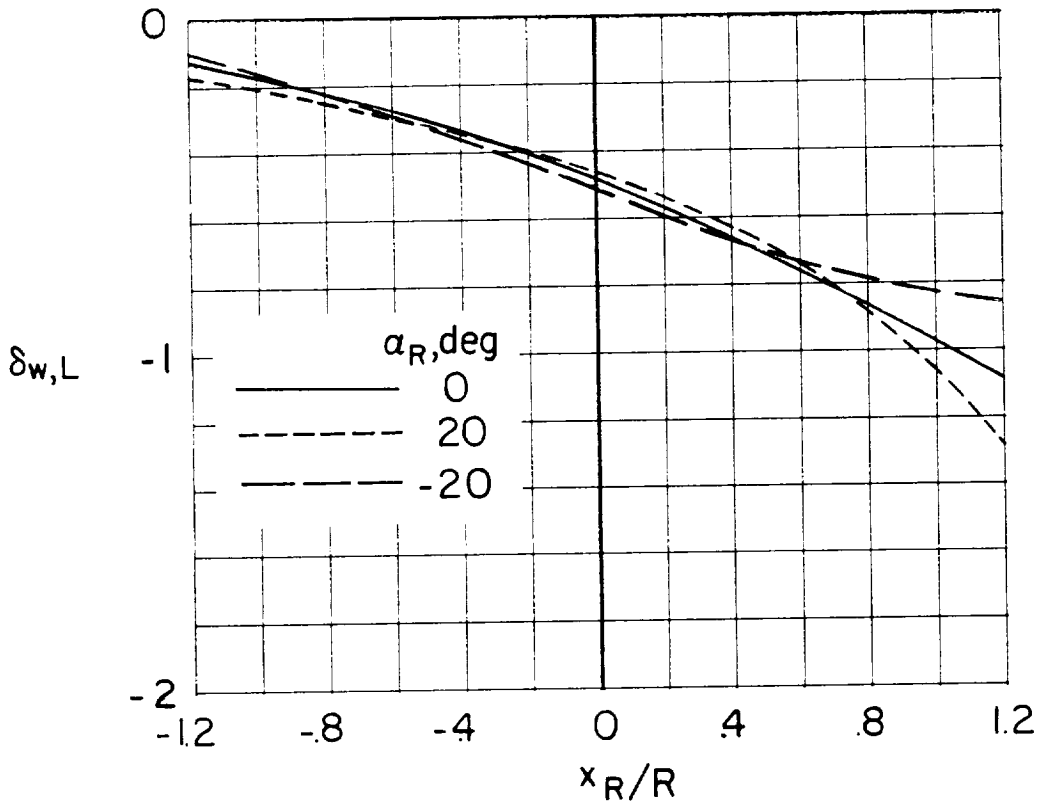

(a) $\chi = 60^0$.

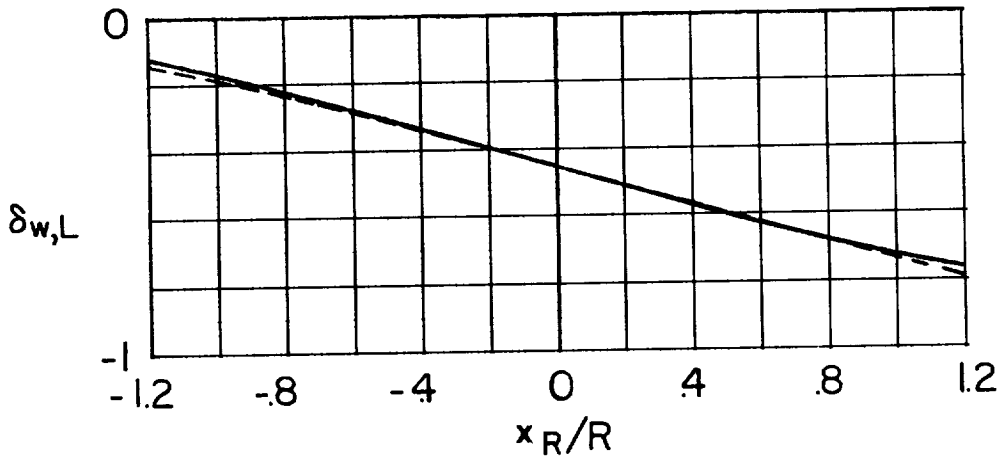

(b) $\chi = 90^0$.

Figure 33.- Effect of angle of attack on distribution of interference factor on longitudinal axis of uniformly loaded rotor centered in closed tunnel. $\gamma = 1.5$; $\sigma_R = 0.5$. At $\chi = 90^0$, the interference factors are symmetrical about $\alpha_R = 0^0$.

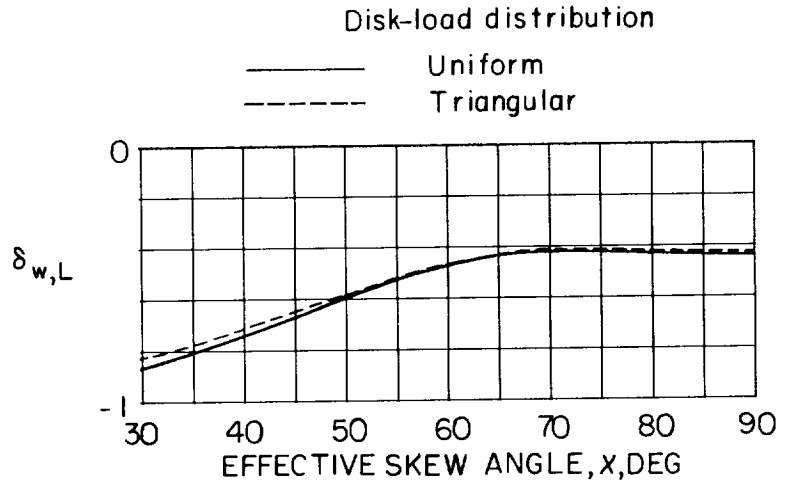

(a) $\alpha_R = 0^0$.

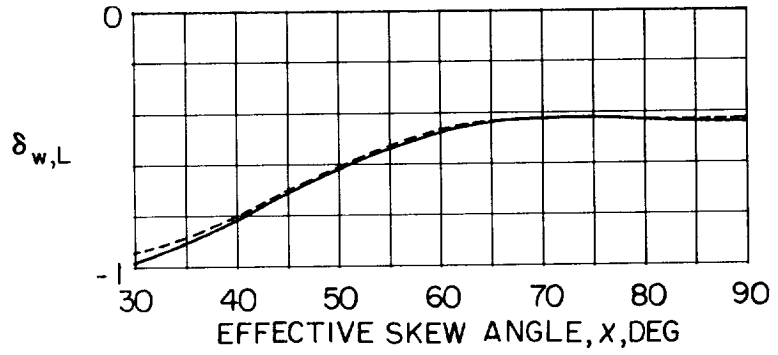

(b) $\alpha_R = 20^0$.

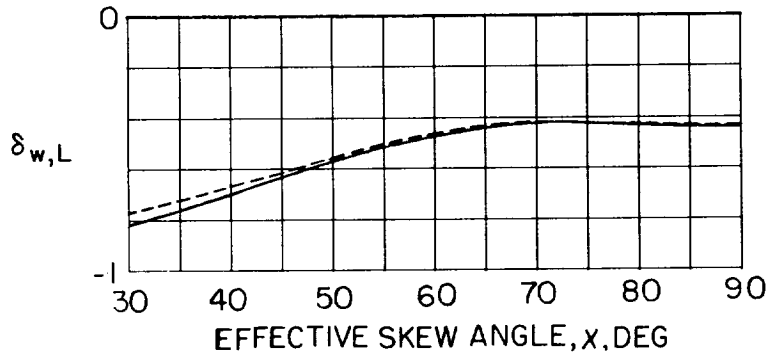

(c) $\alpha_R = -20^0$.

Figure 34.- Effect of disk-load distribution on average interference factor for uniformly loaded rotor mounted in center of closed tunnel. $\gamma = 1.5$; $\sigma_R = 0.5$.

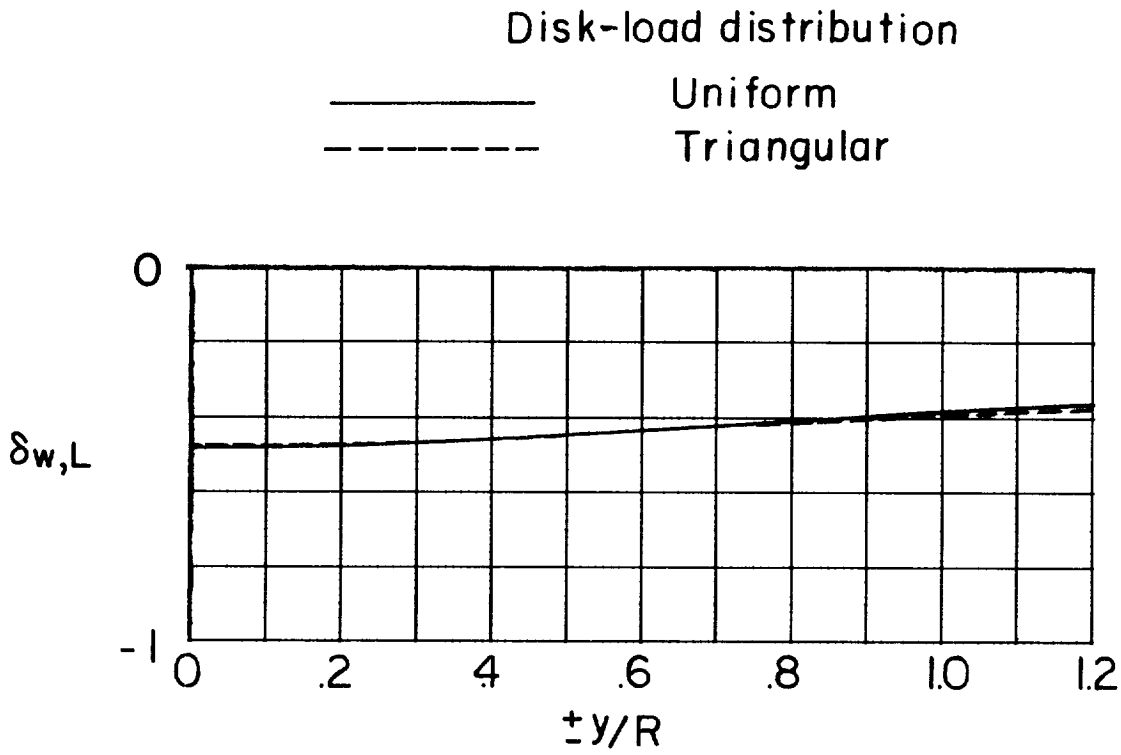

(a) $\chi = 60^{\circ}$.

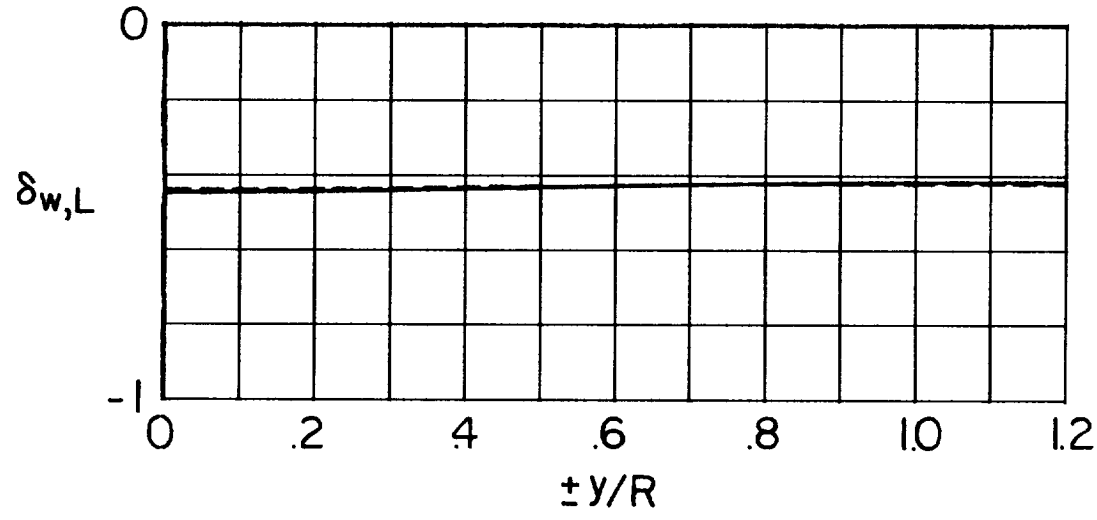

(b) $\chi = 90^{\circ}$.

Figure 35.- Effect of disk-load distribution on distribution of interference factors on lateral axis of rotor mounted in center of closed tunnel. $\gamma = 1.5$; $\sigma_R = 0.5$; $\alpha_R = 0^{\circ}$.

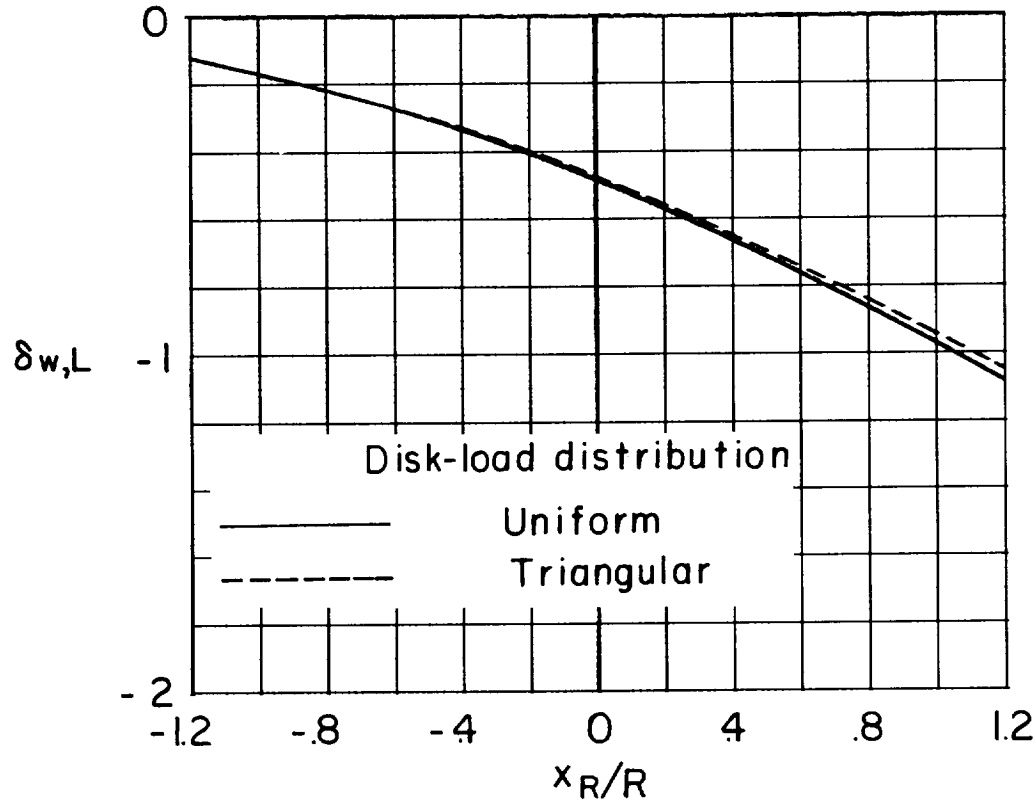

(a) $\chi = 60^0$.

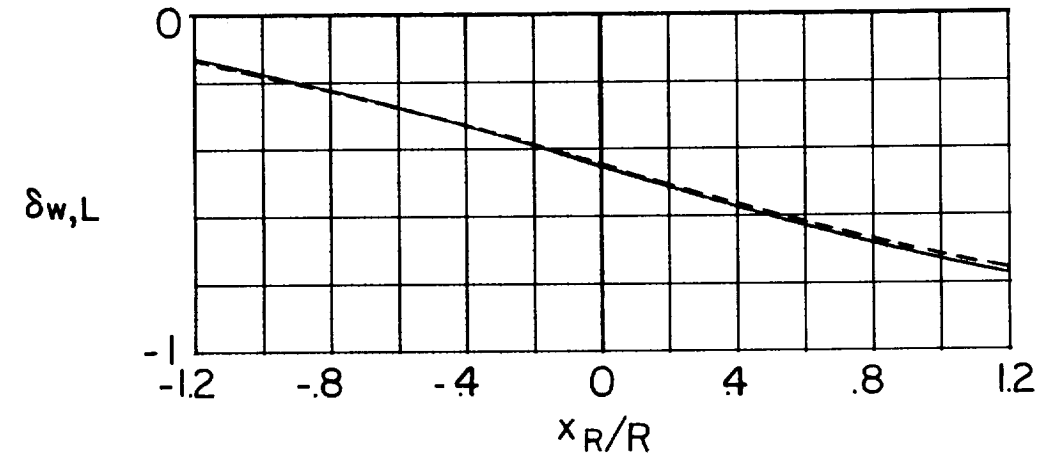

(b) $\chi = 90^0$.

Figure 36.- Effect of disk-load distribution on distribution of interference factor on longitudinal axis of rotor centered in closed tunnel. $\gamma = 1.5$; $\sigma_R = 0.5$; $\alpha_R = 0^0$.

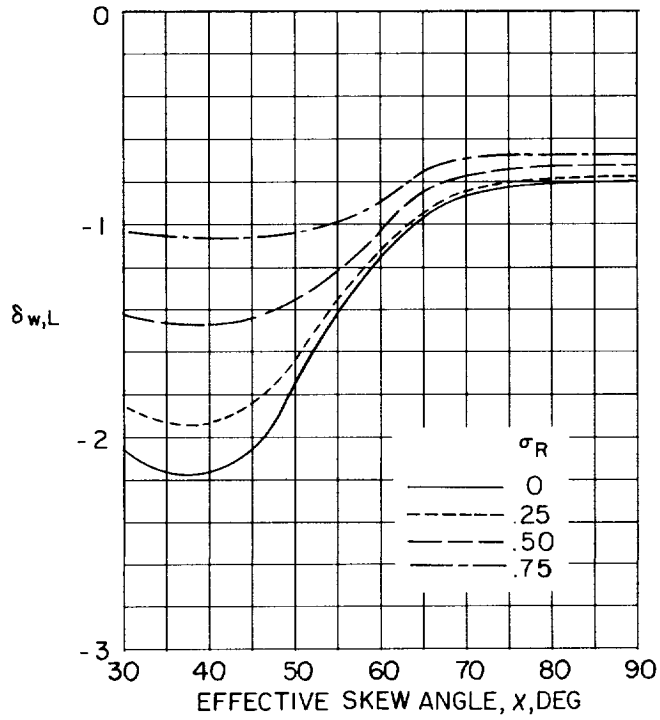

(a) $\frac{l_t}{H} = 0.75$; $\frac{h_t}{H} = -0.075$.

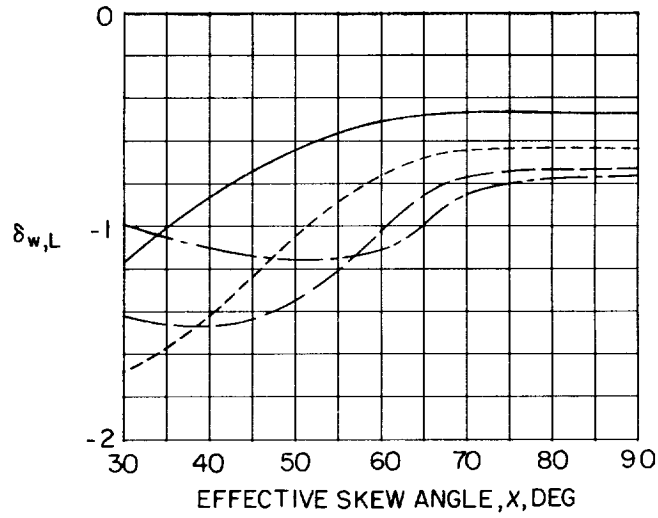

(b) $\frac{l_t}{R} = 1.0$; $\frac{h_t}{R} = -0.1$.

Figure 37.- Effect of diameter-width ratio on interference factor at a zero-span tail behind uniformly loaded rotor mounted in center of closed tunnel. $\gamma = 1.5$; $\alpha_R = \alpha_B = 0^0$.

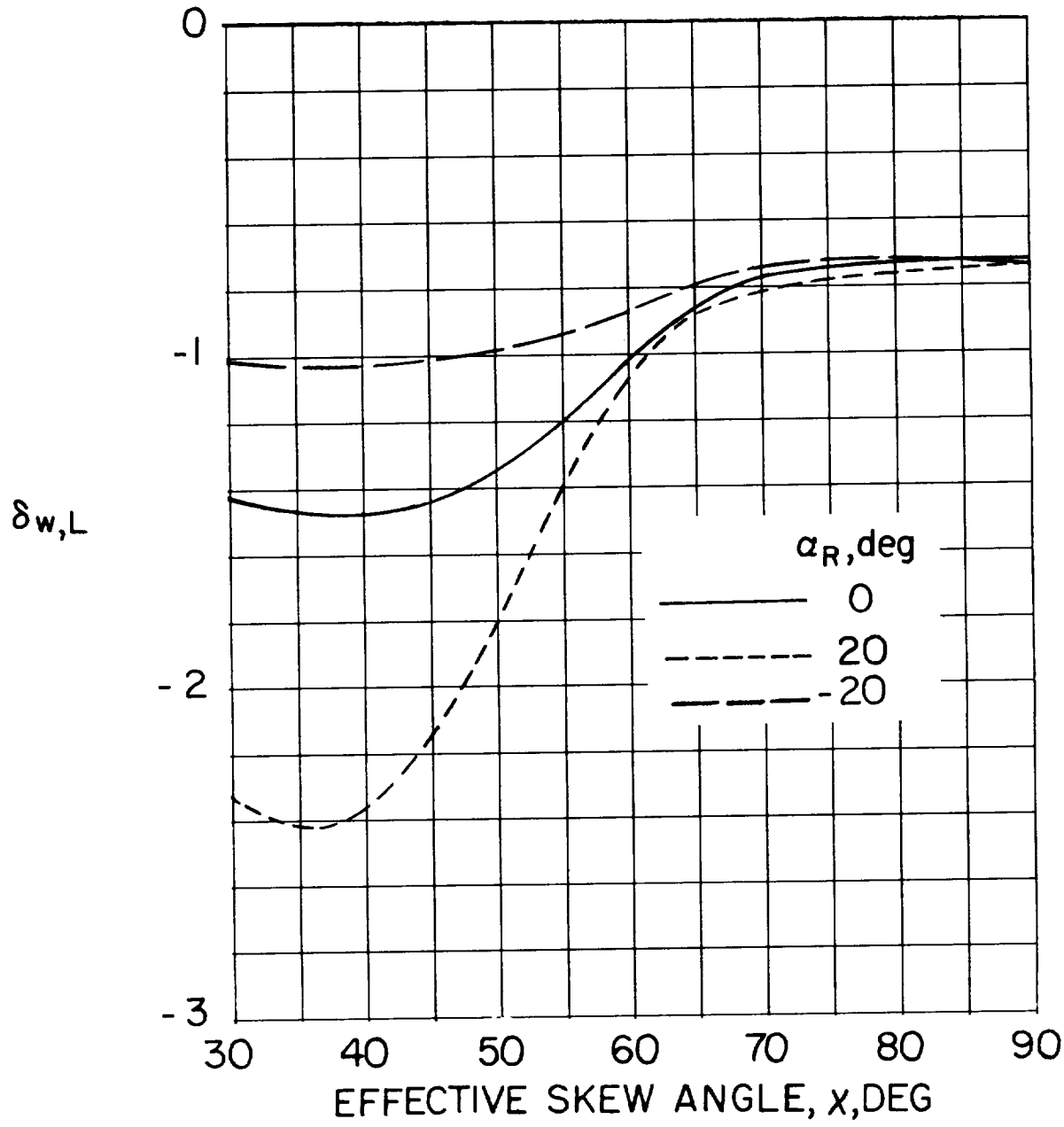

Figure 38.- Effect of angle of attack on interference factor at a zero-span tail behind uniformly loaded rotor mounted in center of closed tunnel. $\gamma = 1.5$; $\sigma_R = 0.5$; $\alpha_R = \alpha_B$; $\frac{l_t}{R} = 1.0$; $\frac{h_t}{R} = -0.1$.

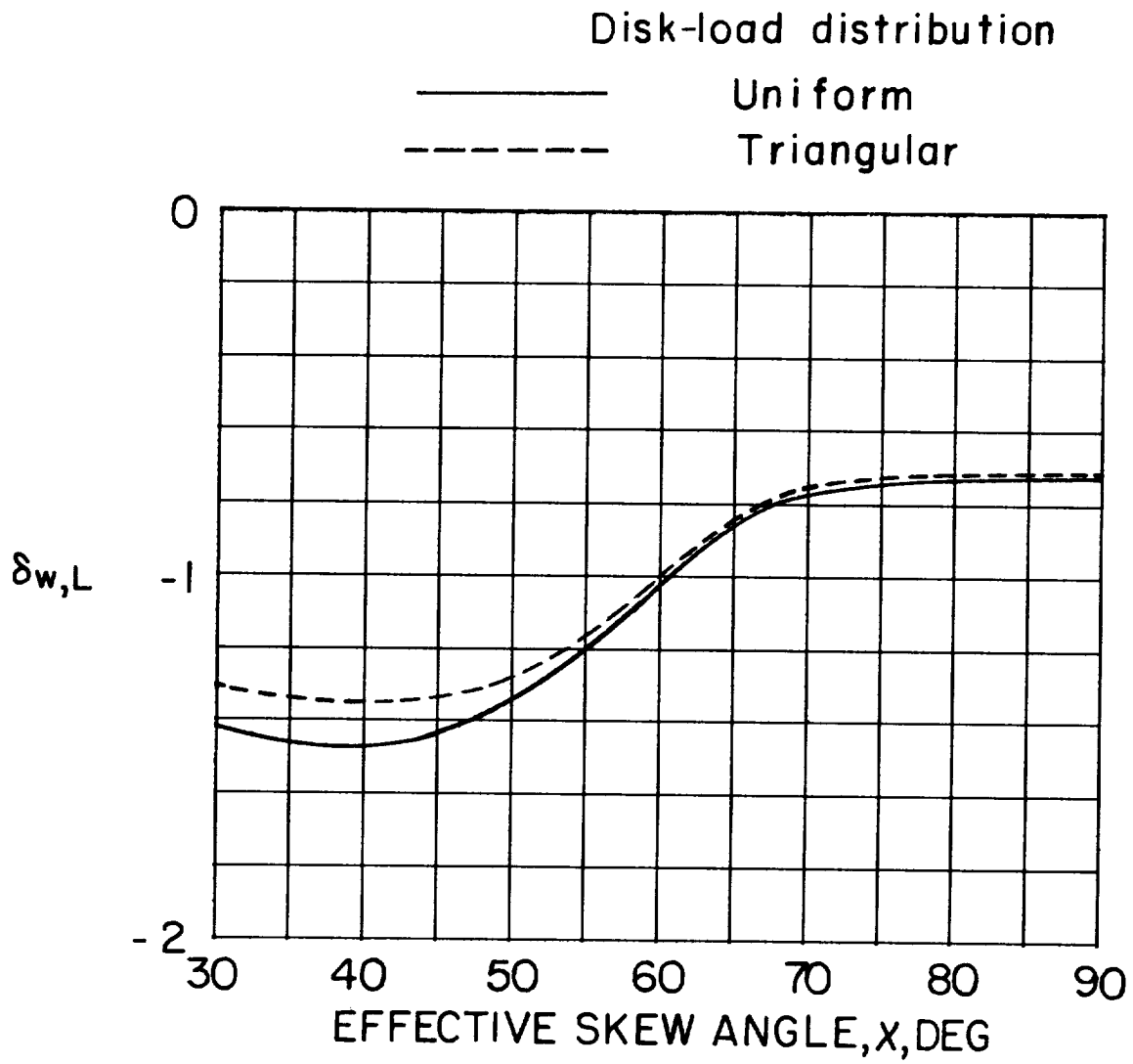

Figure 39.- Effect of rotor disk-load distribution on interference factor at a zero-span tail behind rotor mounted in center of closed tunnel. $\gamma = 1.5$; $\sigma_R = 0.5$; $\alpha_R = \alpha_B = 0^0$; $\frac{l_t}{R} = 1.0$; $\frac{h_t}{R} = -0.1$.

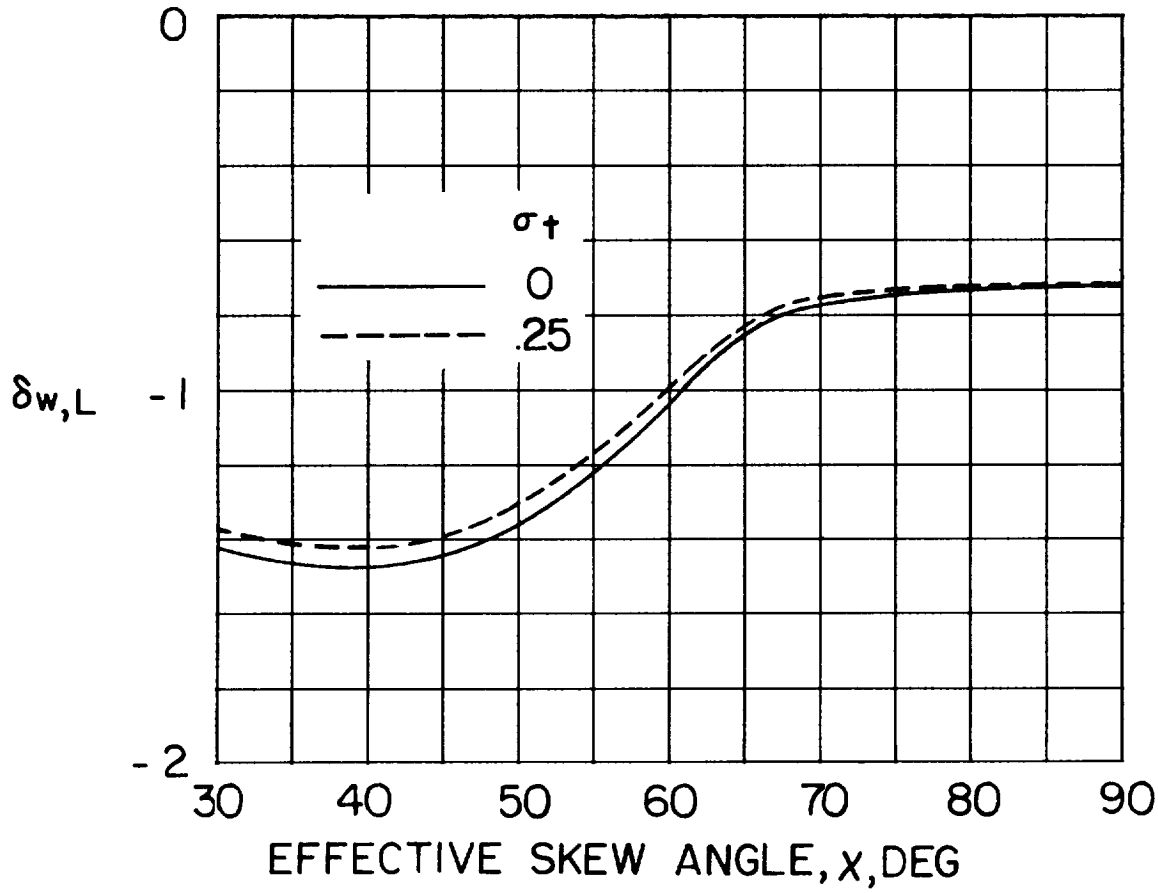

Figure 40.- Effect of tail span on interference factor at tail behind uniformly loaded rotor mounted in center of closed tunnel. $\gamma = 1.5$; $\sigma_R = 0.5$; $\alpha_R = \alpha_B = 0^0$; $\frac{l_t}{R} = 1.0$; $\frac{h_t}{R} = -0.1$.

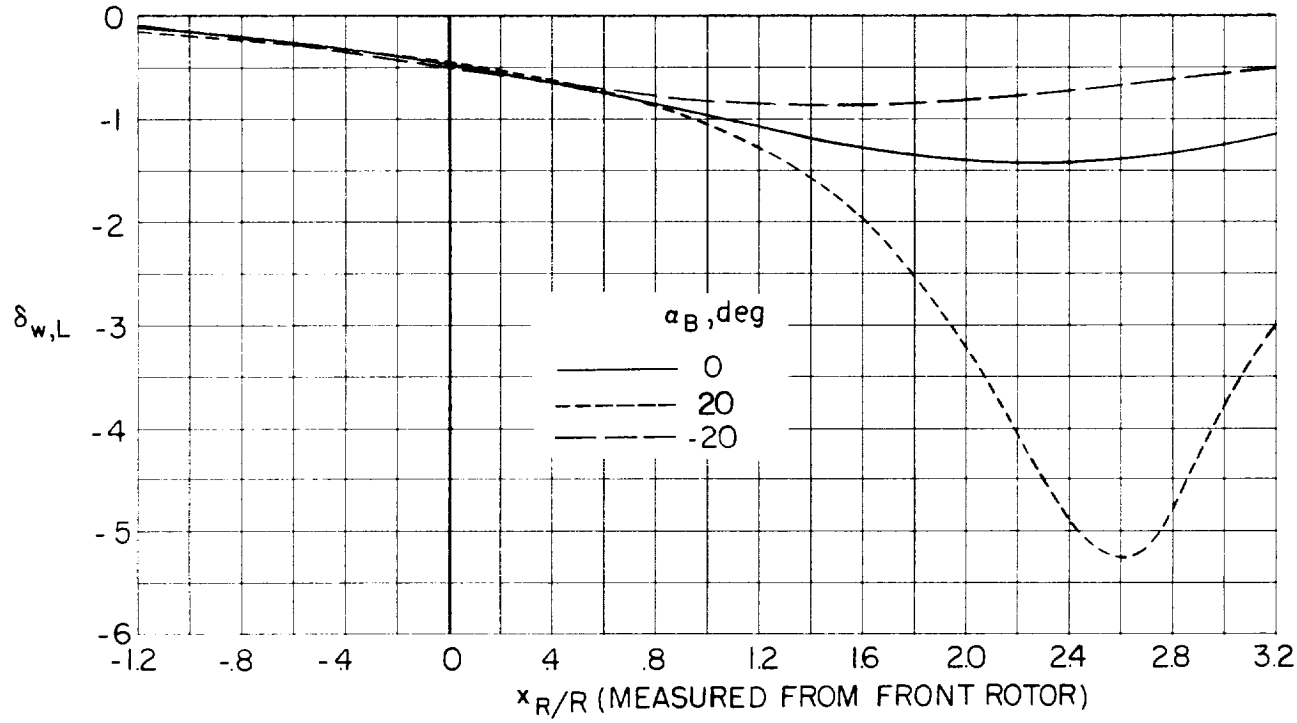

(a) $\chi = 60^0$.

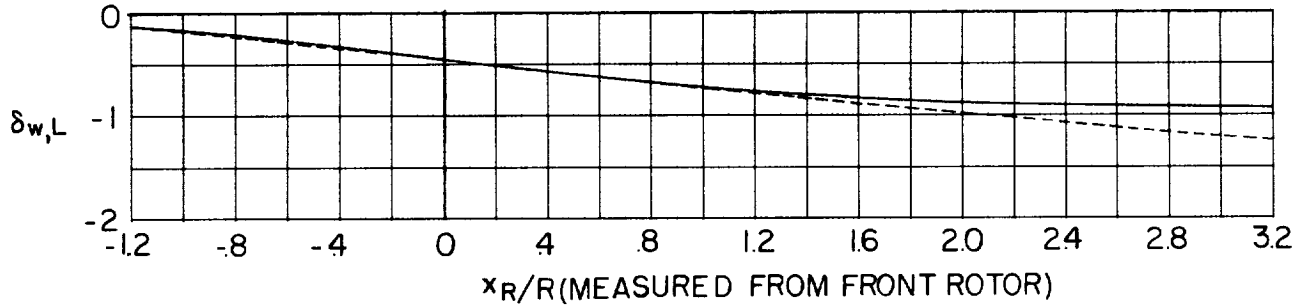

(b) $\chi = 90^0$.

Figure 41.- Contribution of front rotor to distribution of interference factor along longitudinal axis of tandem-rotor system with front rotor centered in closed tunnel. $\gamma = 1.5$; $\sigma_R = 0.5$; $\alpha_{FR} = \alpha_{RR} = \alpha_B$. Effect of angle of attack is symmetrical at $\chi = 90^0$.

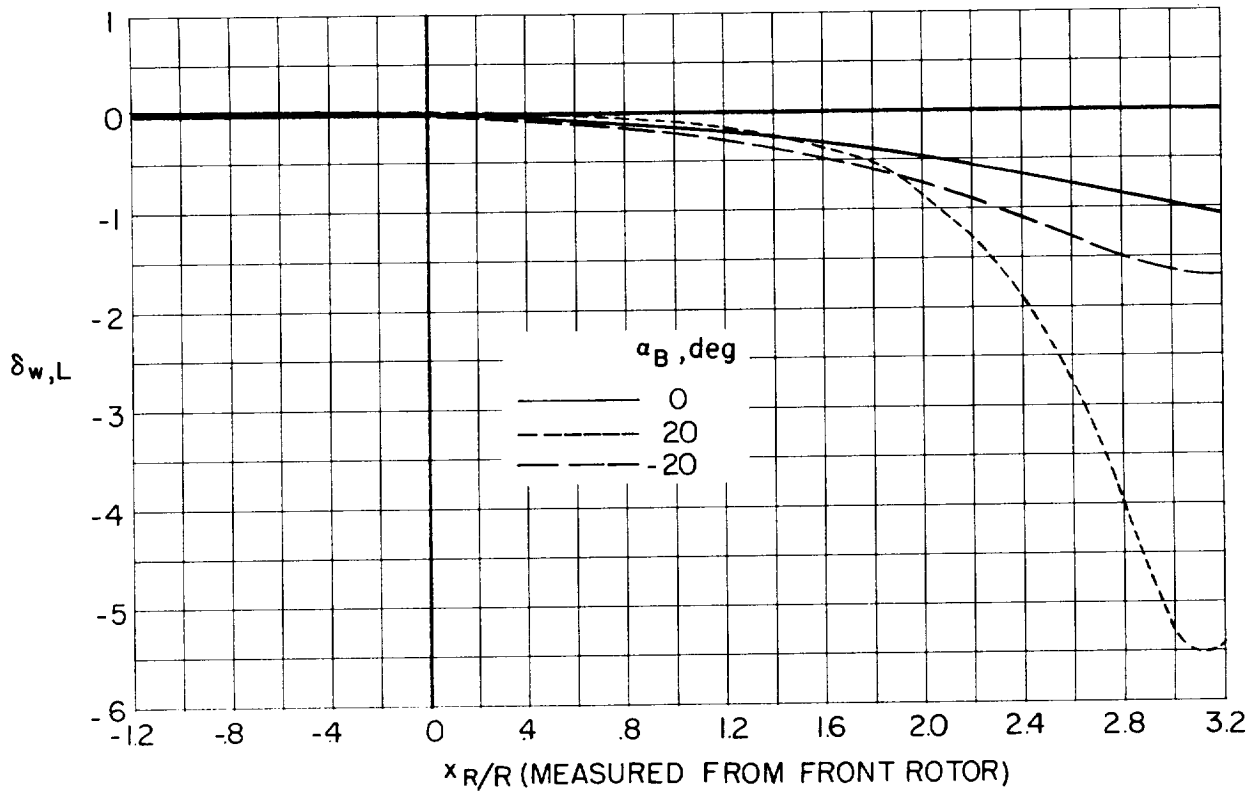

(a) $\chi = 60^0$.

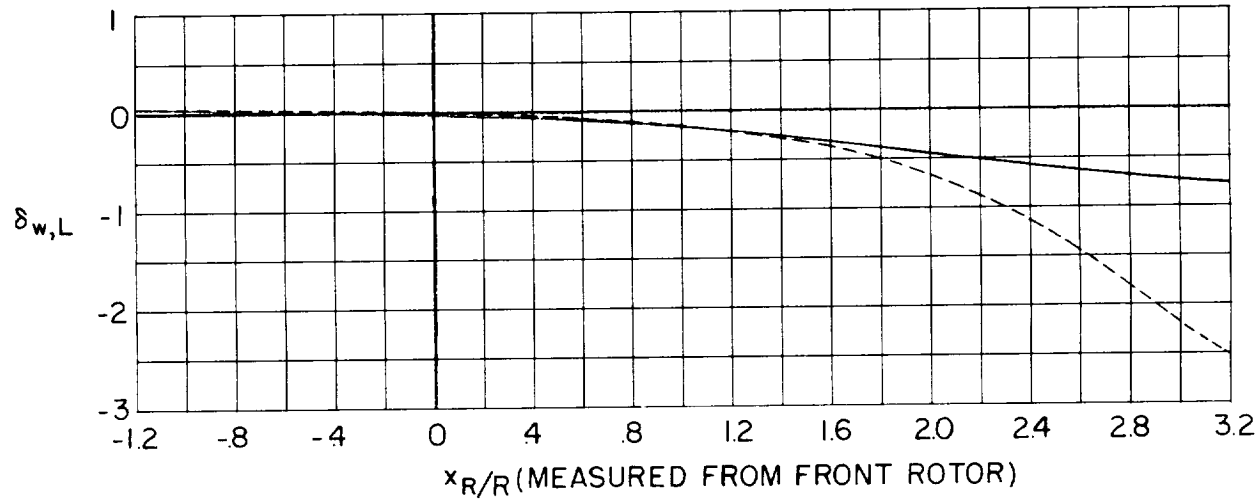

(b) $\chi = 90^0$.

Figure 42.- Contribution of rear rotor to distribution of interference factor along longitudinal axis of nonoverlapped tandem-rotor system with front rotor centered in closed tunnel. $\gamma = 1.5$; $\sigma_R = 0.5$; $\alpha_{FR} = \alpha_{RR} = \alpha_B$; $\frac{l_{RR}}{R} = 2.0$; $\frac{h_{RR}}{R} = 0$. Effect of angle of attack is symmetrical at $\chi = 90^0$.

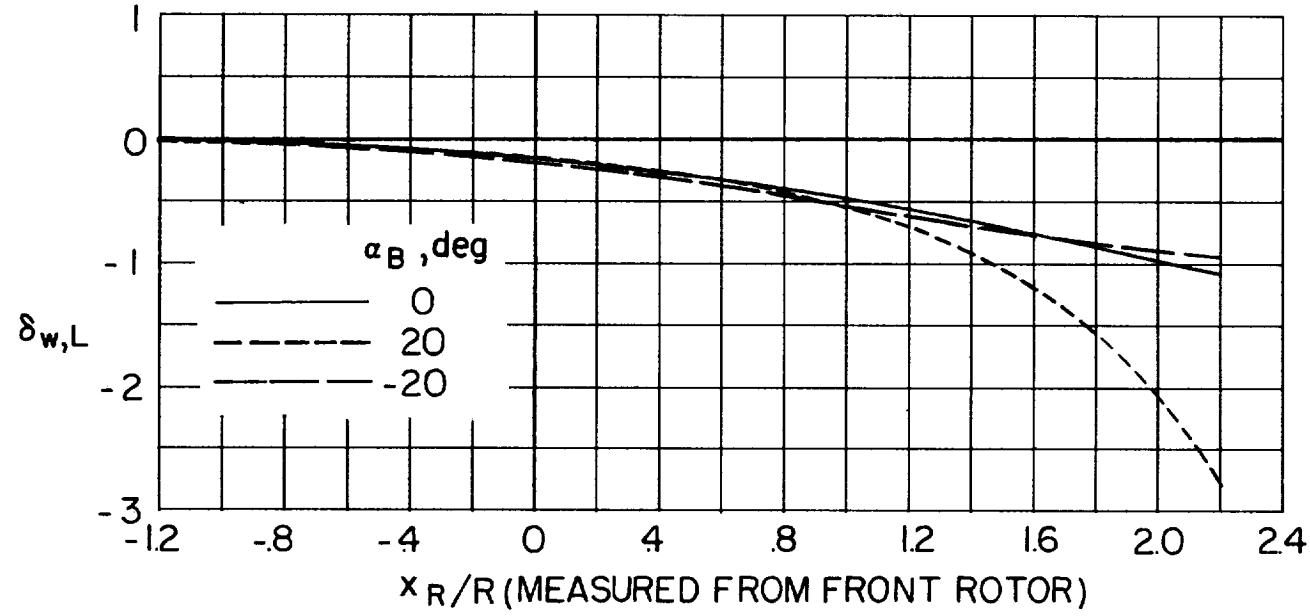

(a) $\chi = 60^0$.

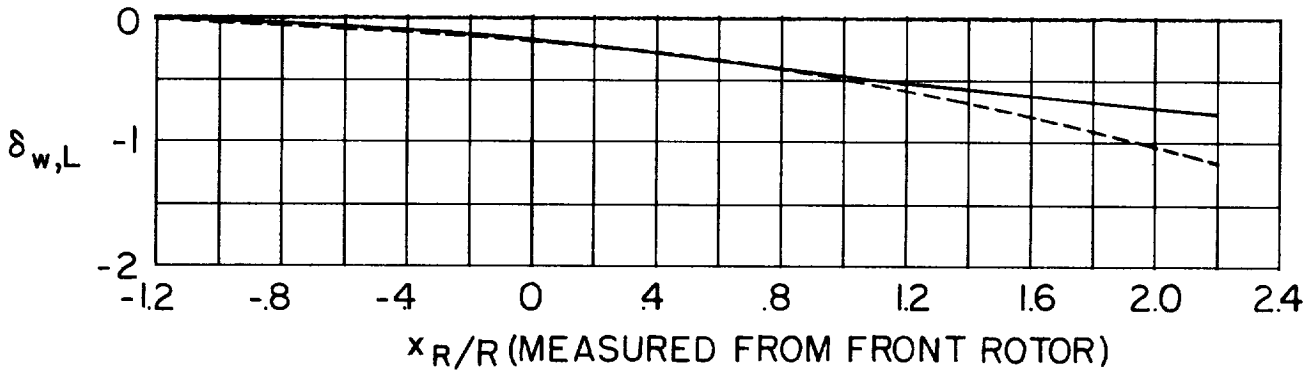

(b) $\chi = 90^0$.

Figure 43.- Contribution of rear rotor to distribution of interference factor along longitudinal axis of fully overlapped tandem-rotor system with front rotor centered in closed tunnel. $\gamma = 1.5$; $\sigma_R = 0.5$; $\alpha_{FR} = \alpha_{RR} = \alpha_B$; $\frac{l_{RR}}{R} = 1.0$; $\frac{h_{RR}}{R} = 0$. Effect of angle of attack is symmetrical at $\chi = 90^0$.

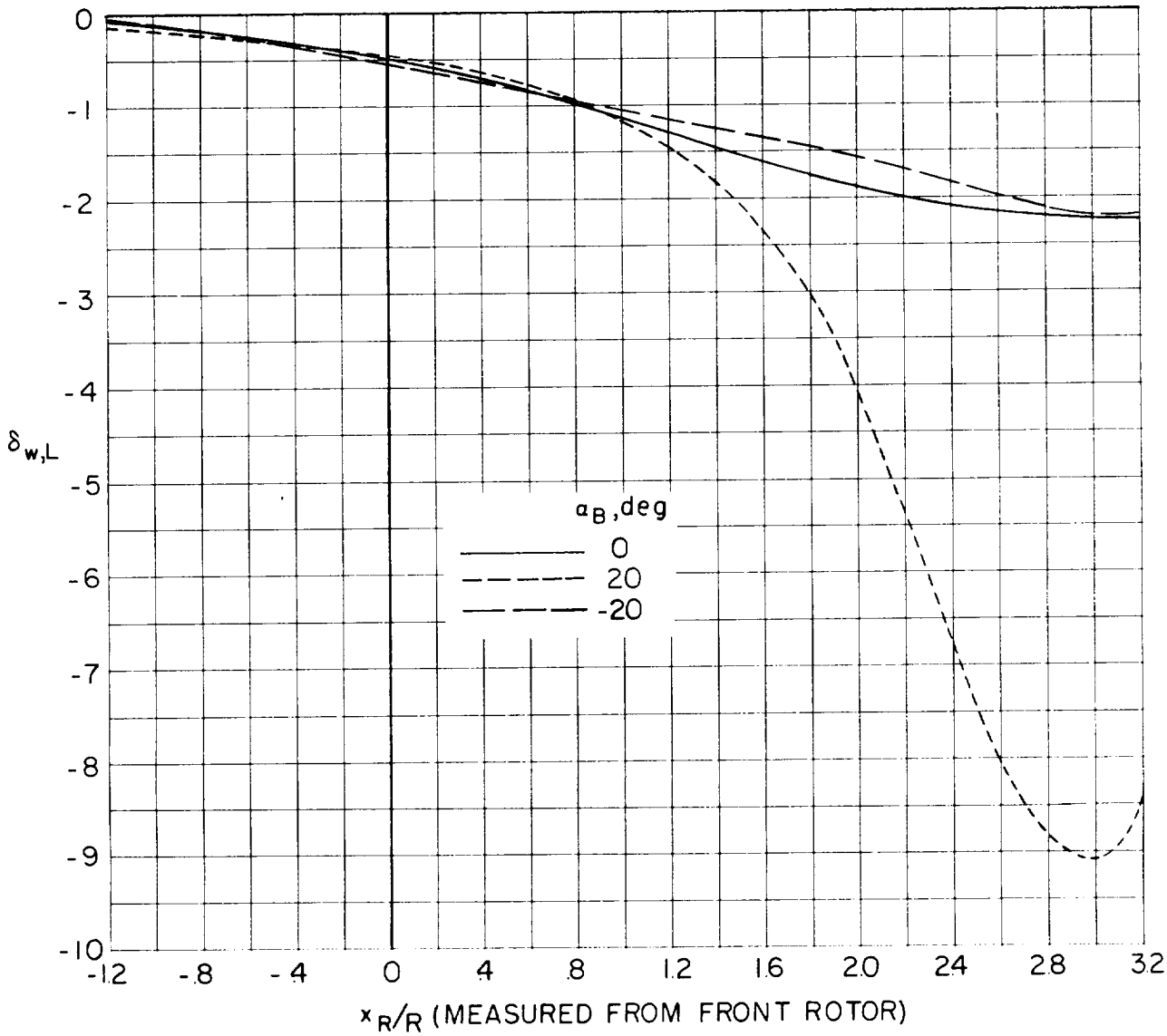

(a) $\chi = 60^0$.

Figure 44.- Distribution of total interference factor along longitudinal axis of nonoverlapped tandem-rotor system with front rotor centered in closed tunnel. $\gamma = 1.5$; $\sigma_R = 0.5$; $\alpha_{FR} = \alpha_{RR} = \alpha_B$; $\frac{l_{RR}}{R} = 2.0$; $\frac{h_{RR}}{R} = 0$.

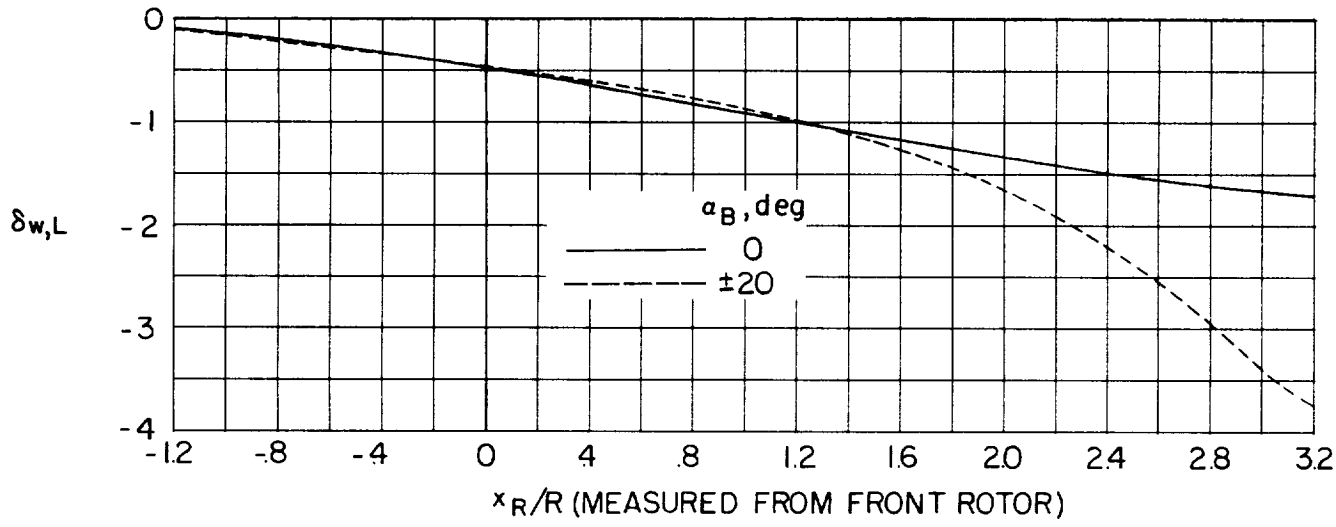

(b) $\chi = 90^0$.

Figure 44.- Concluded.

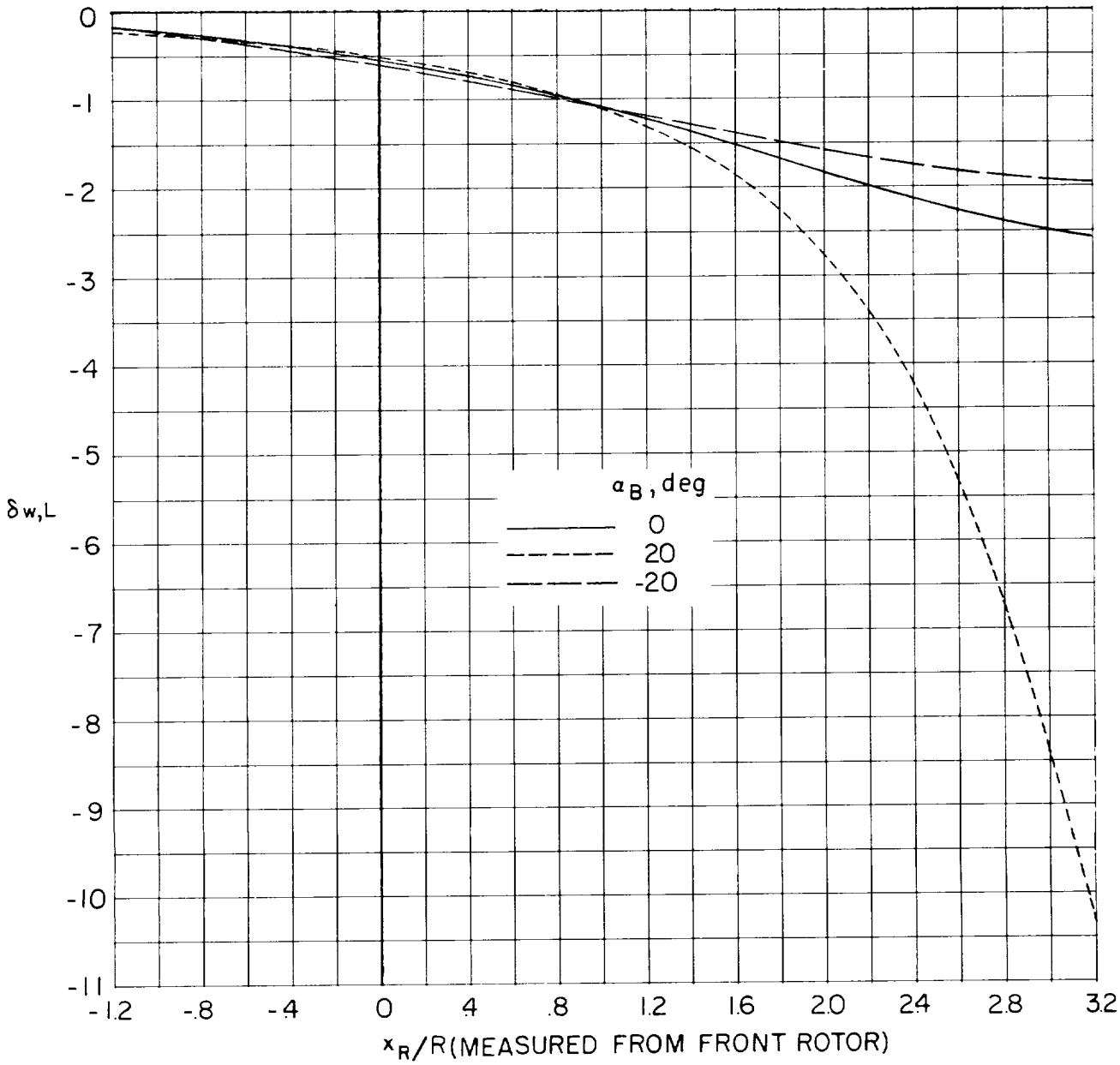

(a) $\chi = 60^0$.

Figure 45.- Distribution of total interference factor along longitudinal axis of nonoverlapped tandem-rotor system with front rotor centered in closed tunnel. $\gamma = 1.5$; $\sigma_R = 0.375$; $\alpha_{FR} = \alpha_{RR} = \alpha_B$; $\frac{l_{RR}}{R} = 2.0$; $\frac{h_{RR}}{R} = 0$.

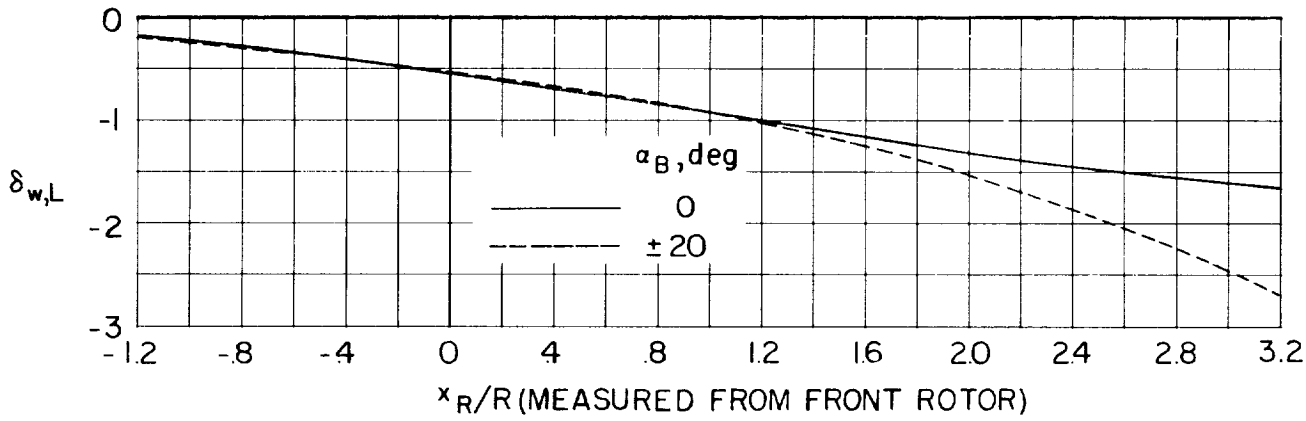

(b) $\chi = 90^0$.

Figure 45.- Concluded.

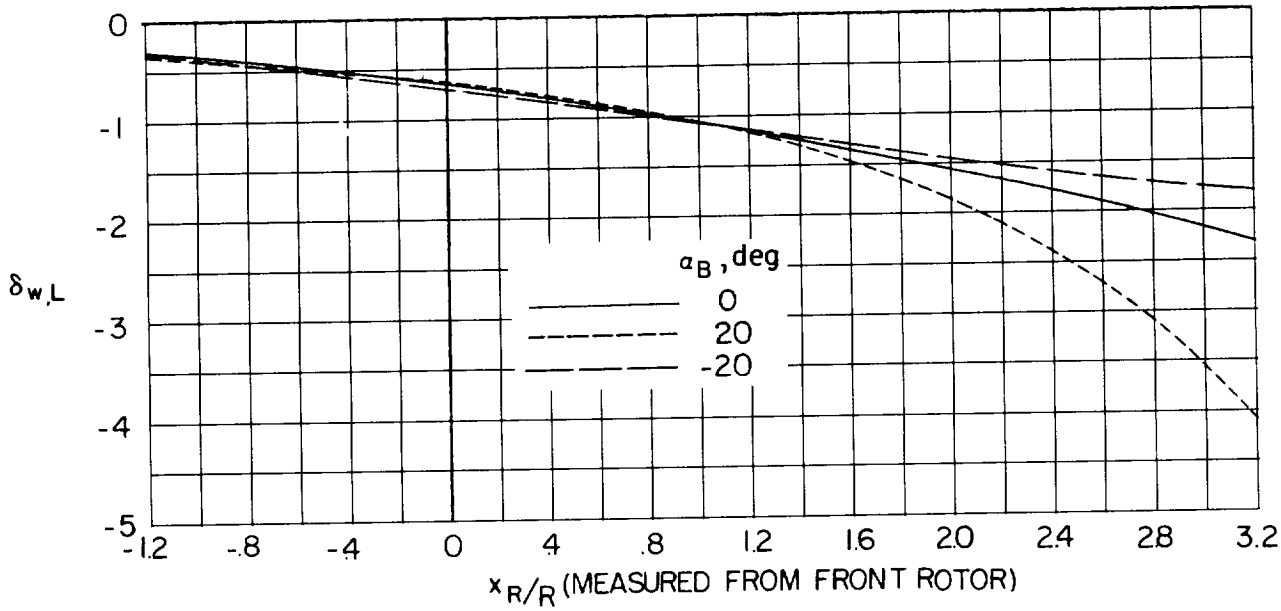

(a) $\chi = 60^0$.

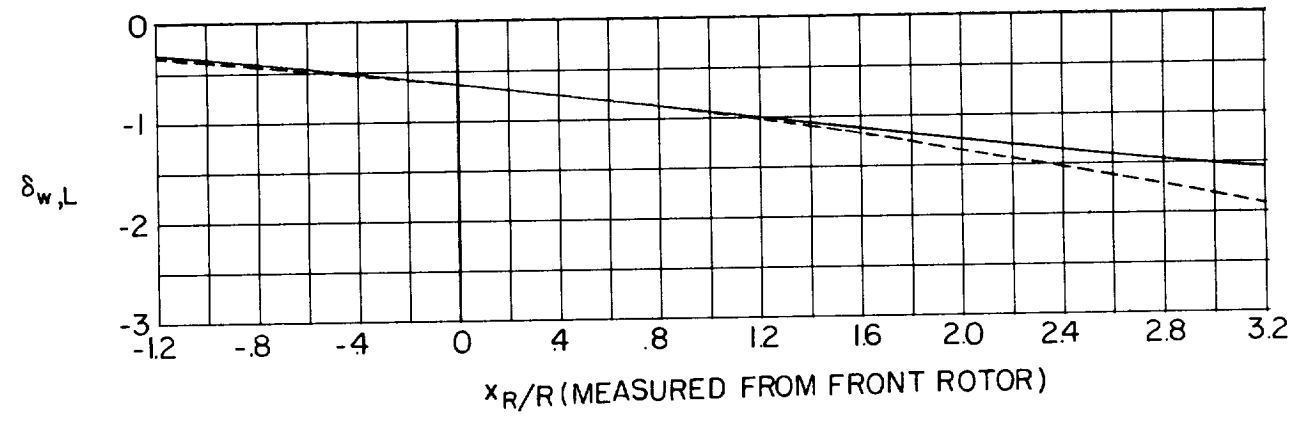

(b) $\chi = 90^0$.

Figure 46.- Distribution of total interference factor along longitudinal axis of nonoverlapped tandem-rotor system with front rotor centered in closed tunnel. $\gamma = 1.5$; $\sigma_R = 0.25$; $\alpha_{FR} = \alpha_{RR} = \alpha_B$; $\frac{l_{RR}}{R} = 2.0$; $\frac{h_{RR}}{R} = 0$. Effect of angle of attack is symmetrical at $\chi = 90^0$.

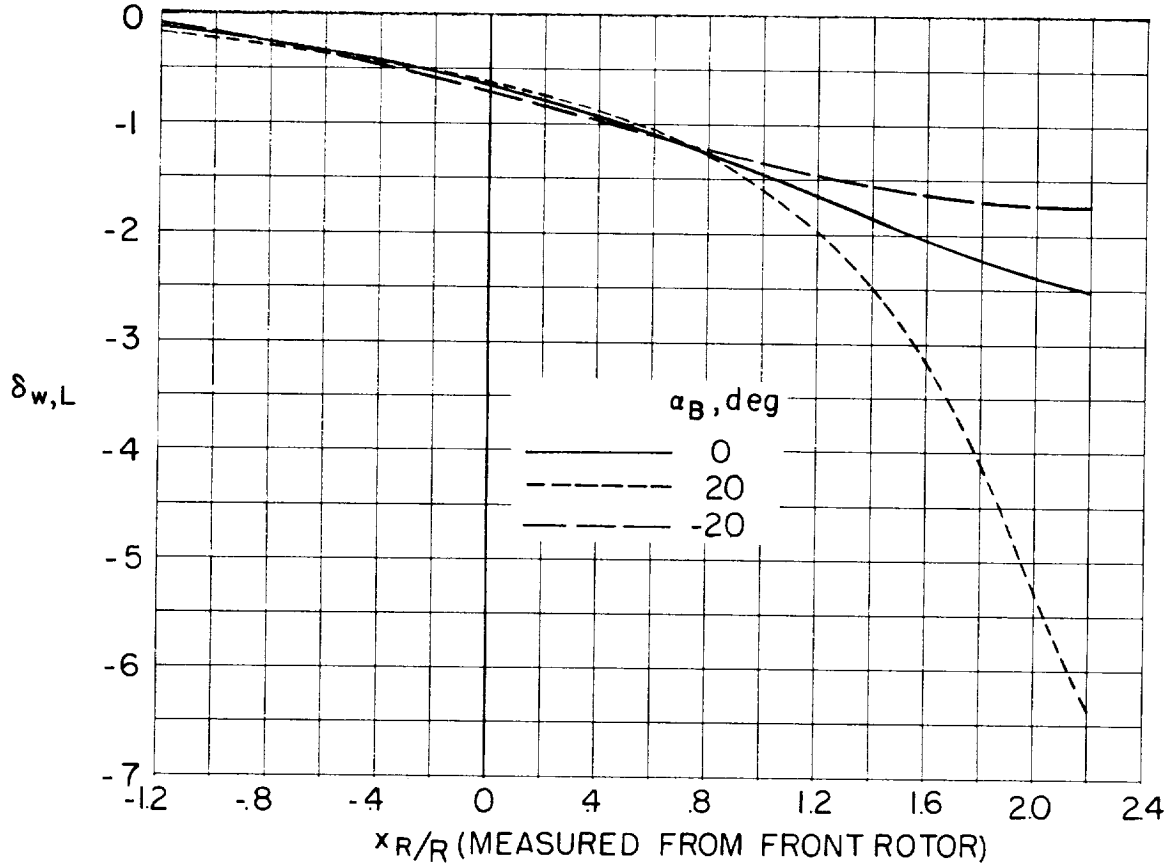

(a) $\chi = 60^0$.

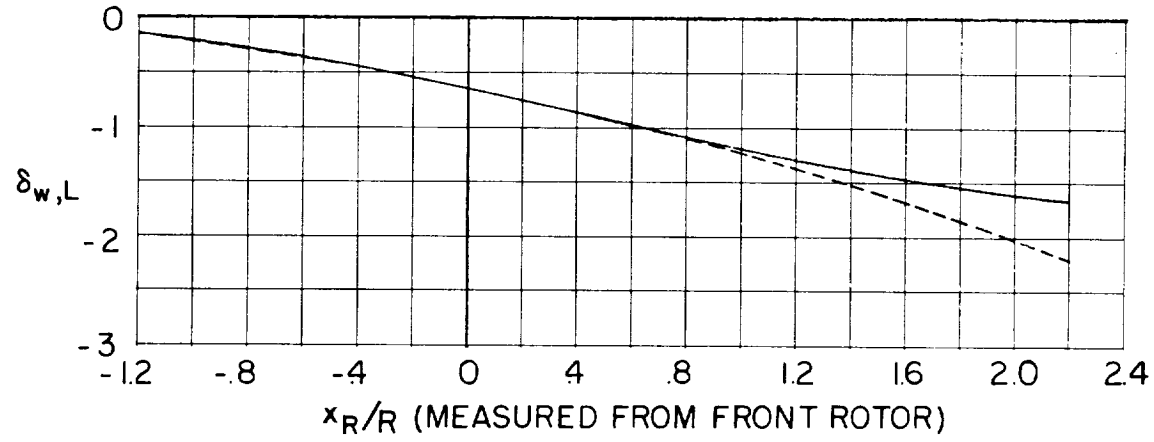

(b) $\chi = 90^0$.

Figure 47.- Distribution of total interference factor along longitudinal axis of fully overlapped tandem-rotor system with front rotor centered in closed tunnel. $\gamma = 1.5$; $\sigma_R = 0.5$; $\alpha_{FR} = \alpha_{RR} = \alpha_B$; $\frac{l_{RR}}{R} = 1.0$; $\frac{h_{RR}}{R} = 0$. Effect of angle of attack is symmetrical at $\chi = 90^0$.

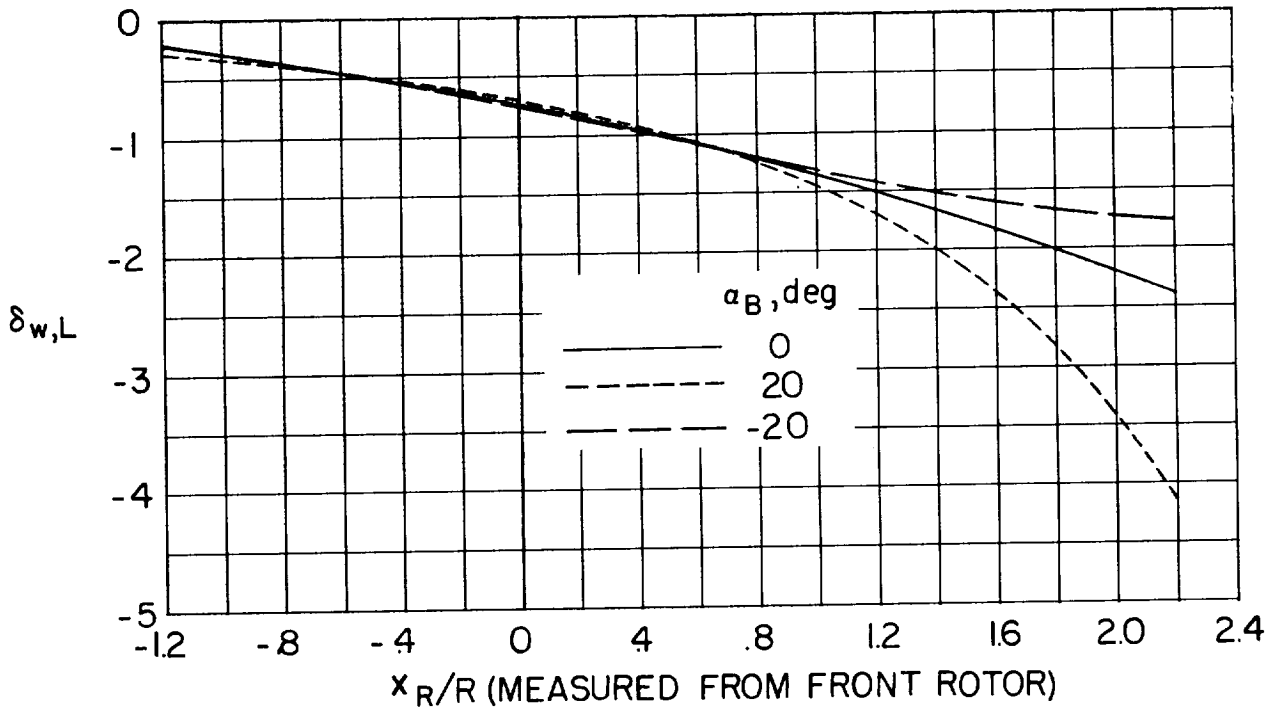

(a) $\chi = 60^0$.

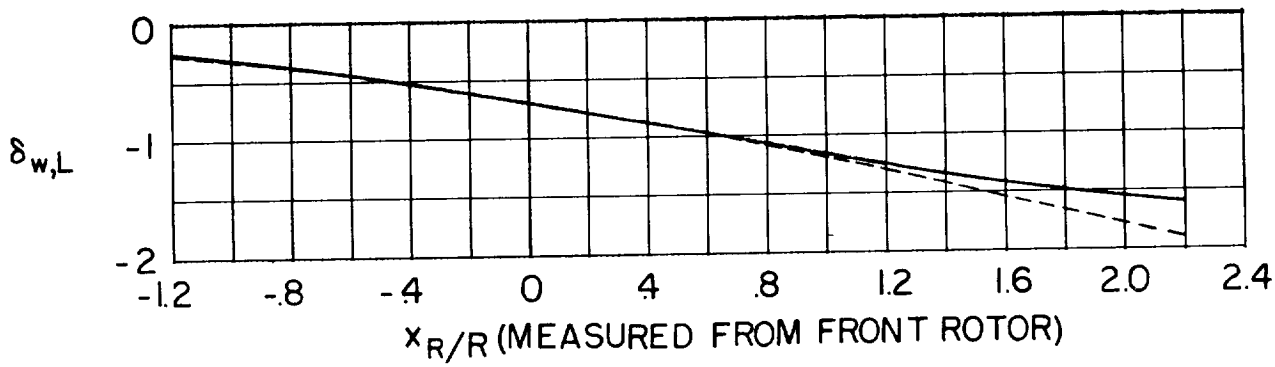

(b) $\chi = 90^0$.

Figure 48.- Distribution of total interference factor along longitudinal axis of fully overlapped tandem-rotor system with front rotor centered in closed tunnel. $\gamma = 1.5$; $\sigma_R = 0.375$; $\alpha_{FR} = \alpha_{RR} = \alpha_B$; $\frac{\ell_{RR}}{R} = 1.0$; $\frac{h_{RR}}{R} = 0$. Effect of angle of attack is symmetrical at $\chi = 90^0$.

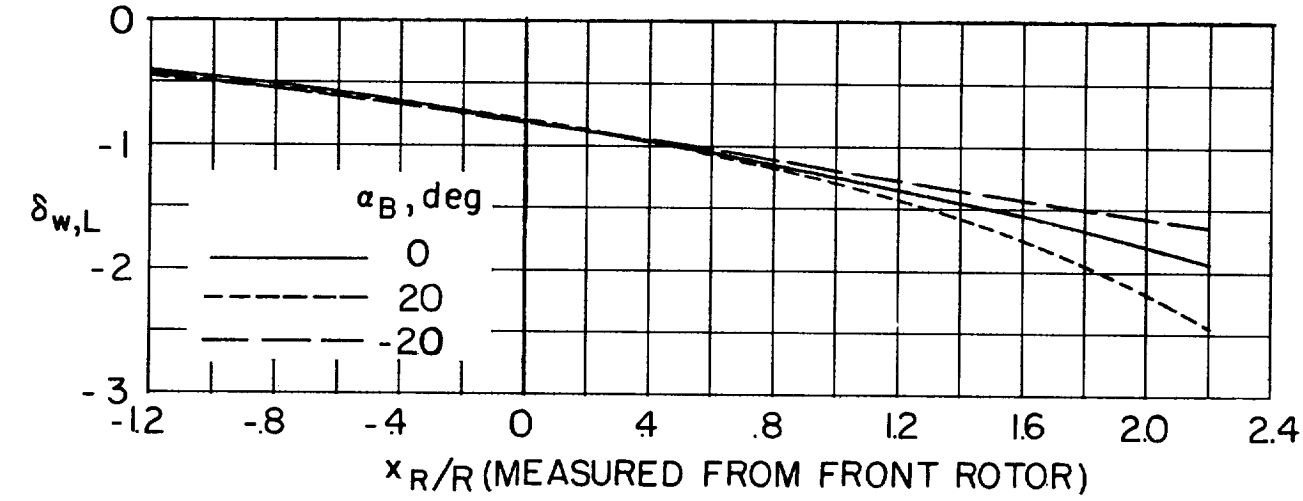

(a) $\chi = 60^0$.

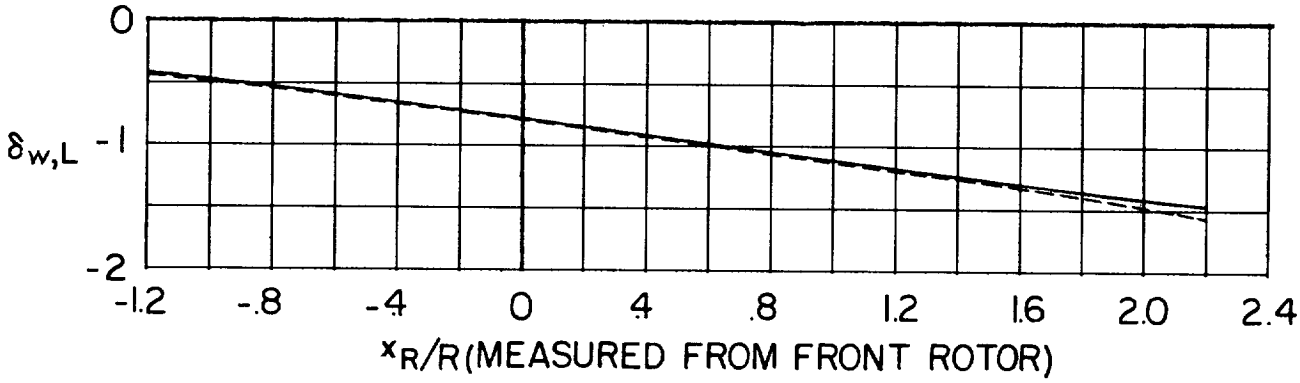

(b) $\chi = 90^0$.

Figure 49.- Distribution of total interference factor along longitudinal axis of fully overlapped tandem-rotor system with front rotor centered in closed tunnel. $\gamma = 1.5$; $\sigma_R = 0.25$; $\alpha_{FR} = \alpha_{RR} = \alpha_B$; $\frac{\ell_{RR}}{R} = 1.0$; $\frac{h_{RR}}{R} = 0$. Effect of angle of attack is symmetrical at $\chi = 90^0$.

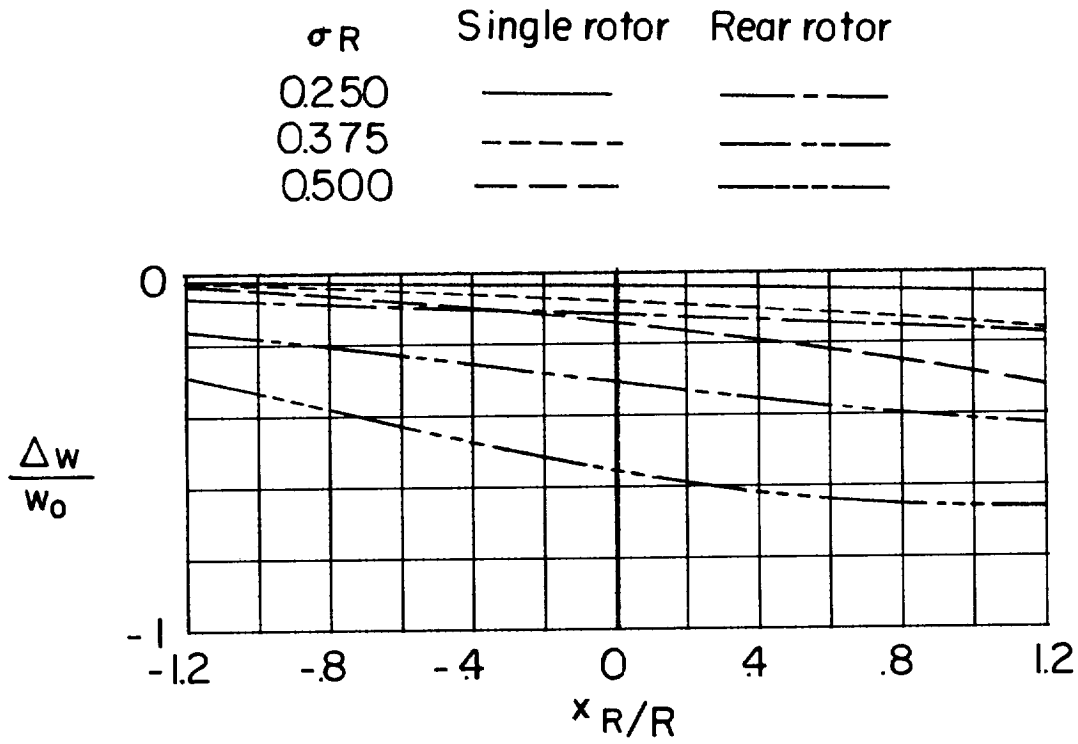

(a) $\chi = 60^{0}$.

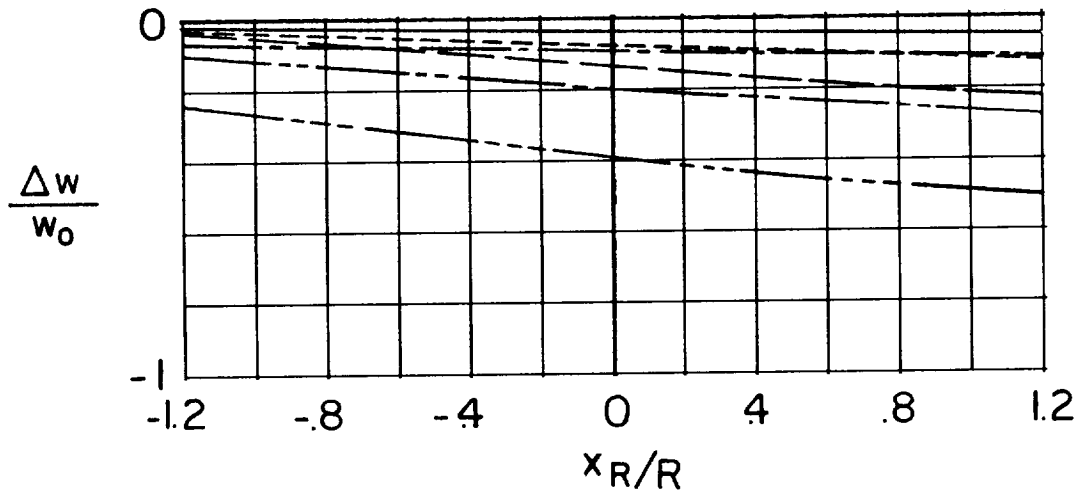

(b) $\chi = 90^{0}$.

Figure 50.- Comparison of interference velocities along longitudinal axis of a single rotor and the rear rotor of a nonoverlapped tandem-rotor system. $\gamma = 1.5$; $\alpha_R = \alpha_{FR} = \alpha_{RR} = \alpha_B = 0^{0}$; $\frac{l_{RR}}{R} = 2.0$; $\frac{h_{RR}}{R} = 0$.

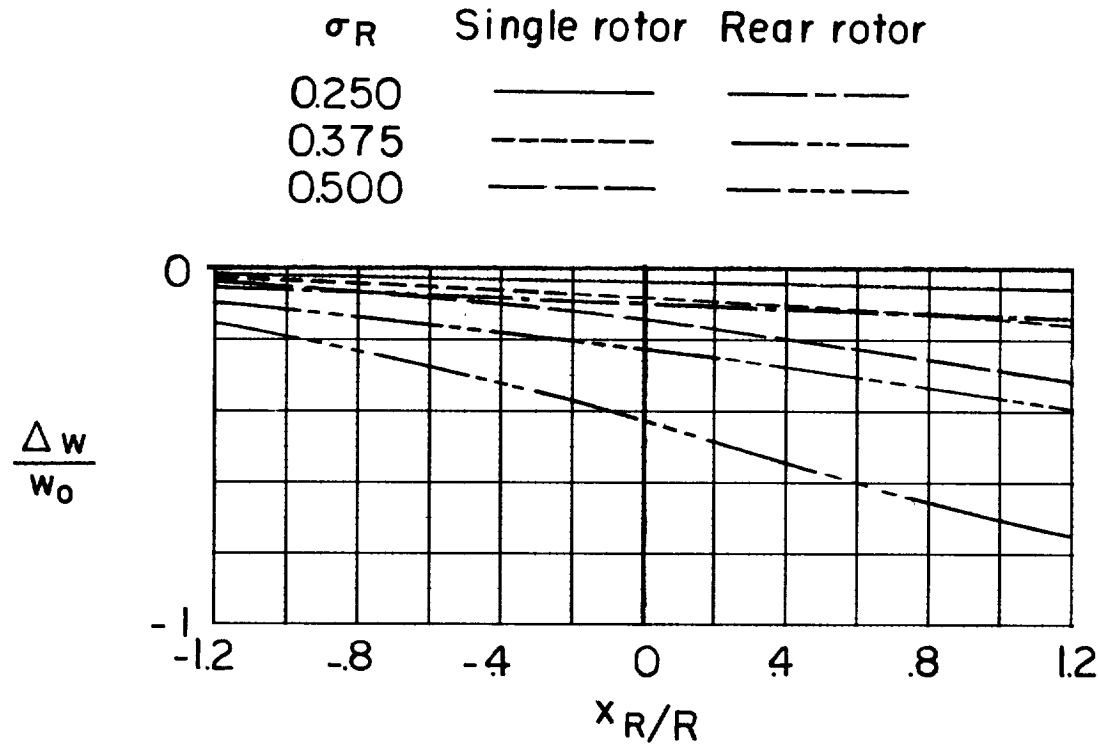

(a) $\chi = 60^{0}$.

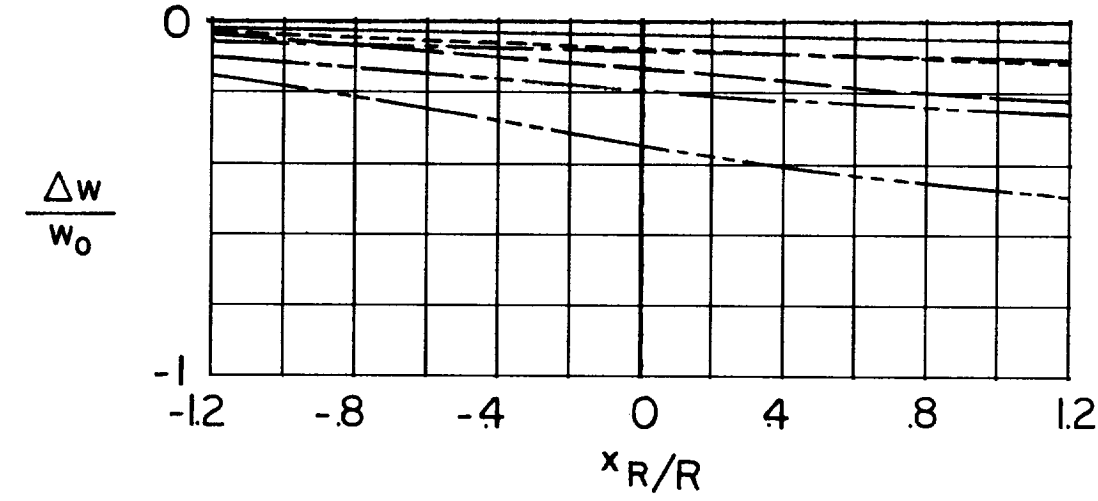

(b) $\chi = 90^{0}$.

Figure 51.- Comparison of interference velocities along longitudinal axis of a single rotor and the rear rotor of a fully overlapped tandem-rotor system. $\gamma = 1.5$; $\alpha_R = \alpha_{FR} = \alpha_{RR} = \alpha_B = 0^{0}$; $\frac{l_{RR}}{R} = 1.0$; $\frac{h_{RR}}{R} = 0$.

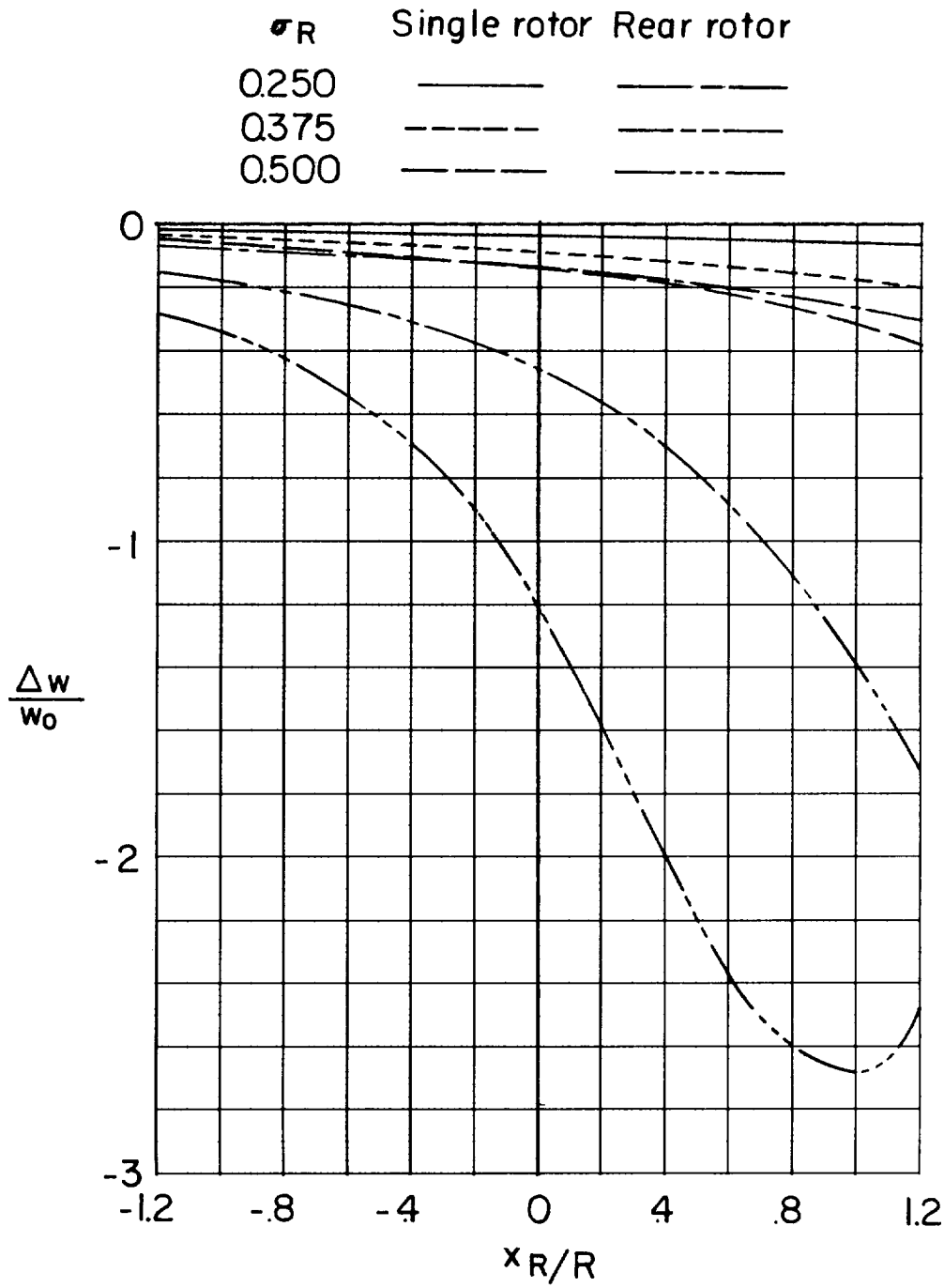

(a) $\chi = 60^0$.

Figure 52.- Comparison of interference velocities along longitudinal axis of a single rotor and the rear rotor of a nonoverlapped tandem-rotor system. $\gamma = 1.5$; $\alpha_R = \alpha_{FR} = \alpha_{RR} = \alpha_B = 20^0$; $\frac{l_{RR}}{R} = 2.0$; $\frac{h_{RR}}{R} = 0$.

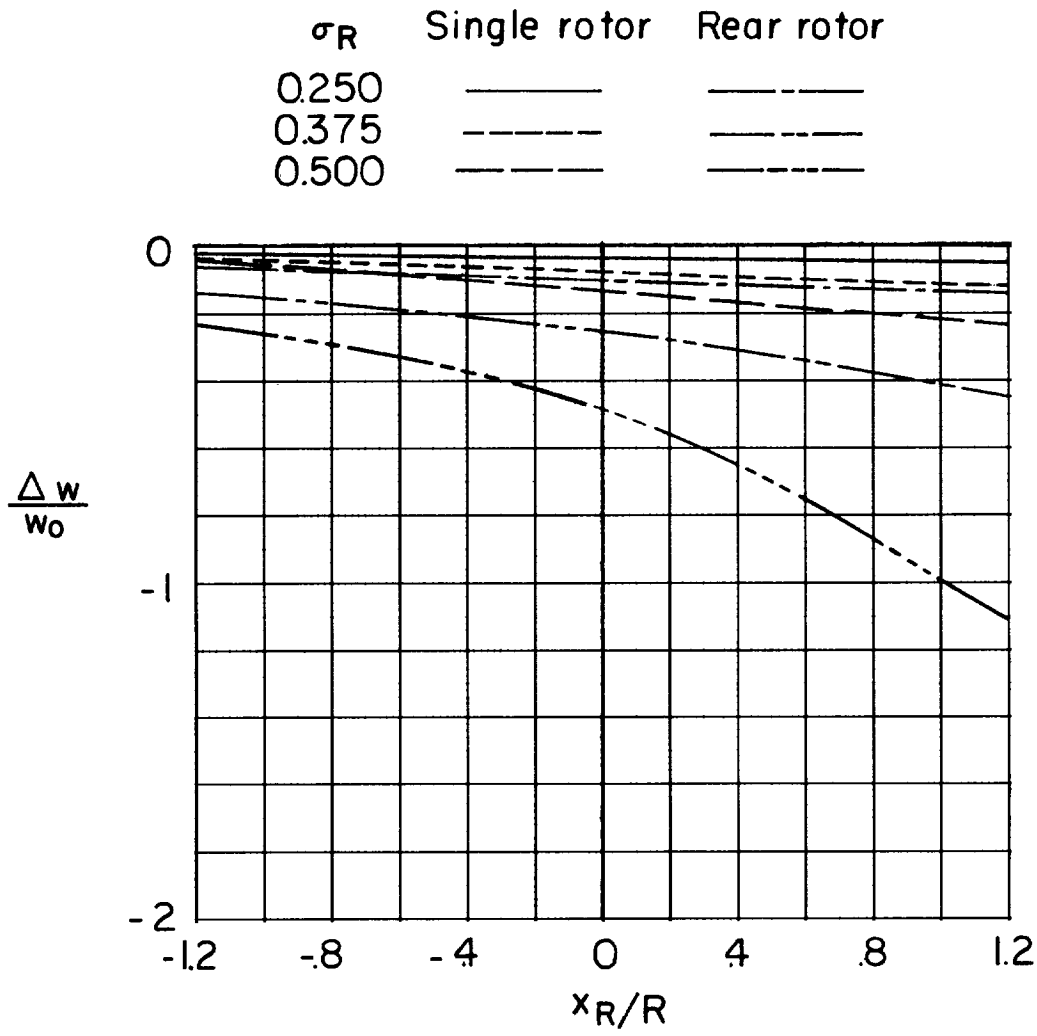

(b) $\chi = 90^0$.

Figure 52.- Concluded.

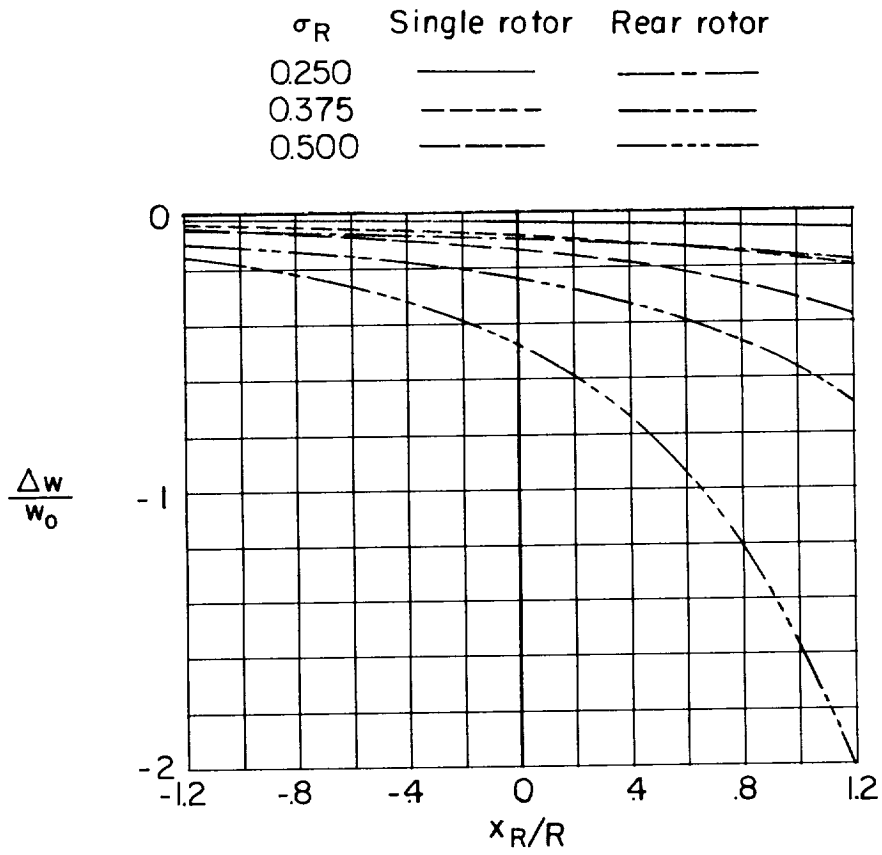

(a) $\chi = 60^0$.

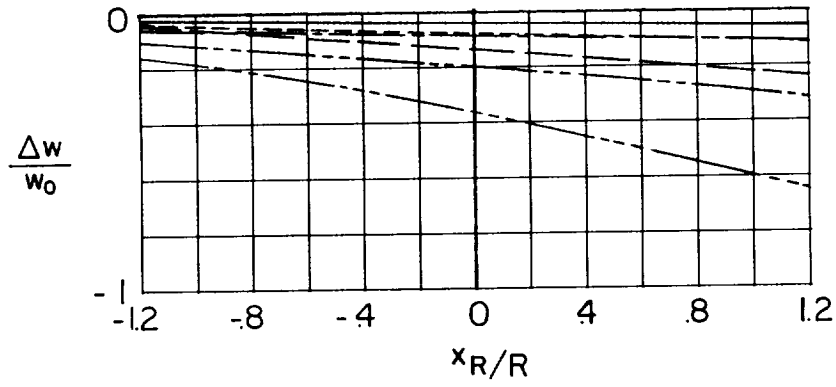

(b) $\chi = 90^0$.

Figure 53.- Comparison of interference velocities along longitudinal axis of a single rotor and the rear rotor of a fully overlapped tandem-rotor system. $\gamma = 1.5$; $\alpha_R = \alpha_{FR} = \alpha_{RR} = \alpha_B = 20^0$; $\frac{l_{RR}}{R} = 1.0$; $\frac{h_{RR}}{R} = 0$.